Abstract

Furthering the Scope, Understanding, and Application of Proteolysis Targeting Chimera

Daniel Paul Bondeson

2018

Modern biomedical research has unveiled many of the complicated processes that underlie life at the most basic of level of cells. This enterprise has shown reversible protein phosphorylation, mediated by kinases, is an integral process whose mis-regulation causes many diseases, including cancer. Current therapeutic strategies targeting kinases have been focused on inhibiting enzymatic activity, and this has led to many approved therapies that extend the life and livelihood of many people.

This thesis explores the limitations of these strategies and a novel chemical biology tool to overcome them. In the first chapter, a brief history of kinases highlights how modern thinking focuses on kinase activity but ignores additional functions of protein kinases. The onco-kinase BCR/Abl is one such example: non-kinase roles of this protein are implicated in maintaining the disease and preventing cure even when the kinase activity is efficiently inhibited. A second example is the pseudokinase ROR2 and pseudokinases in general. These proteins share common structural features of kinases yet are enzymatically inactive and participate in important signaling programs within the cell. These two examples illustrate how inhibition is a limited paradigm of drug discovery.

Chapter two exemplifies recent advances in a strategy to overcome the limitations of inhibition. This strategy is called proteolysis targeting chimera, or PROTAC, and is based on heterobifunctional small molecules which bind to the protein target and recruit it to E3 ubiquitin ligases. The target protein is then ubiquitinated and degraded. While previous iterations of PROTACs have been rather unimpressive, this chapter highlights

the degradation of a protein kinase as well as a nuclear hormone receptor. These PROTAC molecules are unprecedented in their potency, selectivity, and drug-likeness. The chapter concludes by discussing the many recent examples of PROTACs and their application in research and, soon, therapeutic interventions.

Chapter three then asks a basic and important question about PROTAC design. In designing potent degraders, minor structural changes in the molecule can lead to drastic effects on protein degradation. This chapter explores that phenomena, first by using a model system in which PROTAC geometry is finely tuned for degradation. It is shown that the discriminating factor between poor and potent PROTACs is the ability to form a stable ternary complex between the target, the PROTAC, and the E3 ligase. The best PROTACs induce protein:protein interactions between the target and E3 ligase, stabilizing the complex and leading to more potent degradation. In the second part of chapter three, PROTACs are explored which bind to many different kinase targets, but only degrade a subset of possible targets. Again, the discriminating factor between degraded and non-degraded proteins appear to be protein:protein interactions unique to the degraded proteins. This chapter offers biophysical explanations for commonly observed phenomena, and aids in developing design principles for PROTAC molecules.

Having shown PROTAC molecules to be a strategy for potent protein degradation in chapter two and enhancing the understanding of that platform in chapter three, chapter four returns to the two examples listed above. First, potent degradation of BCR/Abl is achieved through a PROTAC designed to target the allosteric site. Next, these compounds are used in initial assays to explore functions of BCR/Abl that are affected by either inhibition or degradation of the protein. Finally, initial studies in patient-derived stem cells are presented. While the viability of these cells is reduced by PROTACs, more nuanced work must be done to highlight differences between degradation and inhibition of BCR/Abl.

Second, initial efforts are made to develop ligands for the pseudokinase ROR2. While these compounds may not have activity on their own, they could be converted into PROTAC molecules which would deactivate all functions of ROR2. A thermal shift assay is used to identify potential ligands of ROR2 which bind with modest affinity. Future work will explore these compounds as well as developing high-throughput screens for pseudokinases in general.

While previous iterations were limited in potency, this study demonstrates that PROTAC molecules can be versatile chemical tools. While outside the scope of this thesis, PROTACs also show promise as therapeutic interventions. By degrading the entire protein rather than just inhibiting one functionality, PROTACs may expand what is currently considered druggable. Many literature examples point to this possibility. With the first PROTAC molecules soon to enter clinical trials, this study highlights the reasons for the considerable excitement surrounding this technology.

Furthering the Scope, Understanding, and Application of Proteolysis Targeting Chimera

A Dissertation
Presented to the Faculty of the Graduate School
of
Yale University
in Candidacy for the Degree of
Doctor of Philosophy

by
Daniel Paul Bondeson

Dissertation Director
Professor Craig M Crews

May 2018

Table of Contents

List of Figures and Tables

Acknowledgements

I am indebted to many people for the work that has gone into this dissertation. First, I must thank Professor Craig Crews. I have always been amazed at his willingness and excitement to entertain even the most trivial of data and scientific discussions. He has provided a fount of ideas: some of them crazy but almost all of them good. He has also endeavored to create a lab environment in which trainees can flourish, and I think he has succeeded in this. The quality of researcher in the Crews' lab is high indeed.

I thank my thesis committee members as well: Professors Karen Anderson and Mark Hochstrasser. I have always enjoyed our discussions. Your warm and patient encouragement has focused my thinking and my work and pushed it in good directions.

I am also indebted to my fellow Crews' lab scientists. I am grateful that I cannot think of a single person in the lab that has not made my science more effective: either by providing helpful insights or a warm smile. Thank you for putting up with me through the years. Special thanks to Dr. Saul Jaime-Figueroa, Dr. George Burslem, Dr. Ian Smith, Dr. Eunwha Ko, Dr. Momar Toure, and Hervé de Laborde for synthesizing the many compounds discussed in this dissertation.

Several Crews' lab members made substantial contributions to this dissertation. Dr. George Burslem has provided a patient ear for "a biologist trying to think like a chemist" and discussions with him have spurred many good ideas. He and I collaborated on the foretininb-omics, BCR/Abl, and pseudokinase projects; he also read through the entirety of an early version of this dissertation, providing helpful remarks for which I am appreciative. Blake Smith has been a valuable co-author, colleague, and friend, bringing a height of enthusiasm and depth of knowledge which pushed the foretinib-omics project to an excellent finished product. I am also grateful for Brian Hamman at Arvinas, for many

stimulating discussions on ternary complex equilibria and for always allowing me to use his reagents and plate-reader. Lastly, Alexandru Buhimschi has been an invaluable colleague and friend for the time that we have worked together. His contributions, mainly to the HaloTag studies, extend well beyond technical acumen: his comments and ideas have changed my way of thinking on many occasions.

Outside of the Kline Biology Tower, I am extremely grateful for the communities I have been a part of, primarily through Trinity Baptist Church, the Rivendell Institute, and the Yale Graduate Student Christian Fellowship. These relationships have changed how I think about *thinking,* which is one of the greatest gifts a person can receive. To Tony, Kim, Joshua, Ben, Fan, Jessica, Heidi, Lucas, Jon and Anita, and Rick and Soozie: Thank You.

To my family, thank you for encouraging me to come to New Haven so many years ago, and thank you for consistently believing in me more than I believe in myself. Your love means the world to me.

Lastly, to Gentley. Your passion, love, joy, and grace has made this last chapter of graduate school far more decent. I cannot wait to start the next chapter with you.

For my father,

I grew up not-understanding Triplet Exciton Dynamics and Spin Lattice Relaxation in $MTPA(TCNQ)_2$ and I may never understand the impact that having your dissertation on my shelf has made.

Jeremiah 33:20 – 22

Chapter 1

Introduction and Literature Review

Preface

The review of protein degradation technologies presented in the latter part of this chapter is a modified version of a review written by me:

Bondeson, D.P., and Crews, C.M. (2017). Targeted Protein Degradation by Small Molecules. Annual Reviews Pharmacology Toxicology. *57*, 107–123.

Biological and biomedical sciences in the 21st century have drastically improved human health. Our understanding of disease, particularly cancer, grows at an accelerating pace and translational efforts have pushed this basic understanding towards effective therapies[1,2]. Talk of “curing cancer” is increasingly common and decreasingly unrealistic.

Much progress is owed to a modern gene-centric mode of thinking that understands that at the heart of human physiology and pathology are *molecules*. Whether it be a focus on large DNA, RNA, or protein molecules, the reductionist view states that the chemistry of life is absolutely essential to understanding the diseases of life. Increasingly, “big-data” techniques have given scientists the ability to rapidly and inexpensively gather information on the multitudes of molecules within cells and to understand the networks within which these molecules operate[3–5].

Increasingly, an understanding of how these molecules have gone awry enables an understanding of the intervention required to fix the problem. 2017 held the first Food and Drug Administration (FDA)-approval of a treatment not based on a tumor’s location but the specific biomarkers of that tumor[6]. This example will be commonplace someday. The feasibility of personalized cancer treatments increases with advances in diagnostics, predictive biomarkers, and an understanding of underlying disease mechanisms[7].

Protein kinases are a class of proteins which have seized the considerable focus modern drug discovery. This class of proteins was described, in 2001, as the “major drug targets” of the century[8]. Many examples of the mis-regulation of these proteins reinforce the *gene*-centric mentality of modern drug discovery. Far more importantly, the selective inhibition of protein kinases has literally transformed some life-ending cancers to lifelong inconveniences.

Protein kinases have a simple function within the cell: catalyze the transfer of a phosphate group from adenosine triphosphate (ATP) to a substrate protein. While simple, the reversible phosphorylation of proteins is a central regulatory mechanism within the cell. Furthermore, when this function becomes mis-regulated, many pathways canonically associated with cancer can become hyper-active: growth, invasion, resistance to cell death, etc. Therefore, the inhibition of kinases, mainly through small molecules which block their enzymatic activity, has led to dozens of FDA-approved therapies[9]. These "major drug targets" are such not without cause.

Despite these successes, inhibitors in general have their limitations. First, inhibition is only achieved when a kinase is constantly associated with the inhibitor[10]. This requires vast excess of the inhibitor. Although some inhibitors can be selective for their desired target, most inhibitors cause side effects by turning off the activity of additional kinases. Second, kinase inhibitors only inhibit kinase activity. While obvious, this drawback leaves the rest of the protein to function per usual, and certain kinases have additional disease-causing functionality aside from their catalytic ability[11].

The focus of this thesis is the development of a new therapeutic strategy to overcome these two limitations. Conceptually, this strategy relies on a small molecule drug which hijacks cellular quality control to *degrade*, rather than merely inhibit, a protein of interest. Because the protein target is degraded, each molecule of drug is capable of turning off many molecules of the target. This allows for lower amounts of drug to be used. Furthermore, because the *entire* protein target is degraded, all possible functions of that target are also inhibited. While this thesis focuses on protein kinases, this strategy can be applied to almost any protein targets.

This introductory chapter has several sections. The first section briefly retells the history of kinases, beginning in the early 1940s when reversible protein phosphorylation

was unknown. This history reveals that despite the enormous benefit from the modern understanding of kinases and their inhibition, many opportunities are missed when inhibition is the only therapeutic intervention available. This section will close with a discussion of two specific examples of protein "kinases" which require alternative interventions.

Possible alternative strategies are discussed in the next section. Broadly speaking, these alternatives are "knock-down" strategies, in which the entire protein is degraded as opposed to inhibiting just one particular domain of that protein. Biomedical research has been accelerated by genetic knockdown tools; unfortunately, these tools are very limited in their therapeutic application. Additional tools are available to readily study protein knockdown, but these too are limited to the research laboratory.

Finally, the chapter closes with chemical knockdown strategies that have shown clinical application in the past. The most successful of these examples have been serendipitously discovered but have paved the way for a more generalizable system. This system will be discussed in the context of its historical limitations. The actual realization of it is the main focus of this dissertation and will be highlighted in subsequent chapters.

Section 1.1: A Brief History of Kinases

1940-70s: Kinases in Glycogen Metabolism

The term kinase comes from the greek κίνησις, meaning movement. The term was first used in the 1920s to describe the movement of phosphate groups by hexokinase between metabolites[12]. The term's use to describe protein phosphorylation developed in the 40s and 50s when an enzyme, glycogen phosphorylase, was found to be regulated by addition or removal of a "prosthetic group[13,14]." In an era before recombinant proteins, affinity tags,

or overexpression in bacterial, this enzyme was isolated from rabbit skeletal muscle by Carl and Gerty Cori and described in 1943.

Phosphorylase could be purified in two forms: form **A** which had enzymatic activity without any added cofactors, and form **B,** which lacked activity without the addition of AMP[13,14]. While form **A** could only be isolated if the enzyme was purified quickly, the Cori group found that phosphorylase converted to form **B** if an unpurified fraction were incubated overnight. The difference between **A** and **B** was the removal of the prosthetic group, which the authors attributed to a prosthetic group removing enzyme. This enzyme could be separated from phosphorylase **A** by precipitation, which allowed the authors to study the prosthetic group-removing enzyme in isolation. Since form **B**, but not **A**, required AMP for activity, they further hypothesize that the prosthetic group was "firmly bound adenylic acid [AMP]"[13].

Studies on this enzyme advanced over the next ten years. With the benefit of hindsight, several findings point toward the prosthetic group being phosphate, and that the removing enzyme is a phosphatase. For example, early studies indicated that phosphate was liberated in this converting reaction[15,16]. Fluoride ions were also shown to inhibit this conversion, which "indicates that fluoride shifts the above balance in favor of active phosphorylase by preventing inactivation"[17]. It was unknown in the 1950s, but fluoride ions are commonly used phosphatase inhibitors.

The details of the inactivation of phosphorylase **A** were revealed by isolating an enzyme that could re-activate phosphorylase **B**. These studies were performed by Nobel Laureates Edwin Krebs and Edmond Fischer. After moving from the Cori lab to begin his own research career, Krebs initiated a collaboration with Fischer. Both researchers had expertise in different areas of phosphorylase biochemistry and sought to understand the two forms of phosphorylase. However, in reproducing the isolation of phosphorylase **A**,

they omitted a filtration step in favor of newer methods in centrifugation. In doing so, they were only able to obtain phosphorylase **B**, the inactive form. Through careful investigation, they found that the filtration step introduced divalent cations into the crude muscle extract[18]. These divalent cations and ATP were required for the conversion of form **B** to phosphorylase **A**. An enzyme was suspected. In a follow-up paper, the authors purified the **B** to **A** converting enzyme and showed that the terminal phosphate of ATPγ^{32}P is transferred onto phosphorylase **B**[19]. The authors stated that "…if ADP is a product, then it would appear reasonable to think of the **B** to **A** conversion as a typical kinase reaction in which the terminal phosphate of ATP is transferred to a specific protein substrate"[19]. When the group later identified ADP as a product, it was firmly established that the "converting enzyme" was indeed a protein kinase[20]. The converting enzyme was termed "phosphorylase kinase."

Krebs, Fischer, and others continued to work on protein kinases, and more examples emerged throughout the 1960s. Because these examples were only in the niche of glycogen metabolism, reversible phosphorylation was as a central regulatory mechanism was not appreciated. Several discoveries late in the 1960s began to widen this scope. For example, kinases involved in other areas of cellular metabolism were described[21]. Likely the largest boom for the kinase field was the discovery of protein kinase A (PKA) by the Krebs group, the activity of which is dependent on cyclic adenosine monophosphate (cAMP) and which phosphorylates and activates phosphorylase kinase[22]. The implications for this were twofold. First, kinases are involved in signaling cascades. Second, because cAMP had already been implicated in diverse cellular processes, it suggested that perhaps protein kinase activity might have a far greater scope than just metabolism.

1970s-1980s: Exploding Understanding and Roles of Protein Kinases

During the 1970s and 80s, examples of proteins kinases began to emerge in nearly every realm of cell biology. By 1987, it was estimated that the human genome might contain upwards of one thousand kinases[23]. It would be impractical to retell the entirety of these years of massive discovery. Therefore, this next section focuses on two cases studies: The Avian Sarcoma Virus (ASV) gene product *v-src* and the epidermal growth factor receptor (EGFR). These examples firmly placed protein kinases at the center of important signal transduction pathways.

The *v-src* gene of ASV was first described in the early 1970s as a non-structural component of the virus that was required for causing oncogenic growth of infected cells[24]. This gene produced a protein product of about 60 kDa[25]. Importantly, this gene was also shown to be closely related to *c-Src*, a cellular gene occurring in normal, untransformed cells[26,27]. In the late 70s, both c-Src and v-Src protein were crudely isolated and found to possess potent kinase activity[28].

Despite the evidence that v-Src had kinase activity and could transform cells, the connection between these pieces of evidence took several years to accumulate. Researchers were limited by their toolset and so relied on large genetic lesions, some of which suggested that the transforming activity of v-Src lay outside its kinase domain[29]. In the mid-80s, however, a slew of papers showed that specific mutations, especially mutating the ATP-coordinating lysine residue 295, that abolished all kinase activity had no ability to transform cells[30], that a particular tyrosine residue was phosphorylated and critical to the activity of the v-src protein[31] and, conversely, that single amino acid substitutions could increase c-Src activity to a transforming levels of activity[32–34]. The residues these groups identified, we know now, are those in the activation loop, where

phosphorylation increases activity, and the C-terminal tail, where phosphorylation causes binding of the protein's SH2 domain and autoinhibition[35].

While c-Src is known now to be only weakly oncogenic[36], the study of c- and v-Src in the 70s and 80s moved kinases further from their initially understood peripheral role in cellular metabolism, to a central position as regulators of integral cellular processes. This central role is also precarious: if a single amino acid change can cause an otherwise normal protein kinase to gain oncogenic functions, these proteins must be critical.

In contrast to the c-Src protein's modest oncogenic potential, the epidermal growth factor (EGF) and its receptor (EGFR) are well-recognized cancer-causing agents. Contemporaneous with the discoveries outlined above for the Src proteins, EGFR was described as a membrane-bound protein with an intracellular kinase activity in 1978[37,38]. The protein was placed at a central role in regulating growth, due primarily to its close similarity to the transforming principle of the avian erythroblastosis virus (AEV). AEV contained a protein, v-ErbB, which was sufficient to induce transformation and highly homologous to portions of EGFR[39]. Researchers therefore hypothesized that v-ErbB had inordinate EGFR kinase activity due to a lack of regulatory mechanisms present on the extracellular domain of EGFR. Several years later, the kinase activity of v-ErbB was confirmed[40,41]. Mutations that abolish kinase activity were discovered to be sufficient to block the transforming ability of the v-ErbB and EGFR proteins[42,43].

The complicated interplay between EGFR kinase activity and binding of EGF received initial clarity in the late 80s, but precise details are still being uncovered today. The epidermoid carcinoma cell line, A-431, provided these initial hints. This cell line possessed elevated levels of truncated EGFR, and a collection of sub-clones displayed a correlation between the amount of receptor present and its mitogenic potential independent of EGF[44–46]. Thus, it seemed, activation of EGFR might be through the action

of dimerization or oligomerization, and experimental evidence suggested that EGF was able to cause rapid dimerization of EGFR which enhanced its kinase activity[47]. This led to a model in which EGF shifted a dimerization/oligomerization equilibrium of EGFR away from a monomeric state[48], which facilitated *trans*-autophosphorylation of the EGFR kinase domains[49], leading to an enhanced ability of EGFR to phosphorylate and activate downstream targets. This model is likely overly simplified and continues to be revised and expanded to this day[50,51].

This cursory historical review has ignored many excellent contributions research, but has endeavored to show some of the narratives that have defined the modern understanding of kinases and their central role in signal transduction and disease[52]. From an initial understanding of kinases in a niche area of glycogen metabolism, to an exploding area of interest where estimates on the number of kinases were overblown and reached into the thousands[23], to a strict, bioinformatic definition of what makes a kinase a kinase[53] and what constitutes the 530 kinases in the human kinome[54], to an enhanced understanding of the three dimensional structure[55,56], the study and understanding of kinases has been an active and ever-changing area of research over the last 60 years. Figure 1.1 outlines some of these advances.

1990 – Present: The case study of the BCR/Abl Tyrosine Kinase

While the basic biological discoveries regarding protein kinases and their integral role within cellular signal transduction characterized this area of research up until the 80s, perhaps the most exciting aspect of the protein kinase field since then has been their therapeutic targeting. Hundreds of clinical trials utilizing agents targeting protein kinases have been undertaken and some have resulted in FDA-approved therapies in 2018: 37 small molecule kinase inhibitors and 5 monoclonal antibodies, all designed to perturb the oncogenic signaling of kinases[9].

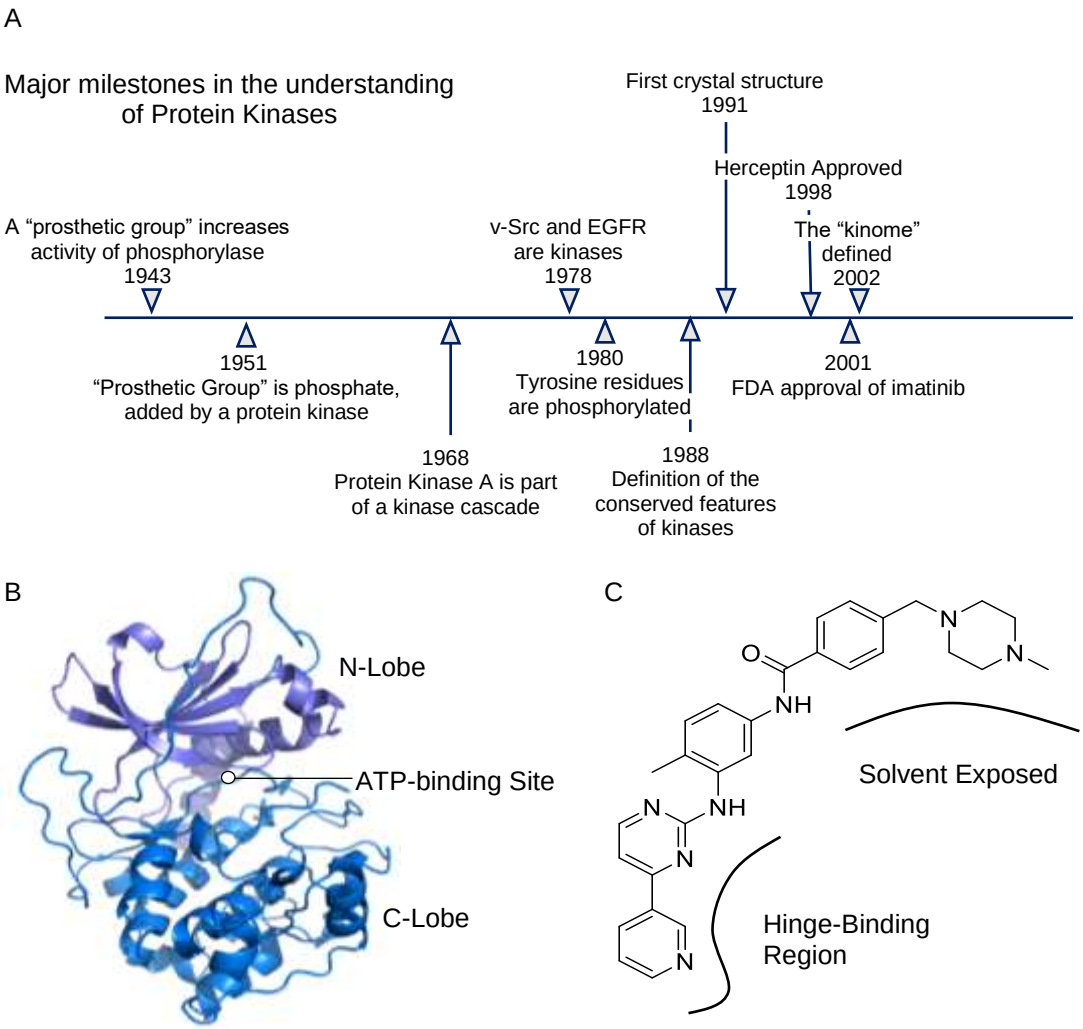

Figure 1.1 Major milestones in the understanding of protein kinases

(A) A small timeline outlining various conceptual and practical advances in relation to protein kinases (B) The first kinase three-dimensional structure published in 1991. Protein Kinase A (PDB Code 2CPK) in its apo state reveals a bilobed structure. The N-lobe is shown in purple, with the C-lobe in blue. No ligand, substrate, or ATP is bound, but the ATP-binding site is indicated. (C) Imatinib is the first small-molecule kinase inhibitor approved by the FDA. Regions of the structure that bind to the hinge connecting the N- and C-lobes (hinge-binding) and solvent exposed regions are indicated.

One of the most well-known examples of a small molecule kinase inhibitor is imatinib (Figure 1.1C). Imatinib inhibits the kinase activity of the oncogenic kinase caused by fusion of the *BCR* and *Abl1* genes and serves as a useful example of both the benefits and limitations of small molecule kinase inhibitors.

Since the 1980s, it was known that almost all cases of chronic myelogenous leukemia (CML) had a translocation of the 9th and 22nd chromosomes, a genetic abnormality termed the Philadelphia chromosome. Researchers such as Owen Witte, David Baltimore, and George Daley discovered that this Philadelphia chromosome produced transcripts with the 5' region of BCR and the 3' end of c-Abl, which produced a large protein that migrated at 210 kDa which they termed BCR/Abl^{p210}. Although there are other "versions" of BCR/Abl that result from related translocation events (e.g. p185 and p160), the most commonly studied form is p210 and will be referred to as simply BCR/Abl[57,58].

The BCR/Abl gene product was shown to possess intrinsic kinase activity and was capable of transforming cells and inducing a CML phenotype in mice[59–63]. In a similar fashion to other studies on kinases, the kinase activity of the BCR/Abl kinase product was shown to be necessary for transformation. To further clarify the role and provide a rationale for the selective inhibition of BCR/Abl, researchers were able to design antisense oligonucleotides (ASO) targeting the junction between *BCR* and *ABL1* portions of the mRNA transcript. Because the ribosome is unable to read through double stranded RNA, these ASO reduced BCR/Abl levels without changing levels of c-Abl levels in normal cells, causing selective inhibition of leukemia cell proliferation over normal cells[64]. Other reports indicated that the small molecules Herbimycin A and various tyrphostin compounds also inhibited BCR/Abl kinase activity, most likely through non-specific mechanisms[65,66]. Although these efforts showed great promise for the development of drugs that might clear

the leukemia while not harming normal tissues, this goal was thought to be highly unlikely. Indeed, even in a report which showed that a small molecule inhibitor could kill leukemia cells *ex vivo*, the authors conclude with this statement:

> "These compounds or more potent analogs that can be synthesized alone or in combination with other differentiating agents such as BCR-ABL1 antisense oligonucleotides may become useful agents to purge transformed cells in bone marrow cultures taken from CML patients in preparation for an autologous transplantation[65]."

It seems that the idea of treating a patient with a kinase inhibitor directly would be far too risky, as the conserved pocket among the different kinases would not allow selective inhibition of an oncogenic kinase. After all, ideas of the "kinome" and consensus kinase domains were just becoming understood and defined[53,55]. Despite this, medicinal chemistry programs continued to develop increasingly specific inhibitors. Serendipitously, in the course of developing inhibitors for Protein Kinase C and Platelet Derived Growth Factor Receptor, a compound was discovered that had selectivity and potent activity towards c-Abl[67,68]. In the first published report of its kind, Brian Druker and colleagues showed that one of these compounds, imatinib (also known as STI-571 and marketed as Gleevec), was capable of inhibiting proliferation of BCR/Abl expressing cells while sparing normal cells, as well as inhibiting the engraftment of tumors driving by BCR/Abl reducing tumor burden[69].

How was this potent and selective cell killing achieved? The crystal structure of imatinib in complex with the c-Abl kinase domain was published in 2000 and provided insights into this question[70]. The kinase inhibitor had already been shown to bind competitively with ATP, and the structure revealed that imatinib bound in the cleft formed between the N- and C-lobes of the kinase domain: exactly where phosphotransfer occurs.

Since all known protein kinases share a similar architecture, previous crystal structures of small molecules bound to protein kinases suggested that binding specificity could only arise from minor variations in primary sequence outside of the canonical kinase subdomains, down to single amino acid changes that might be able to account for specificity[71]. The c-Abl:imatinib crystal structure, however, showed that the kinase domain adopted a different architecture that was more reminiscent of the inactive state of the enzyme. In this state, the “activation loop” of the kinase folds into the active site cleft, occluding access of substrate to the catalytic site and often even blocks the substrate binding site[72]. In the c-Abl:imatinib structure, it appeared that imatinib binds to the activation loop in its natural, inactive state and interacted with residues at the base of the activation loop which are poorly conserved even in closely related kinases. Thus, by forcing the kinase into its inactive state, additional residues that are poorly conserved across the kinome became accessible and could engender specificity[70,73].

The connection between the ability of imatinib to block the tyrosine kinase activity and the ability of imatinib to stop growth of BCR/Abl positive cells has also been elucidated in part. BCR/Abl is very large protein and serves as a node for many different cellular signaling programs. Despite this, major mechanisms of BCR/Abl-induced oncogenesis have been described since the first reports of imatinib were published. By activating the signal transducer and activator of transcription 5 protein (STAT5)[74], BCR/Abl causes cells to upregulate anti-apoptotic pathways and therefore avoid programed cell death[75]. Imatinib counteracts this activity. In a second key pathway, BCR/Abl also suppresses p27, a key cell cycle regulator, to avoid cell cycle arrest and maintain constant cell growth[76]. The details of BCR/Abl ability to promote leukemia are still being uncovered today, and this discussion will continue shortly.

These studies on the potent and selective CML-cell killing ability of imatinib led to clinical trials and its approval by the FDA in 2001[77–79]. Imatinib is justly considered a giant victory for modern drug discovery: chronic myelogenous leukemia was transformed from a disease with a median 5-year survival rate to a chronic yet manageable disease in which the median survival rate approaches that of the general population[80].

The clinical success of imatinib has heralded a new and profoundly effective mindset towards cancer drug discovery, moving away from generally cytotoxic agents towards those which target the specific molecular cause of the disease. Chief among cancer targets are protein kinases, "the major drug targets of the 21st century[8]." In a 2004 census of human cancer genes, "27% cancer genes…encode protein-kinase domains, compared with the 6.3 that would be expected in a random selection of the same number of genes from the complete set of human genes"[81]. Immense pharmaceutical effort is expended towards further defining the role of protein kinases in disease and the development of selective kinase inhibitors. Since the approval of imatinib in 2001, hundreds of kinases have been implicated in cancer and other diseases, and dozens of kinase inhibitors have been approved by the FDA to combat these diseases.

Section 1.2: The Limitations of the Modern "Kinase-Only" Paradigm

This historical review has been far from exhaustive but brings us sufficiently close to a 2018-level of knowledge. While imatinib perhaps remains the most well-known kinase inhibitor-turned therapeutic, the selectivity and potency that were revolutionary at the time are now commonplace or even subpar. Crystal structure of kinases are widespread, and the understanding of kinase autoregulation and regulatory networks has expanded and will continue to do so. With dozens of FDA-approved drugs and more on the way, the therapeutic benefit of understanding kinase biology is having far-reaching effects not only in cancer but also throughout other areas of medicine.

The intention of this review, however, has been to lay the groundwork for a "kinase-only" paradigm. *Paradigm* is a word used often in scientific talks and papers, but rarely is it used rigorously. However, paradigm has a rich philosophical meaning, expounded first and most notably by Thomas Kuhn in his 1961 The Structure of Scientific Revolutions. Kuhn was a sociologist by training and preferred a definition of science that appreciated the irrational and more subjective aspects of the humans that practiced it. As such, he stated that scientists operate under *paradigms*, or schools of thought in which assumptions lay the groundwork not only for the problem solving of "normal science" but also for what constitutes "normal science." Great periods of scientific upheaval, or revolutions, are thankfully quite rare and require the slow accumulation of anomalies that fail to be incorporated into the paradigm.

Since the initial discovery of reversible phosphorylation as a means of controlling protein activity[19] through the modern pharmaceutical effort to target kinases with small molecules[82], a prevailing assumption has been that kinases are just and only that: enzymes that transfer phosphate groups to change the activity of another protein. This assumption is based on very powerful exemplars and narratives which have been explored above.

This assumption, that a protein kinase only transfers phosphate groups, approaches the level of a paradigm in that it dictates the types of questions we ask about kinases. For example, language typical of scientific papers equates "inhibiting the kinase activity" with "inhibiting the entire protein" and leaves no room for other functions of that protein. Furthermore, knocking down the entire kinase-domain-containing protein can often be equated with inhibiting the kinase activity of that protein. These examples, and more, are very common in the literature.

While immense therapeutic value has been born from this paradigm, major limitations are inherent to it. Two examples highlight these limitations. The first has already been introduced and is the fusion oncoprotein BCR/Abl. Despite transforming the outcome of CML, inhibition of BCR/Abl is rarely curative. Kinase-independent roles of BCR/Abl are likely the culprit for this. The second example is the pseudokinase ROR2. Lacking catalytic activity, the "kinase-only" paradigm might preclude this protein's role in disease or choice as a therapeutic target. However, inhibition of this protein's function is unlikely with a traditional inhibitor strategy but would likely have beneficial therapeutic outcomes in a variety of cancers.

Section 1.3: One Domain is Not Enough: Non-Kinase Functions of BCR/Abl

BCR/Abl is a large protein with many different domains. The kinase activity of BCR/Abl is owed to the kinase domain of c-Abl which loses regulatory mechanisms upon fusion with BCR. Two biochemical reasons summarize the general thinking for why the c-Abl kinase activity is hyperactivated in BCR/Abl. First, the N-terminal inhibitory mechanisms of c-Abl are lost because of chromosomal translocation. Whereas c-Abl is tightly regulated by myristylation and auto-inhibitory clamps, these domains are lost in BCR/Abl[35]. Second, the N-terminus of BCR encodes a coiled-coil domain which causes BCR (and by translocation, BCR/Abl) to oligomerize and active the kinase activity[83,84]. Heterodimerization of c-Abl by other means can have a similar effect. A final postulated mechanism for BCR/Abl hyperactivity involves the BCR portion recruiting novel integral signaling proteins into close proximity of the c-Abl kinase domain. This expands the substrate repertoire of c-Abl[85]. Little experimental evidence is available for this last hypothesis.

That BCR increases the activity of c-Abl is well-documented. The idea, however, that BCR only functions to increase the activity of c-Abl is widespread but runs contrary to

significant bodies of research. Here, non-kinase roles of BCR/Abl are discussed as well as their potential role in preventing the cure of CML by traditional kinase inhibitors.

Leukemic Stem Cells are Resistant to BCR/Abl Kinase Inhibition

The existence of leukemic stem cells (LSCs) resistant to imatinib has been a phenomena appreciated since the approval of imatinib by the FDA[86]. Although imatinib has transformed the treatment of CML, patients are required to maintain treatment for their entire lives. Discontinuation of treatment, even in patients in very deep molecular remission, leads to relapse and progression of the disease within six months in almost half of patients[87]. Because of the possibility of mutations arising in this stem cell fraction and causing a relapse even with treatment, as well as the burden of lifelong treatment, new treatments should be investigated to clear these LSCs[88,89].

The underlying mechanisms that drive survival of LSCs is unknown. Initially, it was thought that the BCR/Abl kinase activity in these cells was inefficiently inhibited, either because of enhanced drug efflux mechanisms or poor distribution of the kinase inhibitor to the bone marrow microenvironment housing the LSCs. More recent studies, however, have shown that BCR/Abl kinase activity is almost completely inhibited in these cells, and yet the LSCs are able to survive[90,91].

The most obvious culprit here would be functions disconnected from the BCR/Abl oncogene entirely. This is a theory shared by many research groups[88]. Cancer is rarely driven or maintained by only one oncogenic lesion, even though BCR/Abl is the most well-known example of cancer treatments focused on one particular lesion. As such, several groups have focused on eroding the LSC population through alternate means such as the use of PPARγ antagonists which transcriptionally reduce levels of total STAT5, leading to LSC exit from quiescence and programed cell death[92].

Regardless of these successes, BCR/Abl kinase-independent roles in LSC survival may provide an alternative strategy. What evidence, however, is there that kinase-independent roles of BCR/Abl are in play? A first circumstantial line of evidence will focus on the differences in biochemistry and cell biology between different c-Abl fusion proteins. The second line of evidence is more direct and involves the use of imatinib-treated transplantation models for the disease.

c-Abl is not only found as fusions to BCR/Abl, but a different and more complicated translocation between the 9th, 12th, and 14th chromosomes leads to fusion of the N-terminal portion of the Tel gene to the exact same residues of c-Abl as in BCR/Abl. The Tel gene also encodes an oligomerization domain which causes the hyperactivation of the c-Abl kinase activity: most substrates are shared by both Tel/Abl and BCR/Abl[93–95]. If the kinase domain of c-Abl were the only important player, then one might expect similar disease to be causes by these two fusion proteins. The leukemia induced by these two proteins are similar, but Tel/Abl is completely unable to recapitulate the LSC phenotype and repopulate the disease in secondary recipients[96].

An even more nuanced scenario is observed with the different translocations of BCR/Abl which results in fusion proteins of different molecular weights. p210 is a fusion of residues 1-927 of BCR while p185 only contains residues 1-426. Both forms have the exact same portion of c-Abl as Tel/Abl (i.e. residues 26-1149). p210 is present in ~95% of all cases of CML which originate from a multipotent progenitor cell, whereas p185 is found in ~25% of cases of acute lymphoblastic leukemia which originates from a committed pro-B cell[97]. These phenotypic differences have been noted since the early 90s[62,98,99].

Why such phenotypic differences between p185 and p210? The 501-amino acid difference between the two forms encodes a Dbl-homology (DH) and Plekstrin-homology domains, and certain mutational and biochemical analyses have traced the differences in

disease induced by p185 and p210 to just the DH domain and a Rho guanine nucleotide exchange factor activity therein[100,101]. Recently, two groups independently looked at the interactomes of and phosphoproteomic-changes induced by the different versions[102,103]. One of these studies highlighted how p210, but not p185, was able to increase global expression of several important hematopoietic markers. This indicates that regions outside of the c-Abl kinase activity are involved in promoting survival of leukemic stem cells.

Although looking into the differences between the different c-Abl fusion proteins provides some circumstantial evidence that there are interesting functions outside the c-Abl kinase activity, several reports have provided more direct evidence. Importantly, in a stem cell transplantation model, certain transcriptional changes were induced by BCR/Abl expression that could not be rescued by inhibition of the tyrosine kinase activity by imatinib[104,105]. Counteracting these changes through orthogonal means (e.g. overexpression of the repressed gene) inhibited the ability of leukemic stem cells to engraft and establish the disease in secondary recipients. Furthermore, a variety of other reports have implicated important survival and metabolic signaling pathways as being activated in leukemic stem cells[88,89].

In summary, the mechanisms for the survival of leukemic stem cells in chronic myelogenous leukemia is of therapeutic interest but remain unknown. BCR/Abl-independent and BCR/Abl non-kinase roles have both been implicated in the survival of these cells, but further research is required to distinguish between these two possibilities. A tool to rapidly and potently reduce levels of BCR/Abl, rather than just its kinase activity, would aid in these studies, and options for that will be discussed below.

Section 1.4: Not Even One Domain: Pseudokinases and “Undruggable” Proteins

The preceding discussion focused on non-kinase roles of the oncoprotein BCR/Abl; here a perhaps more obvious class of proteins that also require further study is discussed.

These proteins may provide new opportunities for therapeutic intervention. While the human kinome consist of 528 separate genes, about 10% of these genes lack one or more of the conserved motifs that are predicted to be necessary for catalytic activity[53]. Some pseudokinases have been implicated in disease[106].

One such pseudokinase is Receptor tyrosine kinase Orphan Receptor 2 (ROR2) and will serve as an archetype for this discussion on pseudokinases, their role in disease, and biochemical mechanism of action. ROR2 was first described in 2000 by mutations associated with Robinow and Brachydactyl type B syndrome, both developmental defects that leave afflicted individuals with stunted growth, primarily in their hands[107–109]. As ROR2 is not expressed in adults, it was initially thought to only have development roles[110].

More recent studies have implicated ROR2 in a variety of cancers[111]. Examples include promoting metastasis in melanoma, cell viability in osteosarcoma, and cell proliferation in lung adenocarcinoma[112–114]. The related ROR1 also has enhanced expression in a variety of leukemias and other cancers[115,116]. However, simply overexpression of a gene in a particular cancer cannot be assumed to be causative of these cancers and so causative relationships with known signaling programs and ROR2 must be investigated.

The physiological role of ROR2 is a concern of much research. ROR2 participates in Wnt signaling. In 2003, based on the homology between the extracellular domain of ROR2 and Frizzled proteins, ROR2 was shown to bind Wnt5a and activate non-canonical Wnt signaling[117]. Follow-up studies found that ROR2 is upregulated downstream of Wnt5a and associates with and is phosphorylated by GSK-3β upon stimulation with Wnt5a[118–120]. Other studies indicated that ROR2 facilitates canonical Wnt signaling as well and its role in both pathways is generally appreciated[121,122].

Early studies indicated that tyrosine kinase activity of ROR2 was required for signaling, but all of these studies have been indirect[123]. For example, mutations of residues which abolish kinase activity in other related proteins inhibited ROR2's ability to transmit Wnt5a stimulation. These mutations, however, are in the cleft of the ROR2 kinase domain and would likely change the conformation of ROR2.

Other studies also indicate that ROR2 likely functions without kinase activity. Most importantly, the crystal structure of apo-ROR2 shows an atypical autoinhibitory mode, in which the activation loop is swung into the ATP-binding site and stabilized by a variety of novel contacts[124]. Furthermore, a relatively conserved tyrosine residue among different receptor tyrosine kinases (Tyr555 in ROR2) is swung into the active site in an uncommon manner. Drastic rearrangements of the protein's structure would be required to allow for ATP binding, and unpublished studies from multiple labs indicate that ROR2 does not bind ATP[125]. Most recent publications accept that ROR2 likely functions in the absence of kinase activity.

Thus, the mechanism of ROR2's action is largely unknown, but examples from other kinases shed some light on possibilities. Within the class pseudokinase, there are several mechanisms for transmitting signals. For example, KSR is a scaffolding protein which facilitates the BRAF-MEK-ERK phosphorylation cascade by binding all of them simultaneously. Furthermore, the phosphorylation of KSR, or its binding to small molecules which induce an active-like conformation, allosterically activating BRAF kinase activity[126–128].

Based on the example of KSR, one obvious line of research is to ask why ROR2 adopts such a strange, autoinhibited structure? Could phosphorylation on the activation loop as well as Tyr555 allow ROR2 to adopt a more active-like conformation? It should be noted that the pseudokinase-classifying mutation in ROR2 (GxGxxG -> GxDxxG) would

likely occlude ATP binding *even* in an active-like conformation. However, what might the consequences of such an active conformation be? Unfortunately, no obvious biochemical answers to this question are available.

Therapeutic opportunities for Pseudokinases

What therapeutic options exist for pseudokinases? First, it must be admitted that the genuine classification of most of these proteins *as pseudokinases* is dubious, at best. Choice of model substrate and contaminating kinases in purified fractions are two common issues which plague many publications. If a pseudokinase were to be shown to have genuine kinase activity, then its therapeutic targeting by traditional small molecules would be possible and would follow the general pattern set forth for genuine kinases. The "pseudokinase" integrin linked kinase is one such example[129].

For pseudokinases in which catalytic activity is not the main function of the protein, the serendipitous discovery of allosteric inhibitors may be a path towards therapeutic intervention. KSR is one example of this. Upon discovery of small molecules that could stabilize the active state of the protein, the Dar group set out to identify molecules which stabilized the *inactive* state[130]. These ligands bind with reasonable selectivity (though there's no reason to suspect that more selective ligands couldn't be discovered) and antagonize the function of the protein. This strategy for targeting KSR could very well move towards clinical application.

While some pseudokinases may be druggable through this strategy, the above examples do not lay a clear path towards a generalizable plan for the therapeutic targeting of pseudokinases. An alternative path could instead focus on degradation of these pseudokinases, rather than inhibition. If a strategy could be developed to decrease levels of the entire protein, then one would not need to worry if the protein is in an active

conformation or not. Furthermore, such a strategy could be extended to other undruggable proteins (KRas, c-Myc, etc.) which are the focus of many drug discovery effforts[131].

Section 1.5: Oligonucleotide Knockdown Techniques as an Alternate Strategy

As described above, traditional occupancy-based inhibitors have inherent and technical limitations which leave many protein targets "undruggable." BCR/Abl non-kinase roles and pseudokinases in general would be difficult to target via small molecule inhibitors. Reducing levels of the target protein would circumvent these issues. The following sections review several techniques for reducing protein levels that can aid in the understanding and therapeutic targeting of these undruggable functions. The first focus is on research tools that are unlikely to provide therapeutic benefit. These include genetic strategies such as RNA interference (RNAi), antisense oligonucleotides, and gene-editing techniques as well as technologies which require an orthogonal fusion protein to degrade the protein of interest. These tools have been widely adopted in the research community but are unlikely to advance into therapeutics. Second, "all-small-molecule" technologies that do not require genetic manipulation to degrade the protein of interest will be introduced. This area is inclusive of selective estrogen receptor downregulators (SERDs) and compounds that hijack quality control machinery in order to degrade non-natural substrates (immunomodulatory imide drugs, hydrophobic tagging, and proteolysis targeting chimera).

The oldest and most widely-used technique for altering the expression levels of a protein of interest has been the pre-translational modification of the gene product at the DNA or RNA level. Historically, this technique was used even before polymerase chain reaction (PCR) or solid phase oligonucleotide synthesis were adopted and took the form of mutagenizing the DNA of an organism, isolating a particular phenotype and then cross-referencing that phenotype with a particular genetic change. With an enhanced

understanding of how biological systems process and maintain their genetic material, intentional, specific, and rapid manipulations are now possible. Virtually all modern biomedical research laboratories use some or all of the following techniques: RNA interference, antisense oligonucleotides, or genetic engineering techniques.

RNA interference is the use of small, double-stranded RNA molecules to reprogram an endogenous machinery to degrade the mRNA of a gene of interest. The Nobel Prize in Physiology and Medicine in 2006 was given to Andrew Fire and Craig Mello for their discovery that certain mRNA molecules were expressed but not translated in the nematode *C. elegans*[132]. They found that a double-stranded RNA molecule was capable of potently interfering with the expression of the targeted gene and that the interference only required a few molecules of RNA per cell. This indicated that perhaps a catalytic mechanism was in play[133]. The mechanism for this involves processing of the double stranded RNA into a single-stranded, targeting RNA which is loaded into the Argonaute protein complexes that then recognizes the target mRNA and degrades it[134,135]. Tools are available to aid the researcher in designing RNAi molecules to selectively and potently decrease expression levels of their gene of interest[136], and the interfering molecules can be stably introduced into cellular genomes by the use of short hairpin RNA (shRNA) packaged into lentivirus[137].

In contrast to RNAi, antisense oligonucleotides (ASOs) are designed to bind to single stranded mRNA and block the translation machinery that only recognize single stranded RNA. This technique has been used since the mid-1980s and was used widely to identify various oncogenes as being critical for transformation (including BCR/Abl)[64,138,139]. Although not commonly used in mammalian cells as a research tool (likely because of the ease and potency of RNAi), ASO is highly effective in the zebrafish model. Another benefit of ASO is their ability to not only repress translation, but also, for

example, block a particular exon:intron junction to manipulate the processing of a particular disease-causing gene. This technique, referred to as exon skipping, has resulted in a FDA-approved drug for Duchenne's muscular dystrophy[140].

Directly modifying or engineering the genome provides an irreversible platform for reducing gene levels in organisms. A major downside of both RNAi and ASO is that complete knockdown of the gene of interest is often incomplete, and so data generated through these techniques are tainted by the remaining, albeit low, levels of expression. In contrast to the two knockdown strategies presented above, knock out strategies eliminate genomic copies of the gene of interest and are irreversible. Modern day approaches to accomplish this include zinc finger nucleases and transcription activator-like effector nucleases: these two techniques are likely to be completely replaced with the clustered regularly interspaced short palindromic repeat (CRISPR) system[141]. CRISPR was first identified as a bacterial defense system against viral invasion[142], CRISPR enables the rapid design of a specific cas9-based nuclease to nick DNA sites virtually anywhere within the genome[143–145]. The targeting sequence employed is termed a small guide RNA (sgRNA) which is loaded into the Cas9 nuclease. Upon recognition of the target sequence, the nuclease introduces a single-stranded break, or nick, into the genome, which is repaired through endogenous pathways and typically results in a frame shift which disrupts expression of the gene of interest. If the gene is to be modified, rather than knocked-out, then repair templates can be used to insert DNA encoding affinity tags, fluorescent labels, or the many other recombinant technologies available today[146].

As research tools, these nucleic-acid based technologies have been invaluable in elucidating the functions of a gene of interest. A separate use, forward genetic screens, is a powerful technique to uncover the molecular players in complex phenotypes. A library of lentivirus containing shRNA or sgRNA towards thousands of genes can be designed

and synthesized[147–149]. The library is then delivered to a population of cultured cells such that each cell receives at most one RNA molecule as well as a barcode sequence linked to the gene to be knocked down. By applying a selective pressure (e.g. tumor metastasis) and using next generation sequencing methods to determine relative changes in the amount of each barcode before and after selection, important genes or clusters of genes can be identified whose knockdown/knockout is critical for the phenotype being selected for. Examples include CRISPR screens to uncover genes involved in tumor metastastis[150] or in salamander limb regeneration[151].

A second powerful technique can be used especially in the context of noncatalytic roles of protein kinases, or more generally for multidomain proteins. After knockdown by RNAi methodologies, an orthogonal gene can be reintroduced into the cell that encodes the same protein but is resistant to the RNAi through manipulation of the wobble base on several codons. As is, this provides a powerful validation that the phenotype observed is indeed due to knockdown of the predicted protein. The reintroduced gene can also be modified so that kinase activity would be lacking, for example. If the kinase-dead version of the gene product rescues an observed knockdown phenotype, then the kinase is likely performing some non-catalytic role in the cell[11]. This technique has not been used to study BCR/Abl in LSCs, likely because these cells are rare and do not persist outside the animal for long.

Genetic Knockdown Methodologies in the Clinic

While these genetic knockdown strategies have had lasting impacts on basic research, success stories in the clinic have been limited. While some nucleic acid-based technologies have been approved by the FDA, these approvals are questionable and don't display the efficacy one might hope[140]. Other preclinical tests have been equally underwhelming. An RNAi-based strategy targeting the amyloid-producing protein

transthyretin showed good safety and knockdown (>80%) of the protein of interest for amyloidosis[152]. Transthyretin is produced in the liver, which make it an ideal target for nucleic-acid based therapies because these molecules rarely survive first pass metabolism and accumulate heavily in the liver[153]. Accordingly, in another study looking at the important cancer targets kinesin spindle protein and vascular epithelial growth factor receptor, there was little decrease in the amount of the targeted mRNA in tumor samples, again indicating that delivery was an issue[154].

Overall, the clinical outlook for these classes of drugs still require extensive development. With delivery being a chief concern, more research must be done in enhanced packaging or nanomaterial mechanisms for delivering the drugs[155]. Regardless, the efficacy and future of nucleic acid-based therapeutics is in question[156–158].

Section 1.6: Fusion Protein Technologies for Inducible Protein Knockdown

While oligonucleotide-based knockdown has the benefit of being generalizable (any gene that uses DNA can likely be targeted), these techniques fall short in some areas that small molecules are very effective. Here, several small molecule tools that induce protein knockdown are reviewed. Two general trends will be apparent. First, small molecules have very fast mechanisms of action as opposed to RNAi or CRISPR-based techniques. Oligonucleotide-based techniques, at their fastest, require the protein of interest to be depleted through endogenous degradation pathways, whereas the action of a small molecule can act on minute timescales. The second trend in favor of small molecules is their drug likeness. Small molecules are more easily used in animal models and, typically through considerable effort, to treat human diseases.

I will only briefly summarize several techniques that require genetic engineering to introduce a domain into the protein of interest that allows for small molecule induced degradation. This topic has been reviewed elsewhere[159]. A widely used technique, SHLD,

utilizes a fusion protein that is destabilized unless bound by a ligand. Removal of the ligand causes destabilization of the protein[160,161]. A second technique requires fusion of the protein of interest to the auxin-inducible degron domain and overexpression of a corresponding E3 ligase. In this context, treatment with the inexpensive auxin Indole-3-Acetic Acid allow for rapid depletion of the protein. Researchers have recently used CRISPR/Cas9 to introduce the degron fusion into the genomic copy of the gene of interest, allowing for rapid depletion of the protein[162,163]. A final technique uses fusion proteins and matching small molecules which recruits the protein directly to the proteasome[164] or to E3 ligases[165,166]. Overall, these techniques combine the utility of small molecules with the generalizable features of genetic engineering.

Section 1.7: Serendipitous Discovery of Small Molecule Degraders

The previous technologies are useful as research tools and can possibly validate degradation as a strategy for proteins such as BCR/Abl or ROR2. The preceding paragraphs discuss small molecule knockdown strategies that don't require genetic manipulation. The first two, selective estrogen receptor degrader (SERDs) and immunomodulatory imide drugs (IMiDs), cause degradation of their respective protein targets but do so through rather surprising means. As such, these two strategies are sadly not generalizable.

SERDs were among the first class of compounds identified having the added benefit of inducing degradation of their target protein. ERα is a well-known oncogenic driver for metastatic breast cancer[167]. While ERα modulators have been in the clinic since Tamoxifen was first approved in 1970, spurious ERα *activation* in various tissues led to a need for pure anti-estrogens. Fulvestrant (ICI 182,780 or Faslodex™), was first described in the early 90s as a "pure antagonist" capable of overcoming these partial agonistic issues. Its therapeutic mechanism was soon attributed to its ability to decrease

intracellular ERα levels[168,169], but despite approval by the FDA in 2002, Fulvestrant suffers from poor bioavailability, and is administered by monthly intramuscular injection. New, bioavailable SERDs are entering clinical trials[170,171].

While SERDs may be oldest application of induced-protein degradation, the mechanism by which ER degradation is achieved is not well understood. It is thought that upon binding, a SERD induces conformational changes of the protein, exposing novel hydrophobic motifs that can be recognized by chaperones and trigger degradation[172,173].

Immunomodulatory Imide Drugs

Thalidomide and its derivatives have a storied history due to the initial excitement of their anti-nausea properties being replaced by the horror of their awful teratogenic properties. However, in the mid-2000s, thalidomide, pomalidomide, and lenalidomide were identified as potent agents against a variety of leukemias. In 2010, a major step towards understanding IMiD action was made upon identification of Cereblon (CRBN) as a major target of thalidomide teratogenicity. CRBN is a substrate adapter for the Cullin RING Ligase (CRL) 4a ubiquitin ligase complex, and it was later found that IMiD compounds actually cause the degradation of various target proteins with little structural similarities[174–177].

From a biochemical standpoint, recent studies have also led to an understanding of how IMiDs recruit these new substrates to Cereblon. Crystal structures of the Cereblon-IMiD complex[178,179] and the ternary complex between Cereblon, lenalidomide, and CK1α[180] or GSPT1[181] have confirmed that the IMiD glutarimide moiety binds to a hydrophobic cavity in Cereblon, while the phthalimide ring is free to form contacts with the neosubstrates. The phthalimide ring, in combination with local residues from Cereblon, create a remodeled surface which binds to the substrate proteins. Remarkably, despite a

lack of sequence homology, the three-dimensional structure of the recruitment motif is quite similar between the different neosubstrates. Given the success of novel IMiD analogs to recruit novel neosubstrates, it is likely that many more target proteins can be recruited with this type of strategy. Recently, anticancer sulfonamide compounds were also found to hijack the $CRL4a^{DCAF15}$ complex to induce degradation of neosubstrates[182,183].

Section 1.8: Rational Design of degrading compounds

Whereas SERDs and IMiDs induce degradation of important therapeutic targets, these examples do not provide a clear framework towards a strategy that could be applied to any protein target. This section discusses past efforts towards such a strategy. The general trend is the use of heterobifunctional small molecules. One part of the molecule binds to the protein target (a targeting warhead), while the second either induces misfolding of the protein or recruits it to endogenous degradation machinery.

Hydrophobic Tagging

Hydrophobic tagging was first introduced as a concept in the Crews' lab in 2011[184,185] and a related strategy from the Hedstrom group[186]. Given the clinical success of fulvestrant, which mediates ERα degradation by exposing a hydrophobic patch on the surface of the protein, we hypothesized that a ligand for a protein of interest could be similarly functionalized into a "hydrophobic tag" to induce a partially unfolded state. In this way, a "tagged" protein would partially unfold and then be recognized by the same cellular quality control that recognizes and discards terminally misfolded or unfolded proteins. This strategy has been employed to degrade endogenous proteins like the pseudokinase Her3[187] and the androgen receptor[188] without the need for genetic engineering. However, these compounds typically lack potency, only inducing degradation in micromolar

concentrations and only modestly decreasing protein levels. Furthermore, highly stable proteins may be completely resistant to this strategy.

Previous Generations of PROTACs

As an alternate strategy, recruitment of the protein of interest directly to the ubiquitination machinery could induce degradation. Ubiquitination is an enzymatic process in which E1, E2, and E3 enzymes coordinate to activate, conjugate, and ligate the small protein ubiquitin to proteins. Chains of ubiquitin can be added to the protein, and the chain length and topology dictates a variety of possible cellular outcomes, ranging from activating immunological signaling programs to, apropos to this discussion, degradation[189,190]. Since its first description in the 1970s and 80s[191–193], the known complexity of the ubiquitin system has grown dramatically and new surprises are constantly being uncovered[194,195].

Since 2001, our lab has developed the Proteolysis Targeting Chimera (PROTAC) technology to recruit protein to the ubiquitin proteasome system. PROTACs are heterobifunctional molecules that have discrete binding moieties for the substrate of interest and for an E3 ligase connected by a chemical linker. The first PROTAC, developed in collaboration with the Deshaies group at CalTech[196] consisted of the natural product ovalicin and a peptidic ligand for the CRL1 F-box protein βTRCP. This initial PROTAC demonstrated ternary complex (substrate-PROTAC-E3 Ligase) formation, ubiquitination activity, and limited degradation of its target protein in xenopus extracts[197].

Since these initial studies, many publications have explored both the limitations and potential of the PROTAC technology and several key lessons have been learned. First, different E3 ligases are able of being hijacked by PROTACs for selective protein degradation. β-TRCP, MDM2[198], CIAP[199], and VHL[200] have all been employed for induced protein ubiquitination using a heterobifunctional dimer approach. Second, small molecules

have been employed for either binding moiety. The MDM2 inhibitor Nutlin[198] or the IAP ligand bestatin[201–203] have both been used in PROTACs to engage their cognate E3 ligases. Likewise, small molecules have also been used as substrate-targeting ligands, e.g., small molecule agonists of the retinoic acid receptor[199], Fumagillin and ovalicin for Met-AP2 [204]. Lastly, while not technically a PROTAC, other bifunctional peptides have been used to direct POIs to the lysosome for degradation [205].

Third, and disappointingly, these compounds have been very limited in their potency. Most of these early-generation compounds are, at best, active in the low-micromolar range with only partial degradation of the POI. Since these compounds are large and charged (or at least highly hydrophilic), cell-permeability is a key contributor to this lack of potency, though the low-affinity of these peptides for their targets is also likely to be contributing factor.

Several key advances have taken these peptide studies and enabled the potent and selective degradation of target proteins using the PROTAC approach. These advances are the focus of the rest of this dissertation. These “next generation PROTACs” pave a path to target the BCR/Abl non-kinase roles and pseudokinases outlined in this chapter. In so doing, this tool provides the possibility to rewrite the “kinase-only” paradigm and study and target additional functions of these interesting enzymes.

Chapter 2

Small Molecule PROTACs:

Potent and Catalytic Degradation of Protein Targets

Preface

The work done in this chapter was a collaborative effort with GlaxoSmithKline and Arvinas. I did not perform all of the experiment in this chapter. The RIPK2 and ERRα PROTACs were synthesized by Drs. Ian Smith (GSK) and Eunwha Ko (Yale), respectively. The proteomic experiments were performed under the supervision of Marcus Bantscheff at Cellzome. The RIPK2 western blots were performed by Alina Mares at GlaxoSmithKline. The ERRα degradation experiments in Figure 2.10 (both in MCF7 cells and in mice) were performed by Dr. John Flanigan at Arvinas. Most, but not all, of this work has been published:

Bondeson, DP, Mares, A, Smith, IED, et al. (2015). Catalytic *in vivo* protein knockdown by small-molecule PROTACs. Nature Chemical Biology. *11*, 611–617.

The previous chapter outlined benefits and limitations of modern therapeutic strategies. Most drug discovery efforts are focused on inhibiting protein function, but this effort ignores additional functions of proteins and leaves vast swathes of the proteome “undruggable.” Possible strategies to overcome these limitations were also discussed: proteolysis targeting chimera, or PROTAC, have been limited in potency but conceptually offer a general strategy for inducing degradation of any protein for which a ligand can be developed. This chapter begins by discussing technological advances that enable potent protein knockdown. Potent PROTACs are then introduced, first for the protein kinase RIPK2. These PROTACs have a clearly defined mechanism of action, catalytically causing the ubiquitination and degradation of RIPK2. Next, a different class of proteins is targeted with PROTACs: nuclear hormone receptors via the prototype ERRα. The chapter then closes by highlighting the many examples of PROTACs that have recently been published and outlines gaps in the understanding and application of PROTACs.

Section 2.1: A Small Molecule Ligand for von Hippel Lindau (VHL)

Having outlined the advantages and limitations of “first generation” PROTAC molecules, recent work improving the potency and scope of this technology can now be discussed. An understanding in two advances in the design of PROTACs are first required.

The first advance is the discovery of small molecules which bind to the E3 ligase VHL with high affinity and will be discussed first. A second advance is a conceptual understanding of “linkerology”, or the importance of the chemical linker between the two recruiting elements of a PROTAC. While most earlier generation PROTACs simply connected the two recruiting elements with a synthetically tractable spacer, it is now appreciated that this spacer is absolutely crucial to the activity of PROTAC molecules. The reasons why this is will be discussed more in chapter three.

To overcome the limitations of earlier, peptide-based PROTAC molecules, the Crews' research group undertook the development of a high-affinity, small molecule ligand for the E3 ligase von hippel lindau (VHL)[197,200]. VHL is a member of a Cullin 2-RING E3 ligase complex and is the substrate adapter which recruits HIF-1α to the complex for ubiquitination and degradation[206–208]. Most intriguingly, the HIF-1α protein only binds to VHL when HIF-1α is hydroxylated on several proline residues[209–211]. Structural analysis of the VHL:HIF-1α interaction reveal that the hydroxy proline motif binds in a deep cavity in the VHL structure, that this motif stabilizes a network of hydrogen bonds, and that most nearby residues are dispensable for binding[212]. In fact, a corresponding peptide simply lacking the hydroxylation mark has roughly a 1,000-fold loss in binding affinity compared to the high affinity, hydroxylated version[212].

Based on these observations, it would be expected that small molecules mimicking the VHL:HIF-1α interaction could be designed and synthesized. Using a combination of *in silico* screening, NMR fragment screening, and structure-guided design, a series of VHL ligands with high affinity have been developed[213–217]. These compounds continue to be optimized, with the most potent inhibitors having a dissociation constant (K_D) of less than 100 nM and showing VHL inhibition of HIF-1α degradation in cell culture[217]. Compound **1** (Figure 1.1A) was developed in our lab and binds with a K_D of 185 nM. The crystal structure of Compound **1** bound to VHL shows that the hydroxy-proline moiety of the ligand mimics the HIF-1α mode of binding (Figure 1.1B). The structure, in combination with the plethora of structure-activity relationships, also reveal two solvent-exposed areas of the VHL ligand that could be amenable to attaching a linker and target protein recruiting element without compromising binding of the compound to VHL. These two sites are colloquially termed the left-hand and right-hand attachment points and have both been incorporated into PROTAC molecules (see the HaloPROTACs[166] for an example).

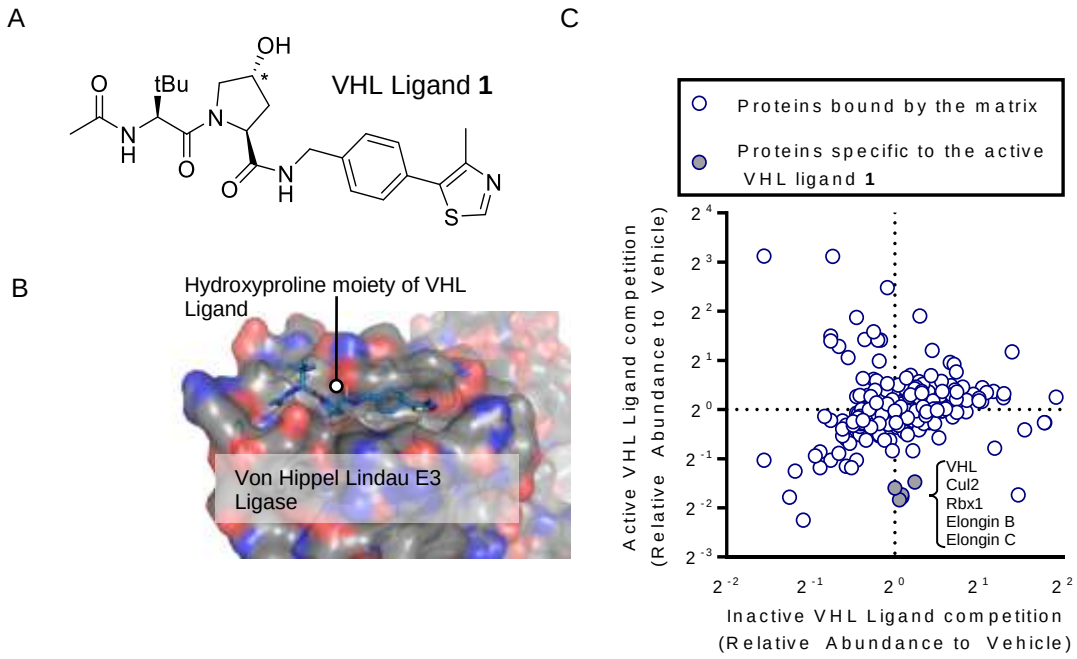

Figure 2.1 A small molecule ligand for the E3 ligase VHL

(A) Compound 1, a hydroxyproline-based ligand for VHL with an affinity of 185 nM. The asterisk indicates the hydroxyproline stereocenter that, when inverted, abolishes binding. (B) Crystal structure of compound 1 bound to VHL (PDB code 4W9H). The ligand binds in a shallow groove along the surface of VHL, with multiple possible linker attachment points. (C) Chemoproteomic approach to assess VHL ligand selectivity. A derivative of compound **1** was immobilized on sepharose, and a whole cell extract of THP-1 cells were incubated after competition with either compound **1** or the inactive control with an inverted hydroxyproline motif. On the Y-axis, the difference between vehicle and Compound **1** control treatment is plotted, while the X-axis shows protein competed with the inactive control compound.

To assess the utility of this VHL ligand we first immobilized the ligand and assessed which proteins from a cellular lysate were precipitated by the ligand. As seen in Figure 1.1C, VHL was efficiently enriched in non-competed samples incubated with the immobilized ligand. Competition with free VHL ligand ruled out the possibility that this effect was simply due to non-specific interactions with the linker or matrix. Along with VHL, the only other proteins that were enriched were other members of an active VHL complex: Elongins B/C, Cullin 2, and Rbx1. This indicates that the VHL ligand is capable of interacting with ubiquitination-competent VHL in a complex cellular extract.

With a high-affinity VHL ligand in hand, we next sought to use this ligand in a potent "all small molecule PROTAC." To validate the utility and scope of this technology, we choose two different classes of substrates: protein kinases and nuclear hormone receptors. Below are presented two PROTACs with unprecedented potency for the protein kinase RIPK2 and the nuclear hormone receptor ERRα.

Section 2.2: The design of PROTACs targeting RIPK2

As discussed in chapter one, protein kinases are a class of proteins with immense therapeutic value, and an area where potent protein knockdown could possibly subvert more functions of protein kinases (see especially chapter four) as well as overcome mutations that confer resistance to typical ATP-competitive inhibitors. Therefore, we developed a PROTAC to the serine/threonine kinase RIPK2.

RIPK2 is a key mediator in both the innate and adaptive immune responses. It mediates NOTCH signaling, and has also been implicated in cancer[218]. RIPK2 was chosen as a model substrate due to the presence of a highly selective and potent inhibitor (Figure 2.2A). The crystal structure of the RIPK2 ligand revealed a solvent-accessible site from which a linker could be built (Figure 2.2B). This RIPK2 inhibitor developed by GSK binds RIPK2 with a K_D of 500 pM. Even the closely related RIPK3 is bound with a K_D of 200 nM,

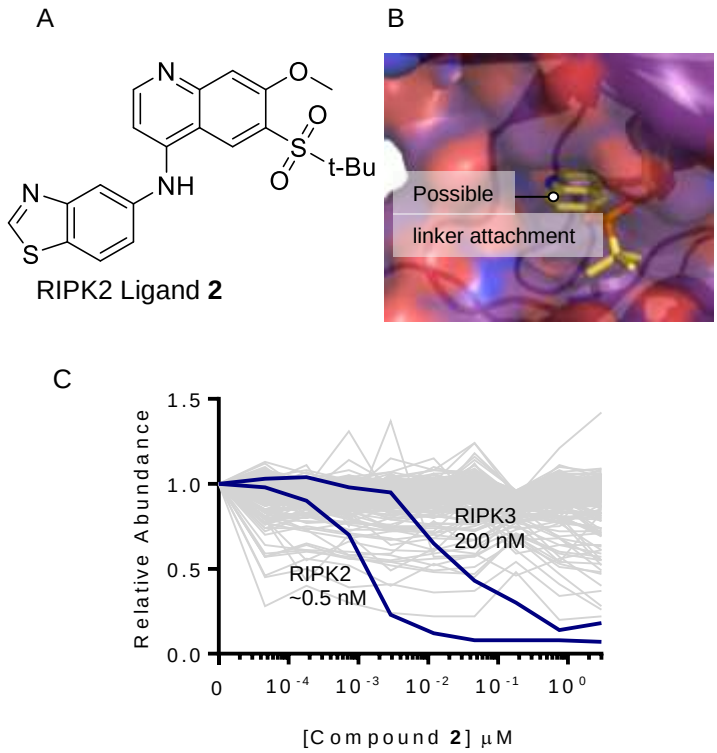

Figure 2.2 Characterization of the RIPK2 binding ligand.

(A) Chemical structure of RIPK2 inhibitor **2** (B) From PDB 5J7B, an analog of Compound **2** bound to the Kinase domain. The solvent exposed linker attachment point on the quinazoline ring is highlighted. (C) KinoBead™ analysis for the selectivity of compound **2**. THP-1 lysates were incubated with compound **2** followed by precipitation of proteins with immobilized kinase inhibitors. After precipitation and washing, proteins were eluted with SDS and subjected to trypsin digestion and tandem mass spectrometry. Roughly 300 proteins were identified in the precipitate, but the only proteins whose abundance decreased with increasing concentrations of compound **2** are highlighted in blue: RIPK2 and RIPK3.

giving a selectivity of over 200-fold, and a survey of other kinases by the KinoBeads™ platform indicates even greater selectivity. This selectivity is important for a proof-of-principal study in order to eliminate any false negative compounds due to off-target binding that might decrease the amount of RIPK2 degradation observed.

Based on the affinities of compounds **1** and **2** for their respective targets, we designed and synthesized the RIPK2 PROTAC **3** and negative control **4** (Figure 2.3). Based on the activity of a small panel of compounds, the 14-atom polyethylene-glycol-based linker was used to connect the RIPK2 and VHL ligands. Inversion of the three sites on the VHL ligand moiety, indicated by asterisks, gives the control compound **4**, which should not be able to bind to VHL but would still bind and inhibit RIPK2 to a similar extent.

We next evaluated each step in PROTAC-mediated degradation in turn. For RIPK2 to be degraded by the PROTAC **3**, several biophysical thresholds must be met. First, the protein needs to from a ternary complex with RIPK2 that is sufficiently stable to mediate ubiquitin transfer. Second, the VHL complex must access lysine residues on RIPK2 and efficiently transfer ubiquitin. Finally, RIPK2-conjugated ubiquitin must accumulate fast enough to be recognized by the proteasome, rather than being kept at shorter chain lengths by deubiquitinating enzymes (DUBs).

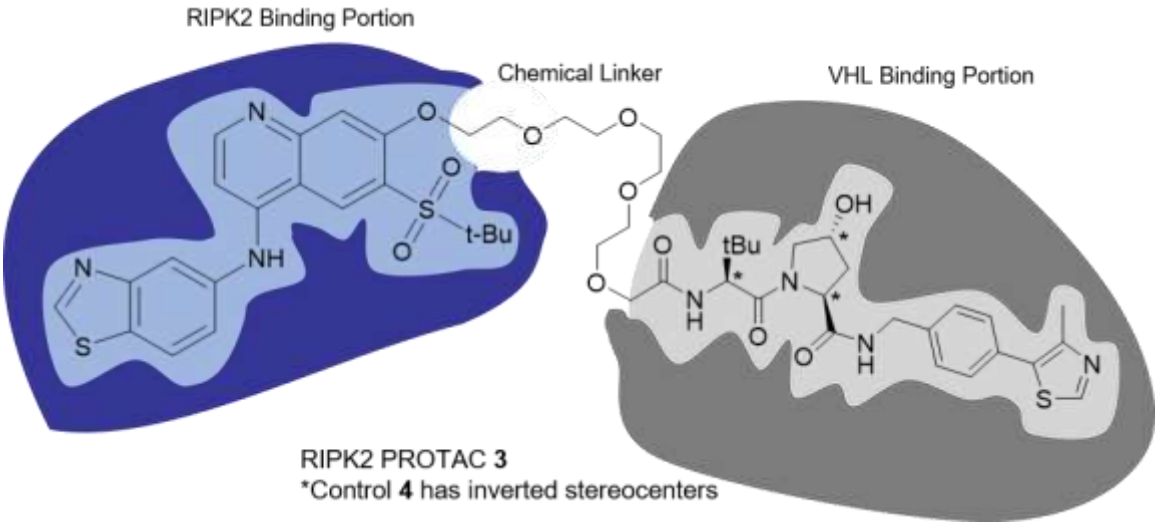

Figure 2.3 PROTAC 3 designed to degrade RIPK2

The RIPK2-binding compound **2** and the VHL binding ligand **1** were connected by a flexible chemical linker on sites predicted to not disrupt binding. The two binding portions are highlighted with the blue and gray cartoons. The VHL ligand has three stereocenters, marked by asterisks, which are inverted in control **4** and should abolish binding to VHL.

Section 2.3: Ternary Complex Formation by the RIPK2 PROTAC

To assess the ability of PROTAC_RIPK2 to form a stable ternary complex with VHL, we used co-immunoprecipitation. THP-1 cell lysates were first preincubated with Compound 3 to pre-form the VHL:PROTAC:RIPK2 complex and then passed over amino-link beads preincubated with anti-VHL antibody. After washing away unbound proteins, the precipitated proteins were analyzed by immunoblotting. As seen in Figure 2.4, only in the presence of the active PROTAC 3 and VHL IP was RIPK2 detected in the western blot (top panel). IgG and inactive PROTAC control 3 were all unable to precipitate RIPK2. To determine the selectivity of proteins interacting with VHL, precipitated proteins were also subjected to unbiased and quantitative mass spectrometry analysis (bottom panel). RIPK2 peptide levels were increased by as much as 20-fold in the presence of 30 nM active PROTAC **3**. Interestingly, at 300 nM PROTAC **3**, the levels of RIPK2 detected decreased, corresponding to the “hook effect” of PROTAC function which is explained next.

Because PROTAC molecules act as bridging molecules to form a ternary complex between an E3 ligase and substrate proteins, their ternary complex versus dose response profiles do not look like typical agonists. At low concentrations, no ternary complex is formed, while at middling or optimal concentrations, much of the PROTAC molecule is successfully bridging its two binding partners. At even higher concentrations, however, PROTAC molecules effectively saturate both of the binary interactions (E3:PROTAC and PROTAC:substrate) and inhibit further formation of the ternary complex. This phenomenal is observed across many classes of bridging molecules and is colloquially referred to as the hook effect. That the PROTAC molecule displays such a hook effect is further evidence for the proposed mechanism of action.

A further observation of Figure 2.4 is worth noting here. While the active PROTAC **3** binds to VHL with a K_D of roughly 650 nM (some affinity is lost upon addition of the linker,

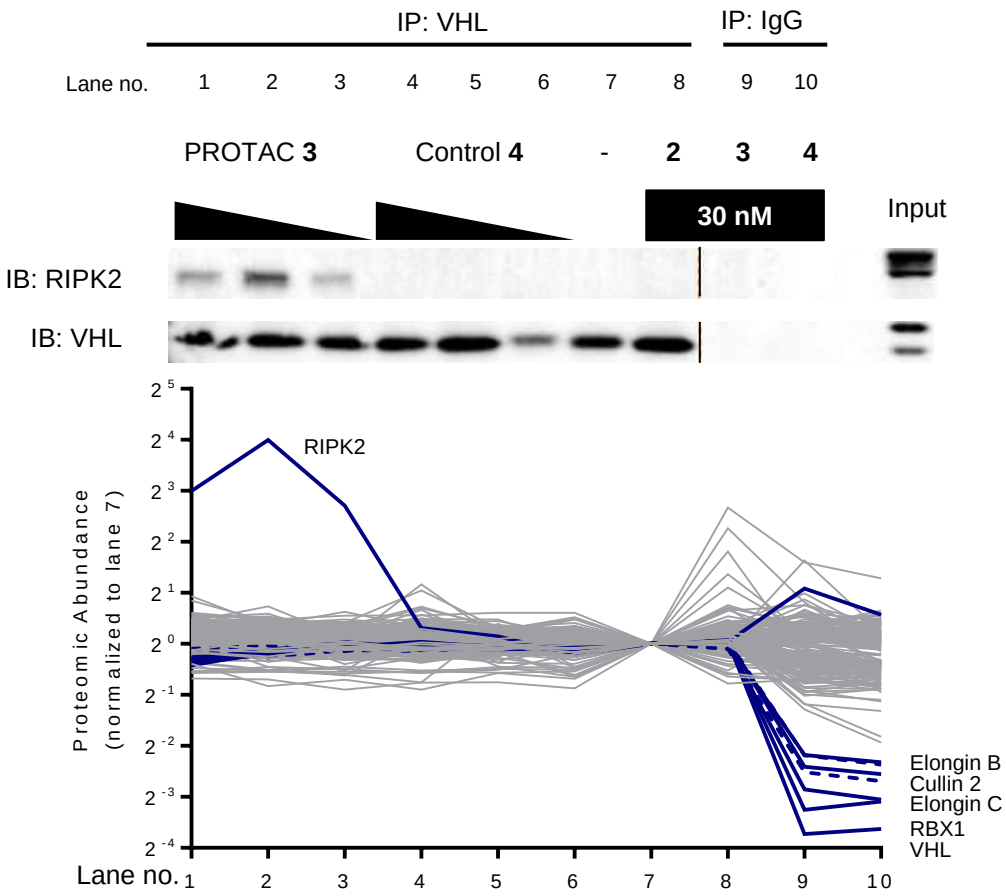

Figure 2.4 RIPK2 forms a ternary complex with VHL in the presence of PROTAC

THP-1 whole cell extracts were incubated with the indicated compounds and immobilized IgG Control (Lanes 9 and 10) or anti VHL Antibody (Lanes 1-8). PROTAC **3** and PROTAC **4** were employed at 3, 30, or 300 nM. After antibody incubation, precipitated proteins were eluted with SDS and subjected to western blotting (top) or TMT-labeling and LC/MS/MS analysis (bottom). Relative proteomic abundances are shown normalized to the vehicle-treated, VHL IP sample (Lane 7). Expected members of the ternary complex are highlighted in solid blue bars; additional proteins that co-precipitated with VHL (GALK1, ZSCAN29) are dashed blue lines.

unpublished data), the ternary complex effectively forms at concentrations well below that and is even decreasing at concentration less than the affinity for VHL. Additionally, no additional proteins were precipitated with the PROTAC including the closely related RIPK3. According to predictions based on ternary complex equilibria, protein:protein interactions between the E3 ligase and substrate may be favorable or unfavorable, and thus left- or right-shift the association curve, respectively. This may explain the increase in potency of RIPK2 association and the decrease/lack of association for RIPK3. This point will be examined more fully in chapter three.

Section 2.4: PROTAC-mediated Ubiquitination of RIPK2

Having shown that the active PROTAC **3** is able to induce association of RIPK2 and VHL, we next sought to evaluate whether this ternary complex is sufficient to induce ubiquitination of RIPK2. To do so, we expressed recombinant VHL E3 ligase complex (VHL, Elongin B, Elongin C, Cullin 2, and Rbx1) using a baculovirus/insect cell expression system and purified it to homogeneity using standard techniques. This complex is capable of being neddylated and of rapidly inducing ubiquitination of a HIF-1α-mimetic peptide (Figure 2.5A, B).

RIPK2 protein was next auto phosphorylated with radioactive ATP in order to label the protein for *in vitro* ubiquitination reactions. By incubation with ATPγ^{32}P, a single band was apparent when the protein was run on a gel and ^{32}P imaged using a phosphoimager screen (Figure 2.5C). To determine the efficiency of autophosphorylation, RIPK2 was incubated with cold ATP, digested with tryspin, and phosphorylated peptides were detected by LC/MS/MS (Keck Mass Spectrometry Facility, Yale University). Figure 2.5D shows the results of this analysis. Many peptides were identified as being phosphorylated even in the absence of ATP, likely due to autophosphorylation during the purification of

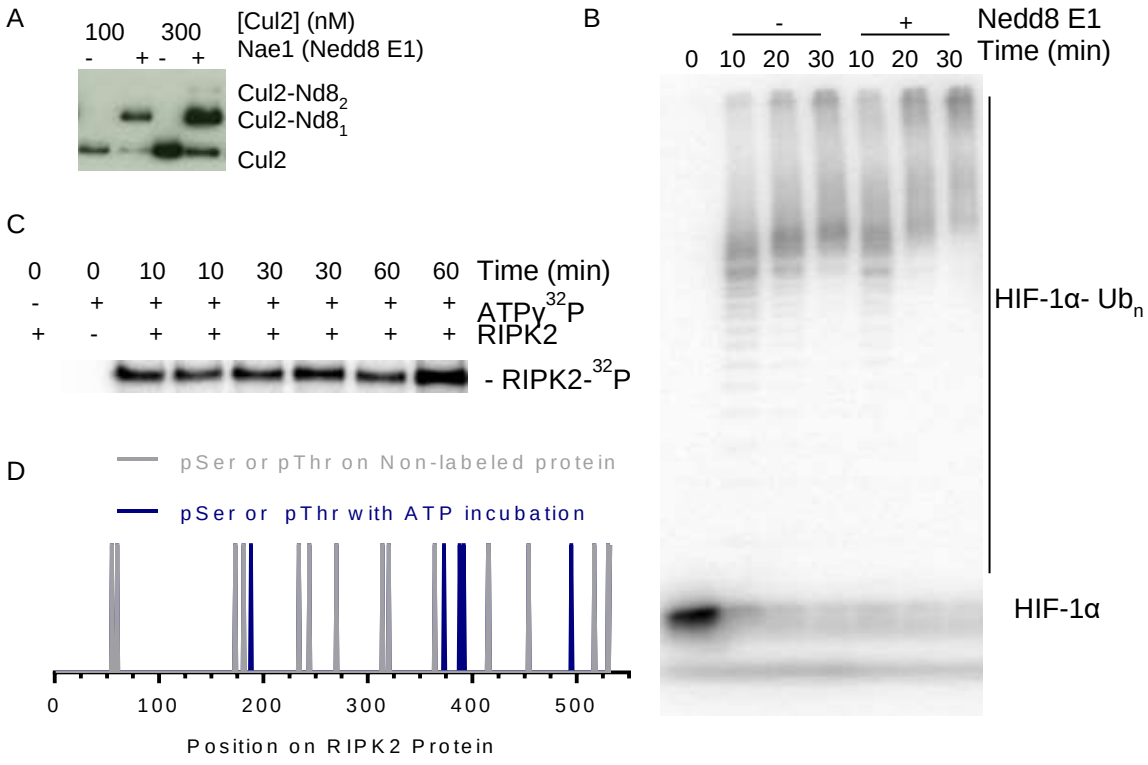

Figure 2.5 Preparing the substrate and enzymes for PROTAC mediated ubiquitination of RIPK2.

(A) The Cullin 2 complex is efficiently neddylated in the presence of Nae1. (B) The HIF-1α peptide was incubated with PKA and ATPγ^{32}P and, in parallel, the Cullin 2 complex was incubated with Nedd8 and Nae1. At time zero, labeled peptide, neddylated Cullin 2 and VHL complex, the E2 enzyme Cdc34, Ubiquitin, and ATP were added and aliquots were withdrawn at the indicated times and quenched by SDS. The reactions were then resolved on SDS-PAGE and imaged on a phosphoimager screen. (C) Full length purified RIPK2 protein was incubated with ATPγ^{32}P for the indicated times. Samples were quenched with SDS, resolved by SDS-PAGE, and imaged using a phosphoimager screen. (D) Profiling of phosphorylation sites on RIPK2. An autophosphorylation reaction was performed as in (A) with unlabeled ATP, and tryptic digest of the protein were precipitated with TiO_2 and subjected to LC/MS/MS for phosphorylation site profiling. Some sites were identified as being phosphorylated in the absence of the ATP-incubation (gray), indicating sites phosphorylated through the purification process. Five sites were unique to the protein after kinase reaction (blue), and so a constant stoichiometry of five was used to convert from moles of ^{32}P to moles of RIPK2.

the protein. Regardless, three novel phosphorylation marked were noted on the protein. Thus, we assumed that five molecules of ^{32}P would be added per molecules of RIPK2.

In vitro ubiquitination reactions were performed as outlined Figure 2.6A. The RIPK2 protein is labeled with ^{32}P and then mixed with PROTAC and VHL to form the ternary complex. In parallel, the E1 (UbE1), E2 (Ubc5, except in Figure 2.6C), and ubiquitin are mixed to pre-charge the E2 enzyme. At time zero, these two mixtures are combined and incubated at room temperature for a set period of time. As seen in Figure 2.6B, higher molecular weight conjugates of RIPK2 are readily apparent after an overnight reaction. Ubiquitinated RIPK2 appears with increasing concentrations of PROTAC **3** and exhibits a dramatic hook effect, such that almost no ubiquitination is observed at 5 μM PROTAC **3**.

We next sought to determine the chain type of ubiquitin that was added to RIPK2. For RING-type E3 ligases, chain type is largely determined by the E2 conjugating enzyme used, and so three different E2 enzymes were surveyed. Cdc34, UbcH5, and UbcH4 were all assessed for their ability to ubiquitinated RIPK2, with UbcH4 giving the most profound ubiquitination in terms of both substrate modified and extent of polyubiquitin chains (Figure 2.6C). This is the most commonly used E2 used in *in vitro* settings, presumably because of its high activity. Next, a variety of ubiquitin mutants were purchased and added to the *in vitro* reactions in lieu of wild type ubiquitin. These mutants have lysine to arginine mutants at those positions off of which poly-ubiquitin chains are extended. Methylated ubiquitin, in which all lysine residues are chemically methylated, was also used for its near inability to form polyubiquitin chains (it can still form chains off of the N-terminus, though most ubiquitination enzymes are incapable of this). Interestingly, there was little difference between the extent of poly ubiquitination of RIPK2 with K29R, K48R, or K63R, or a triple mutant of all three (Figure 2.6D). As these lysine residues are the most commonly used

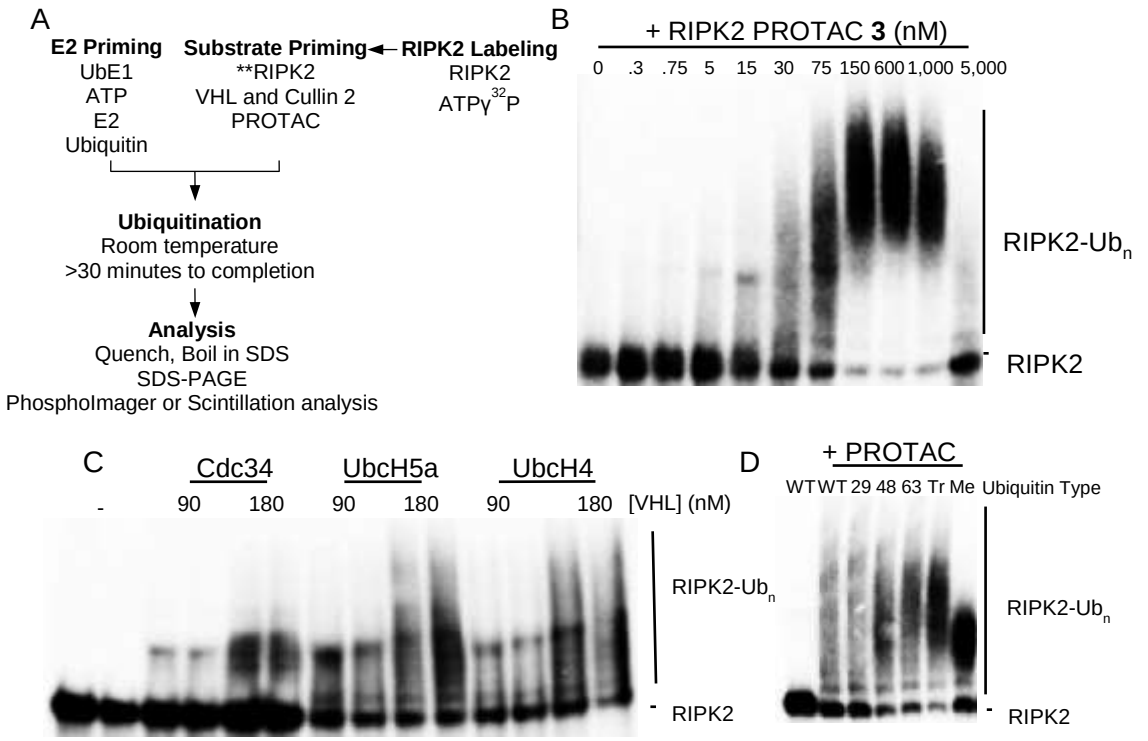

chain-extensions for degradation signals, it could be the case that this *in vitro* system lacks

Figure 2.6 Development of an *in vitro* ubiquitination assay to study PROTAC activity

(A) Schematic of the reaction. ^{32}P RIPK2 is incubated with VHL and PROTAC while E1, E2, and Ubiquitin are incubated to pre-charge the E2. These two separate reactions are then mixed and incubated at room temperature until quenching with SDS, resolution by SDS-PAGE followed by downstream analysis. (B) RIPK2 PROTAC **3** is capable of near complete conversion of RIPK2 into higher molecular weight conjugates after a 16hour ubiquitination reaction. Higher doses of PROTAC 4 lead to decreased yield of ubiquitinated PROTAC, corresponding to the “hook effect.” (C) Choice of E2 enzyme changes the efficacy of the ubiquitination reaction. Three different E2 enzymes were analyzed for their impact on RIPK2 ubiquitination. (D) Ubc4 catalyzes promiscuous ubiquitin chain type formation. Different mutants or modifications on ubiquitin were employed. Wildtype (labeled WT); K29R (labeled 29); K48R (labeled 48); K63R (labeled 63); the K29R, K48R, K63R triple mutant (labeled Tr); chemically methylated to block all chain extension (labeled Me).

relevance with respect to lysine selectivity (see below for efficient degradation of RIPK2 in a cellular context). An alternative explanation is that the lysine residues modified by this system are promiscuously chosen, giving the system flexibility with respect to substrate selection. Furthermore, using methylated ubiquitin, there appears to be as many as five ubiquitin molecules added to RIPK2, indicating that many lysine residues on RIPK2 are accessible for ubiquitination. Overall, these results indicate that the *in vitro* system is rather promiscuous with respect to lysine selectivity; whether this is physiologically relevant will be discussed in chapter three.

An important prediction of PROTAC mechanism of action, and a clear advantage of PROTAC molecules is their ability to supra-stoichiometrically modify substrate proteins. Whereas traditional occupancy-based inhibitors are limited to 1:1 inhibition (i.e. one inhibitor molecule inactivates one protein molecule), PROTAC should be capable of inducing multiple rounds of ubiquitination, and in a cellular context, degradation. We next sought to use the *in vitro* ubiquitination system to verify that supra-stoichiometric ubiquitination was possible with PROTACs.

PROTAC **3** and its inactive control **4** were then used to ubiquitinate RIPK2. In a time-course experiment, increasing amounts of PROTAC **3** increased the rate of RIPK2 ubiquitination, as would be expected (Figure 2.7A). With 200 nM PROTAC **3**, nearly all of the 500 nM RIPK2 substrate was consumed after 35 minutes of reaction. The inactive control **4** showed no ubiquitination at 35 minutes at any concentration tested.

To quantitatively determine stoichiometry, the gel shown in Figure 2.7A was silver stained, and the entire lane above unmodified RIPK2 (corresponding to RIPK2-Ub) was excised and a specific activity of ^{32}P was measured. Because of the sensitivity of ^{32}P detection, an absolute number of moles of ATP in a gel slice could be quantified by liquid

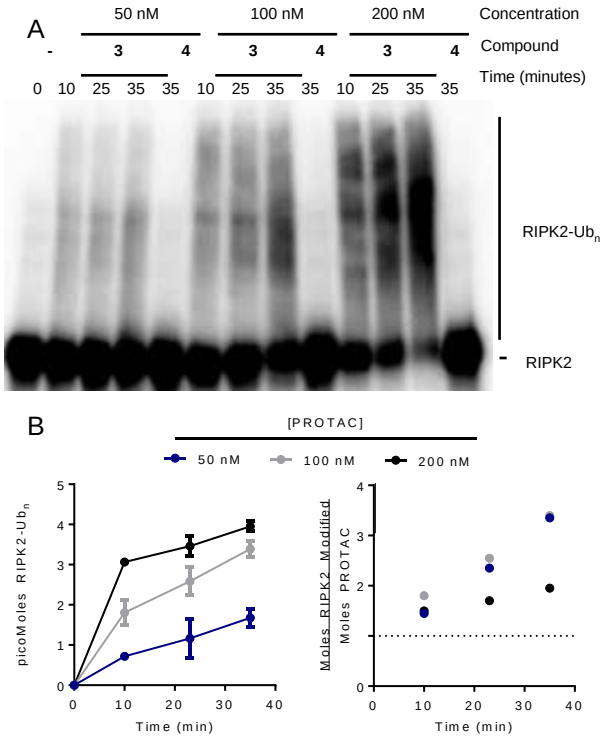

Figure 2.7 Demonstration of catalytic ubiquitination of RIPK2 by PROTACs

(A) *In vitro* ubiquitination of RIPK2 was performed as outlined in Figure 2.6A. Either RIPK2 PROTAC **3** or the inactive control **4** were incubated at various concentrations and various times. After quenching, the samples were resolved by SDS-PAGE and the gel was exposed to a PhosphoImager screen to image ubiquitinated product. (B) The gel in (A) was silver stained, and bands corresponding to unmodified RIPK2 were excised, as well as the entire lane above unmodified (thereby corresponding to ubiquitinated RIPK2). The gel slices were then analyzed by liquid scintillation to determine the amount of ^{32}P present, which was then converted to moles of RIPK2. Left, the number of moles of RIPK2 modified are plotted over time. Right, the ratio of RIPK2 modified to amount of PROTAC employed is calculated over time, with the dashed line indicating where this ratio indicates that PROTACs are acting catalytically. Error bars represent standard error of the mean for two replicates.

scintillation analysis. Moles of ATP could then be converted to moles of RIPK2, assuming that 5 moles of ^{32}P were added to each mole of RIPK2 (see Figure 2.5 above). As expected, at the 35 minutes time point, each of the different PROTAC 3 concentration conditions had supra-stoichiometric amounts of ubiquitinated substrate (Figure 2.7B, left chart). The turn-over number ranged from 2-3.5, robustly confirming the event-based nature of PROTAC molecules (Figure 2.7B, right chart). These numbers are inherently limited in the amount of substrate in the reaction, as well as an assumption that ubiquitinated substrate is just as likely to re-enter the VHL complex and inhibit non-ubiquitinated substrate. In a cellular context, the "catalytic turnover" of RIPK2 might reach far greater values.

Section 2.5: Selective Degradation of RIPK2 in Cells

Having confirmed the ability of PROTAC 3 to efficiently induce a ternary complex between VHL and RIPK2, and that this complex catalytically ubiquitinates RIPK2 *in vitro*, we next sought to determine if this compound is capable of reducing RIPK2 levels in an *in cellula* context. We chose the monocyte culture model THP-1 because of their high expression of RIPK2.

After a 16-hour treatment with PROTAC **3** ranging from 0.5 nM to 30 µM, levels of RIPK2 were almost completely depleted in a dose-responsive fashion (Figure 2.8A). Two quantitative measures are useful for describing PROTAC function. The first, DC_{50}, corresponds to the concentration at which half maximal degradation is observed. This is often confused with a concentration at which 50% of the substrate protein is degraded, but as many PROTAC molecules do not deplete 100% of substrate, DC_{50} is a more useful measure for comparing between compounds. A second term, D_{max}, refers to the maximal degradation observed for a PROTAC.

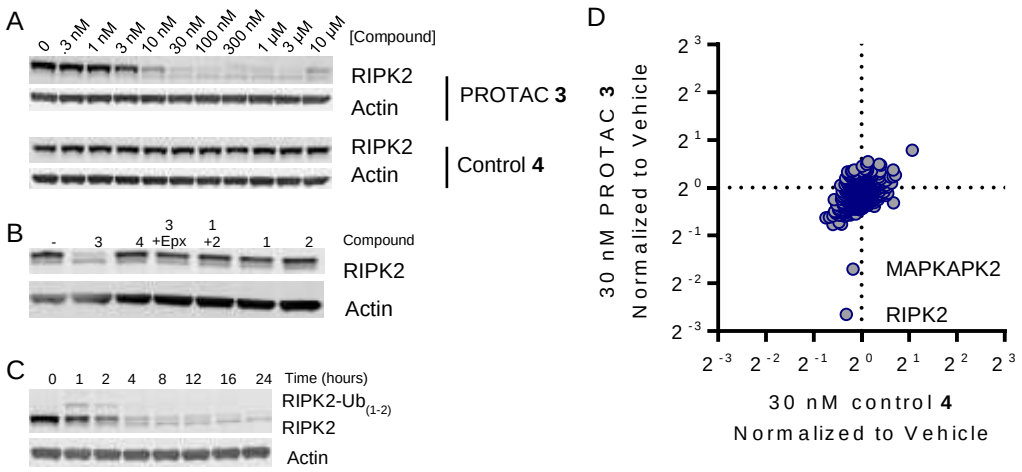

Figure 2.8 PROTAC-mediated Degradation of RIPK2 in cells

(A) Dose responses of PROTAC **3** and the inactive control **4**. THP-1 monocytes were treated with the compounds at the indicated concentrations for 16 hours, and RIPK2 and Actin protein levels were analyzed by western blotting. (B) Controls to confirm the mechanism of PROTAC-mediated degradation. All treatments were for 16 hours with 30 nM compound, with the exception of epoxomicin which was added one hour before treatments and used at 1 μM. The lanes, from left to right, are vehicle; PROTAC **3**; Control **4**; PROTAC **3** and pretreatment with the proteasome inhibitor epoxomicin (Epx); VHL and RIPK2 ligand cotreatment (compounds **1** and **2**); VHL ligand **1** alone; RIPK2 ligand **2** alone. (C) Time course of PROTAC-mediated degradation. THP-1 cells were treated with 30 nM PROTAC **3** for the indicated times. At early times, a higher molecular band appears which is likely ubiquitinated RIPK2. Later time points show a decrease in this, as well as the RIPK2 band. (D) THP-1 cells were treated for 24 hours with either PROTAC **3** or control **4**. Cell extracts were digested with trypsin, TMT-labeled, and relative abundancies of proteins were determined with LC/MS/MS. The Y-axis shows the abundance of more than 7,000 proteins after treatment with PROTAC **3** relative to vehicle treated cells. The X-axis is the same but for control **4**. Therefore, proteins only degraded by the PROTAC should be decreased along the X=1 line.

PROTAC **3** has a DC_{50} of roughly 500 pM and a D_{max} of 97% (observed at 30 nM): this is a very potent compound. As expected, a hook-effect is observed at higher concentration of PROTAC 3, with 75% of the untreated protein remaining at 30 µM (unpublished data). Several interesting observations should be noted. First, roughly 90% of the protein is degraded over roughly 4 orders of magnitude (3 nM to 10 µM), indicating that the hook effect is unlikely to overly complicate dose regimens in a clinical context. This may be a concern when contemplating a new therapeutic entity such as PROTACs, but it seems to be an unwarranted concern based on this data.

Second, it is interesting to contemplate the factors that lead to such potent degradation at such low concentrations, especially considering the dissociation constants for VHL and RIPK2 of 650 nM and 2.5 nM, respectively (PROTAC **3** binds with weaker affinity than parent ligands **1** or **2**; data not shown). At 3 nM, even assuming perfect cell permeability, roughly 1% of VHL and 50% of RIPK2 should be bound by the PROTAC, further indicating that the dose-response curves for PROTAC-mediated degradation is left-shifted relative to the individual binary association curves. This is due either to the catalytic effect or due to protein-protein interactions which stabilize the ternary complex relative to the binary species.

Regarding the catalytic effect, no copy number estimates are available for RIPK2 in THP-1 cells. However, a some reports that in HeLa cells, RIPK2 protein is present at roughly 18,000 copies per cell[219,220]. With a HeLa cell volume of 1500 μm^3, intracellular RIPK2 concentrations are likely in the 20 nM range[221]. Again, with 3 nM PROTAC **3** capable of degrading 20 nM RIPK2, this indicates that the PROTAC is acting catalytically.

We next sought to confirm that the degradation of RIPK2 was due to the proposed mechanism of action. Several controls were used. First, the enantiomer negative control compound **4** does not degrade RIPK2 over any concentration tested (Figure 2.8A). This

compound is the perfect control for assessing PROTAC functions, as it has a nearly identical binding profiles for RIPK2 and maintains the same physio-chemical properties, such as cell permeability, as PROTAC **3**. Additionally, proteasome inhibition by epoxomicin blocks PROTAC-induced degradation, and neither the RIPK2 nor VHL ligands alone or in combination are capable of degrading RIPK2 (Figure 2.8B). These control experiments confirm that degradation of RIPK2 by PROTAC **3** requires VHL engagement, requires that the two warheads be physically connected, and requires a functional proteasome. This is in contrast to many other mechanisms of ligand-induced degradation[222].

Cells require rapid and robust mechanisms to sense and adapt to changes in oxygen levels. As such, HIF-1α levels begin to increase mere minutes of exposure to hypoxic conditions and, when re-oxygenated, HIF-1α protein is degraded with a half-life of only 8 minutes[223]. To assess how degradation of RIPK2 compares to the rapid degradation of HIF-1α, time-course experiments were performed. As seen in Figure 2.8C, more than half maximal degradation was observed within two hours of PROTAC **3** treatment and protein levels continued to decline until less than 10% of protein remained after 4 hours. Intriguingly, at the earliest time point a band appeared above RIPK2 which is likely ubiquitinated RIPK2. This band disappeared over time. These data indicate that RIPK2 degradation via PROTAC treatment is not as rapid as HIF-1α, which is unsurprising for a non-natural substrate which likely has a lower affinity for VHL and is less likely to have optimally poised lysine residues for ubiquitin transfer and degradation by the proteasome[224–226].

Finally, to assess the specificity of RIPK2 degradation by PROTAC **3**, treated lysates were subjected to whole cell proteomic analysis to quantify over 7,000 proteins. As seen in Figure 2.8D, RIPK2 peptide levels were decreased by more than 8-fold at 30

nM. Only one other protein, MAPKAPK2, was decreased in response to RIPK2 treatment, indicating that this compound is highly specific. Interestingly, binding of the RIPK2 ligand **2** to MAPKAPK2 was not detectable at 3 μM (Figure 2.2C) but this protein is degraded at 30 and 300 nM by active PROTAC **3** but not by the inactive control **4**. Possible explanations for MAPKAPK2's degradation involve a left-shift in potency due to favorable protein-protein interactions (see discussion on p38α and foretinib-based PROTACs, chapter three), bystander degradation (in which the target of a PROTAC exists in a protein complex, and other members of that protein complex are also ubiquitinated) or some post-transcriptional effects. This last possibility is unlikely because 1) MAPKAPK2 levels are decreased within 6 hours and 2) the inactive compound **4**, which likely efficiently inhibits RIPK2 kinase activity, does not decrease levels of MAPKAPK2. In short, it is quite unclear why MAPKAPK2 levels are decreased.

In summary, the RIPK2-degrading PROTAC **3** is capable of inducing a stable ternary complex between VHL:PROTAC:RIPK2, which induces the ubiquitination of RIPK2 and subsequent degradation. In contrast to previous technologies, PROTACs have a very clear and well-defined mechanism and are capable of highly specific degradation.

Section 2.6: Degradation of the Nuclear Hormone Receptor ERRα

Having successfully targeted a member of the protein kinase family, we also sought to evaluate the ability of PROTAC molecules based on VHL ligand **1** to degrade another class of proteins: nuclear hormone receptors. This is another class of protein with immense therapeutic value as has been especially demonstrated for the androgen and estrogen receptors in prostate and breast cancers, respectively. Nuclear receptors act as ligand-switchable transcription factors held in the cytosol by association with chaperone proteins until a small molecule ligand binds to the protein. This binding event changes the conformational of the protein, inhibits the association with chaperones, and allows for

nuclear localization for the receptor which can then bind to its cognate DNA element and activate transcription.

Therapeutic targeting of nuclear hormone receptors typically takes the form of small molecule which compete for binding with the cognate ligand, and yet do not induce the activating conformational change. Genetic changes which upregulate either the cognate ligand or the receptor, or hyperactivate the receptor leading classic hallmarks of cancer. Therapeutics such as Tamoxifen[227,228] and Bicalutamide[229] are common examples non-steroidal antagonists of estrogen and androgen receptors, respectively, which have changed the course of these diseases. Common mechanisms of resistance, however, are through mutations in nuclear hormone receptors which change the outcome of antagonist binding, so that these compounds have no effect or, commonly, bring about agonistic effects.

Nuclear hormone receptors are thus a class of proteins where degradation through a small molecule would perhaps overcome this kind of mutation. While the targeting receptor may mutate to render the ligand agonistic, if the protein is being degraded no deleterious outcome will be seen. As such, even early reports of PROTAC molecules focused on degrading nuclear hormone receptors[197,230–232]. Furthermore, non-chimeric small molecules have been shown to induce degradation of nuclear hormone receptors, most predominantly the estrogen receptor. Fulvestrant is an FDA-approved pure antiestrogen and degrades the receptor by pushing out a structural helix, exposing a hydrophobic patch which causes the recognition and degradation of the receptor by protein-homeostasis machinery within the cell[168,169,172,173]. Despite the success of fulvesterant and more potent selective estrogen receptor degraders (SERDs)[233], a clear and generalizable path towards designing such compounds which degrade nuclear

hormone receptors is not feasible. Thus, PROTAC molecules provide a unique opportunity for degrading an important therapeutic class of proteins.

To provide a proof-of-principle that the VHL small molecule ligand could be used to recruit an E3 ligase for degradation of a nuclear hormone receptor, we sought to degrade the Estrogen Related Receptor alpha (ERRα). This receptor is considered a master controller of energy homeostasis, regulating the a variety of pathways from mitochondrial biogenesis, gluconeogenesis, oxidative phosphorylation, and fatty acid metabolism[234,235]. Furthermore, dysregulation of ERRα is implicated in the increase energy consumption required by cancers[236,237]. Small molecule targeting of ERRα has yielded several compounds with modest potency, including some serendipitously discovered to decrease ERRα levels[238,239]. In addition to a generalizable means of inducing degradation, we hypothesized that the PROTAC platform could also improve upon the potency of a mediocre compound.

We started with Compound **5** given its selectivity for ERRα over other isoforms and the availability of a crystal structure[239] to ensure that modifications to the parent ligand would negligibly affect binding affinity (Figure 2.9A,B). Additionally, **5** does not reduce levels of ERRα by itself, and so is a good candidate to study PROTAC-mediated degradation (Figure 2.9C). By addition of varying linkers attached to the VHL ligand, a small panel of ERRα-targeting PROTACs was generated. The best compound is shown in Figure 2.10A as compound **6**, and the inverted stereocenter control compound is compound **7**. This compound has a much shorter linker than the RIPK2 PROTAC **3**. As shown in Figure 2.10B, **6** degrades ERRα with a DC_{50} of <100 nM and a D_{max} of ~85% after 8 hours. This illustrates that no one linker composition is likely to be broadly applicable. The control **7** decreased ERRα levels only slightly. This perhaps indicates that

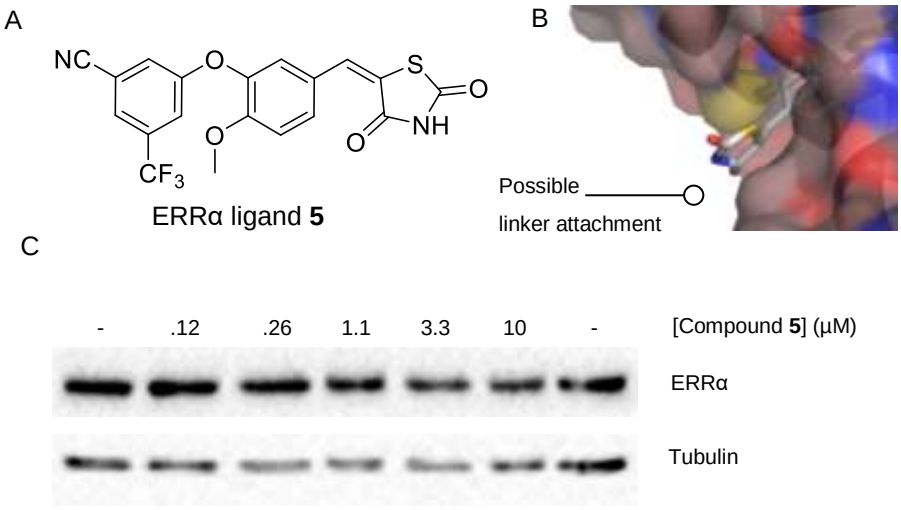

Figure 2.9 Compound **5** is a ligand for the nuclear hormone receptor ERRα.

(A) The diaryl ether compound **5**, a selective ERRα ligand[239]. (B) Crystal structure of ERRα (PDB Code 3K6P). The structure indicates that the thiazolidinedione moiety of compound **5** is solvent exposed and would make an ideal linker attachment point. (C) Unlike other ERRα antagonists, compound **5** does not destabilize ERRα. 3T3-L1 cells were treated for 16 hours with compound 5, and ERRα and tubulin levels were assessed by western blot.

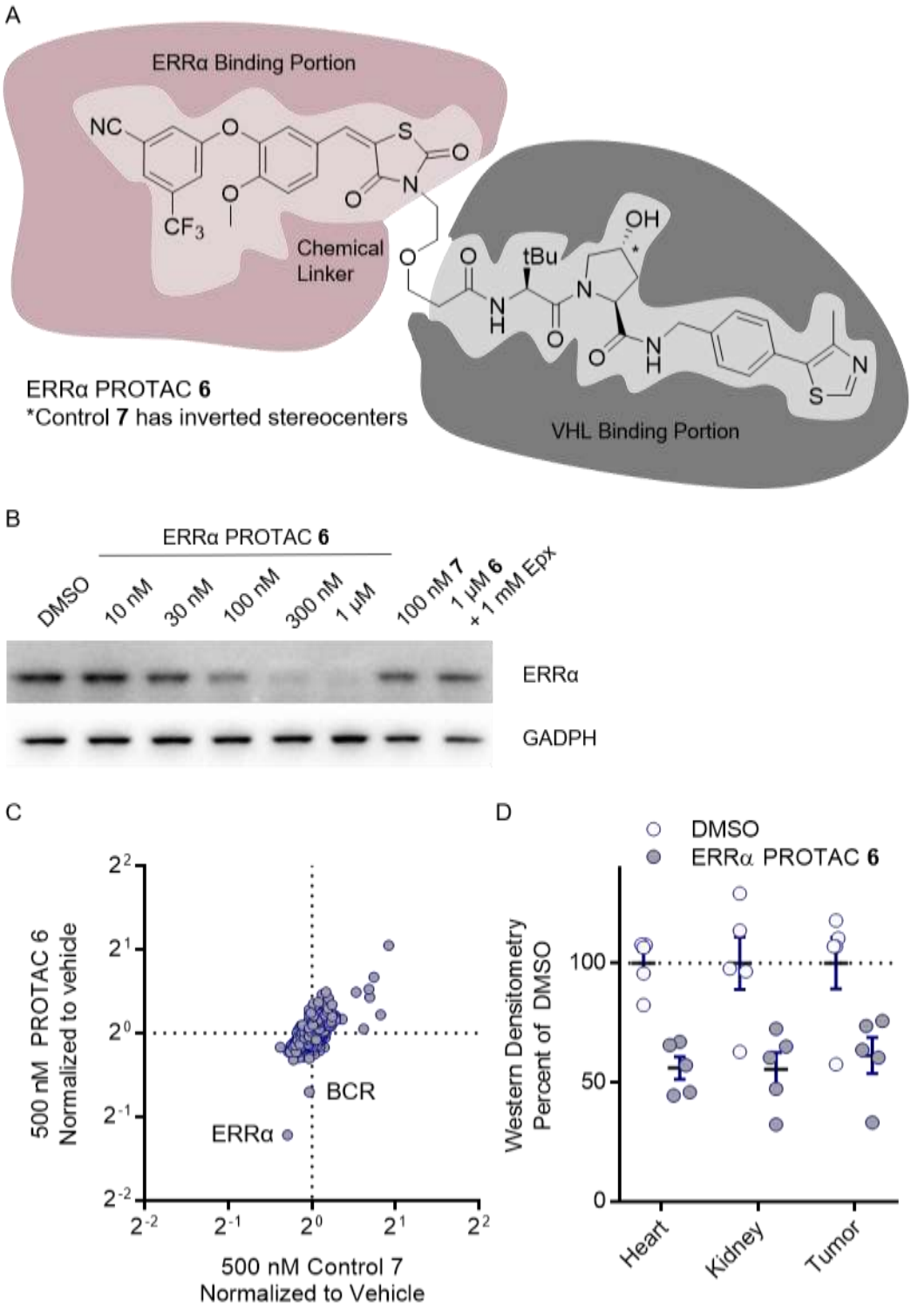
A
ERRα Binding Portion
NC
O
S
O
N
O
O
CF3
Chemical
Linker
O
O
tBu
OH
N
H
N
O
O
N
H
N
S
ERRα PROTAC 6
*Control 7 has inverted stereocenters
VHL Binding Portion
B
ERRα PROTAC 6
DMSO
10 nM
30 nM
100 nM
300 nM
1 μM
100 nM 7
1 μM 6
+ 1 mM Epx
ERRα
GADPH
C
500 nM PROTAC 6
Normalized to vehicle
2^2
2^1
2^0
2^-1
2^-2
BCR
ERRα
500 nM Control 7
Normalized to Vehicle
D
DMSO
ERRα PROTAC 6
Western Densitometry
Percent of DMSO
100
50
0
Heart
Kidney
Tumor

(from previous page)

Figure 2.10 ERRα PROTAC **6** degrades ERRα

(A) The structure of PROTAC **6**. The ERRα compound (**5**) is linked via a short chemical linker to the VHL ligand (**1**). The hydroxyproline motif in the VHL ligand is indicated by an asterisk, and is inverted in the epimer control **7**. (B) Compound **6** degrades ERRα in a PROTAC dependent manner. In lanes one through six, increasing concentrations of compound **6** were incubated with MCF7 cells for 8 hours before western analysis. Lane seven is 100 nM treatment with compound **7** and lane eight is 1 μM compound **6** with a 1 mM pretreatment with epoxomicin. (C) Degradation of ERRα is specific. MCF7 cells were treated for 24 hours with 500 nM compound **6** or **7**, and then over 7000 proteins were quantified by whole cell proteomics. (D) PROTAC **6** degrades ERRα in a mouse. Mice were harvested five hours after a series of four doses 8-hours apart, and the levels of ERRα in various tissues were analyzed by immunoblot and quantified.

although the ligand alone does not destabilize the protein, addition of a linker might change the protein:ligand conformation in such a way as to destabilize the protein, as has been reported for the androgen receptor[240]. Proteasome inhibition was also capable of blocking PROTAC-mediated degradation of ERRα (Figure 2.10B).

Given that Compound **5** shows good selectivity for other ERR isoforms, we hypothesized that compound **6**-mediated degradation would also show good selectivity[239]. We therefore treated cells and the total proteome of whole cell lysates in a similar manner as before. As expected, ERRα was the main protein decreased after treatment with the active PROTAC **6** and no proteins were decreased after treatment with the inactive control **7** (Figure 2.10C). One other protein was decreased after treatment with PROTAC **6**: a relatively understudied protein Breakpoint Cluster Region or BCR. As before, given that BCR is not decreased by the inactive control **7**, either this protein is directly degraded, or indirectly via inhibition of ERRα. This compound's effect on BCR is discussed more fully in chapter four.

Having robustly shown that these compounds behave according to the proposed mechanism of action, we next sought to highlight the functional benefit of PROTAC-mediated degradation. While other knockdown techniques, most notably RNAi or other nucleic acid-based technologies, have been employed to reduce protein levels, one major drawback is the poor pharmacological properties of these techniques. The large nucleic acid molecules are cleared by the liver in most mouse models and are thus not able to distribute to the needed site of action. For this reason, we evaluated the ability of PROTAC **6** to knockdown ERRα in various tissues in a simple mouse xenograft model.

After large, bidaily injections, various tissues of a mouse were harvested. The levels of ERRα were evaluated along with the amount of PROTAC that reached the tissue.

As seen in Figure 2.10D, the levels of ERRα were reduced by almost 50% in the heart, kidney and a tumor xenograft. Additionally, levels of the PROTAC were measured and found to be 80-100 μM in these tissues and slightly less in the plasma (data not shown). These data are encouraging but also highlight the difference between generating a chemical probe and a therapeutic. While the levels of PROTAC **6** measured in these tissues are very high (more than 100x the DC_{50} observed in cell culture), ERRα knockdown is only modest. This is likely due to high plasma protein binding. However, that a molecule not optimized in any way for pharmacokinetic properties is still able to distribute to various tissues and effect protein knockdown is encouraging indeed.

Because of the well-known oncogenic functions of VHL, in which mutations in VHL inhibit engagement and degradation of HIF-1α, we next assessed whether HIF-1α was stabilized in response to PROTAC treatment. In a cell line expressing the oxygen-dependent degradation domain of HIF-1α fused to luciferase[241], hypoxic conditions would increase luciferase activity in cell lysates which can be mimicked by treatment with the iron-chelating compound deferoxamine mesylate (Figure 2.11). Treatment with ERRα PROTAC **6** had no effect at any concentration, while only 30 μM of **3** had any effect**.** Given that PROTAC **3** efficiently degrades RIPK2 at 30 nM, this indicates a therapeutic index of at least 1,000.

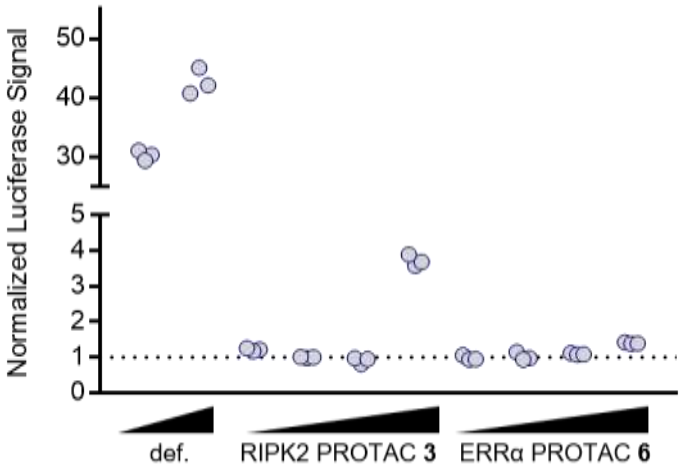

Figure 2.11 PROTACs only modestly inhibit endogenous VHL activity

The oxygen dependent degradation domain of HIF-1α was fused to luciferase and expressed in SH-SY5Y cells. After a four-hour treatment with the indicated compounds, cells were lysed and luciferase activity was measured per manufacturer instructions. Values represent three technical replicates normalized to DMSO treatment. Treatment concentrations are as follows: 0.5 or 5 mM deferoxamine mesylate (def.); RIPK2 PROTAC **3** (30 nM to 30 μM); ERRα PROTAC **6** (30 nM to 30 μM).

Lastly, we also evaluated the ability of the PROTAC to functionally inhibit ERRα activity. As discussed earlier, ERRα is a master regulator of energy homeostasis, and one commonly used model for this is an adipogenesis model. In a 3T3-L1 pre-adipocyte cell line, treatment with high concentrations of insulin and the phosphodiesterase inhibitor IBMX causes these cells to differentiate into adipocytes and accumulate large lipid droplets. This process can be measured via RT-qPCR analysis of the mRNA for various adipocyte-related genes and is inhibited upon ERRα antagonism[242,243]. As seen in Figure 2.12, the mRNA levels of various metabolism-related genes (*AP2* and *UCP1)* significantly rise over 8 days after differentiation. These levels are decreased by treatment with the parent warhead **5**, the PROTAC **6**, or the inactive control **7**. These results indicate that the PROTAC is capable of inhibiting the activity of ERRα, but that this inhibition is not much more potent than the parent warhead, and that simple inhibition of ERRα is sufficient to block its adipogenic activity. Because inhibition is sufficient, and addition of the linker and VHL ligand to compound **5** likely decreases the affinity of PROTAC **6** for ERRα, it might be expected that PROTAC **6** and control **7** would be weaker inhibitors for ERRα activity.

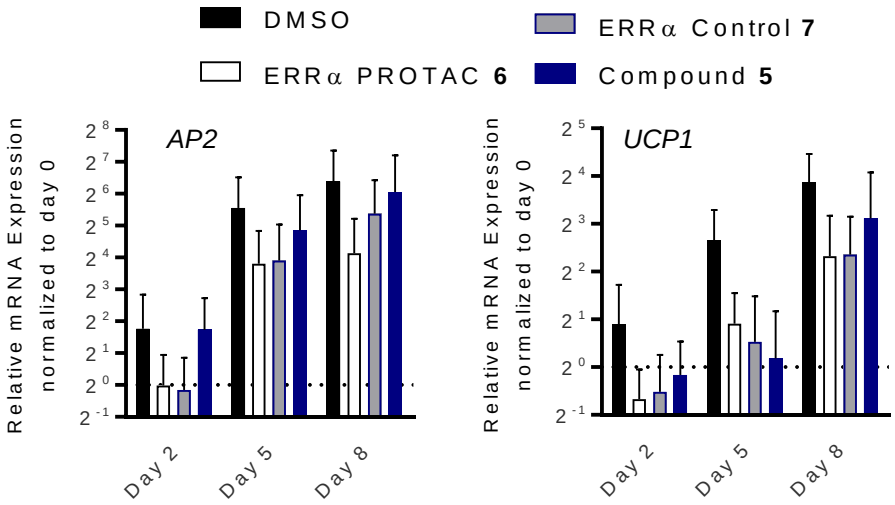

Figure 2.12 Adipogenesis is inhibited by ERRα antagonism

At 80% confluency, 3T3-L1 cells were induced to differentiate with IMBX, insulin, and dexamethasone and cotreated with the indicated compounds. After the indicated times, cells were lysed with trizol and then frozen at -80. After the completion of the time course, RNA from all samples were extracted in parallel and AP2 and UCP1 levels were quantified by RT-PCR. Technical duplicates were averaged, and error bars represent standard error for the mean for biological duplicates.

Section 2.7: Discussion

Proteolysis targeting chimera, or PROTAC, were first published roughly 15 years ago but was limited to a chemical biology parlor trick because of a lack of potency. Early generation compounds were based on PROTACs or weak affinity ligand and so lacked potency, cell permeability, or both[196,244]. The compounds presented in this chapter, however, are designed based on high affinity ligands and achieve near complete protein knockdown at low nanomolar concentrations. These compounds are also well characterized, possessing a clearly defined mechanism of action, and exquisitely specific, knocking down the desired protein without major off-target effects.

Recent advances in the PROTAC technology also includes expanding the repertoire of available E3 ligases. While the development of VHL-recruiting PROTACs was only possible because of the Crews' lab investment in developing high affinity ligands, thalidomide and its derivatives have been serendipitously discovered as potent ligands to the Cullin 4a-based E3 ligase Cereblon (CRBN)[245]. Thalidomide has a checkered history due to its teratogenic effects, but the discovery that it binds CRBN and induces neo-substrate degradation has caused a renaissance in its study[174–176]. Structural studies have revealed that these thalidomide derivatives are capable of remodeling the surface of CRBN, making new binding interfaces where new substrates can bind and be degradaed[180,181].This discovery prompted the use of thalidomide as a recruiting element in PROTACs. CRBN-recruiting PROTACs are as efficacious as VHL-recruiting PROTACs[246–249].

The broad use of two E3 ligases (VHL and CRBN) in the PROTAC platform prompts the question of whether there would be added benefit in more and different E3 ligases. In a report from our lab, we noted that the VHL E3 Ligase was unable to degrade the oncoprotein BCR/Abl even when testing various linker lengths[250]. The reasons for this

are unknown, but we hypothesized that different E3 ligases might have different degradation capabilities, and indeed CRBN was capable of degrading BCR/Abl. Another report from our lab used a chemical genetic strategy to query which E3 ligases could be amenable to PROTAC-induced hijacking[251]. Additionally, the inhibitor of apoptosis (IAP) proteins have been widely used in a subset of PROTACs called selective and non-genetic, IAP-based protein erasers (SNIPERs)[199,201,202,252,253]. A potentially powerful use of different E3 ligases (other than patent breaking) may be the use of tissue-specific E3 ligases. For example, if a PROTAC were designed to recruit the E3 ligase Mage A3, which is normally not expressed in adults but is widely expressed over a variety of cancer, target protein degradation could possibly be achieved selectively in tumor tissues[254].

A key benefit of the PROTAC technology is the catalytic nature of these compounds. Rather than acting only when bound to the protein of interest, a PROTAC is capable of exerting its effect (ie ubiquitination and degradation) on one molecule, dissociate, and repeating its effect on additional molecules of target protein. This turnover effect is a likely cause of the enhanced potency of the RIPK2 PROTAC. Indeed, other compounds have been shown to possess unrelated catalytic mechanisms of action which contribute to their potency[255]. The catalytic numbers generated in this study represent a conservative demonstration of catalysis and are limited here by the confines of the assay. Actual catalytic values are likely to be much higher. For example, in an *in vitro* context in which ubiquitinated protein is not degraded nor removed from the system, the ubiquitinated product can compete for binding to VHL:PROTAC and inhibit further unmodified protein from being ubiquitinated. This issue would not be present in the cell.

The most exciting application of PROTACs molecules is to disease-relevant proteins currently considered undruggable. Because current therapeutics broadly rely on a strategy of inhibiting protein active sites, many proteins (~80% of the proteome) lay

outside the realm of current therapies, but examples such as c-Myc and KRas illustrate how these proteins can still play important oncogenic roles[131,256]. The application of PROTACs here is obvious, as the entire protein would be degraded: what is not so obvious is the means by which PROTACs will be targeted to the undruggable protein of interest. Additionally, because most screening technologies rely on enzymatic activities as a readout, robust technologies for identifying and developing small molecules must be developed[257]. Such technologies perhaps include NMR-based screening, the thermal shift assay, DNA-encoded libraries, and others. In addition, many proteins possess more than one functional domain, and so using a PROTAC to degrade the entire protein may provide additional benefit[11].

The complete scope of PROTACs is yet to be realized, but so are many of the drawbacks. Because PROTACs function through a unique mechanism of action, additional factors that haven't been taken into account for previous inhibitors may come into play. For example, protein with extremely fast turnover rates might not be targeted by PROTACs for therapeutic benefit. In such a case, the protein is endogenously turned over so rapidly that the decrease in half-life by PROTACs is negligible. Accordingly, fast re-synthesis rates or feedback mechanism might also limit the efficacy. Additionally, new mechanisms for resistance might be discovered: mutations that inhibit VHL binding to PROTAC or mutations of acceptor lysine residues.

PROTACs also exist outside of the realm of small molecules currently considered drug-like[258]. These molecules are in a zone between typical small molecules and biologics, and so the pharmacokinetic properties of PROTACs may interfere with their clinical use. Indeed, the ERRα PROTAC showed very modest *in vivo* activity which indicated poor properties. Despite this, many publications have since shown good activity with PROTACs in mouse models[246,259], with some unpublished studies even indicating good bioavailability

with oral administration. The future of PROTACs as clinical agents, therefore, is promising[260].

Chapter 3

The Biochemistry of PROTACs:

Furthering the Understanding of Targeted Protein Degradation

Preface

The work in this chapter is largely my own, but several Crews' lab colleagues helped immensely in developing the ideas of this chapter. Alexandru Buhimschi performed the *in vitro* ubiquitination and VHL pulldown assays for HaloTag, as well as preparing the HaloTag mutants. Jing Wang performed the docking and MD simulations for HaloTag and p38α studies. Dr. Saul Jaime-Figueroa synthesized the foretinib-based PROTACs. Blake Smith and George Burslem performed the western blotting in Figures 3.8, 3.11, and 3.13 and 3.15. The mass spectrometric analysis of ubiquitinated lysines was performed by the WM Keck Foundation Biotechnology and Resource Laboratory. The whole cell prteomics experiment was performed by the Thermo Fisher Scientific Center for Multiplexed Proteomics. The HaloTag work is soon to be written and submitted for publication, while the foretinib-based PROTAC work is already published:

Bondeson, DP, Smith, BE, et al (2017). Lessons in PROTAC Design from Selective Degradation with a Promiscuous Warhead. Cell Chemical Biology. *25*, 78–87.e5.

Chapter two introduced improvements in proteolysis targeting chimera, or PROTACs. These next generation small molecules are capable of potent degradation of many different protein classes, and there is considerable excitement for their therapeutic application. However, a basic understanding of how this technology works is required, and that is the focus of this chapter. A key conceptual advance moved PROTACs from modest tool compounds to potent degraders: the appreciation that the linker connecting the targeting warhead and the E3 ligase must be optimized for each target protein. The reasons for this are discussed in this chapter. First, a model system in which there is a very fine “sweet spot” of linker length for degradation is introduced, and the differences between good and bad degraders are investigated biochemically. Second, a promiscuous kinase inhibitor turned PROTAC allows us to ask how many of the dozens of potential targets are degraded. As only a subset is degraded, we then apply the principles gained from the initial model system to understand this selective degradation. Overall, this chapter uncovers the importance of protein:protein interactions between the E3 ligase and target protein for efficient degradation.

Section 3.1: Why are some PROTACs Better than Others?

One intriguing observation from the development of the RIPK2 and ERRα PROTACs was the strict dependency on a particular linker geometry for efficient degradation of the protein. This is a phenomenon that has been observed in many other PROTAC development projects, and rational design of the correct or best linker has not been possible. A more robust biochemical understanding of how the design of PROTAC linkers, colloquially termed “linkerology”, influences PROTAC function could hopefully aid in the design process as well as lead to more potent PROTACs.

As an artificial substrate, it is important to examine how this protein might interface with the endogenous machinery, mimic the endogenous substrate, and thus perhaps

lessons learned from other E3 ligase:substrate interactions may also apply to PROTAC targets. The studies of RIPK2 in chapter two were presented in such a way as to de-convolute the several steps required for a PROTAC to induce degradation: Binding to the substrate protein, formation of a ternary complex, ubiquitination of the substrate followed by recognition of that ubiquitinated protein by the proteasome (Figure 3.1). In this cascade of activities, where is discrimination possible?

A first model might focus on the binding of the PROTAC molecule to the protein(s) and formation of a ternary complex (substrate:PROTAC:E3 ligase). In such a model, it can be imagined that as long as the substrate protein is in close proximity to the E3 ligase, it will be ubiquitinated and degraded. In this model, successful PROTACs would be those that facilitate the most stable ternary complex possible, possibly even through protein:protein interactions between the E3 ligase and the substrate protein[261]. PROTACs could then be thought of as a specific example of a "heterodimerizer" or stabilizers of protein:protein interactions (SPLINTs)[262]. Unsuccessful PROTACs, then, are those that do not allow this ternary complex to form, either through being too short and not allowing simultaneous binding or being too long and enforcing an entropic penalty on folding the linker into an optimal orientation.

A second hypothesis might instead focus on the ubiquitination of the target protein as being the most discriminating step in PROTAC function. Under this idea, the linker is designed in such a way to orient a lysine into some sort of "ubiquitination zone[224,263]." Perhaps, additionally, not just any lysine will do. Particular lysines may not be structurally disordered enough for ubiquitination or for the partial unfolding needed for unfolding and threading through the proteasome[226]. Other lysine residues might reside in patches that are highly prone to deubiquitination, and thus only briefly exist in a state amenable to proteasome recognition[264].

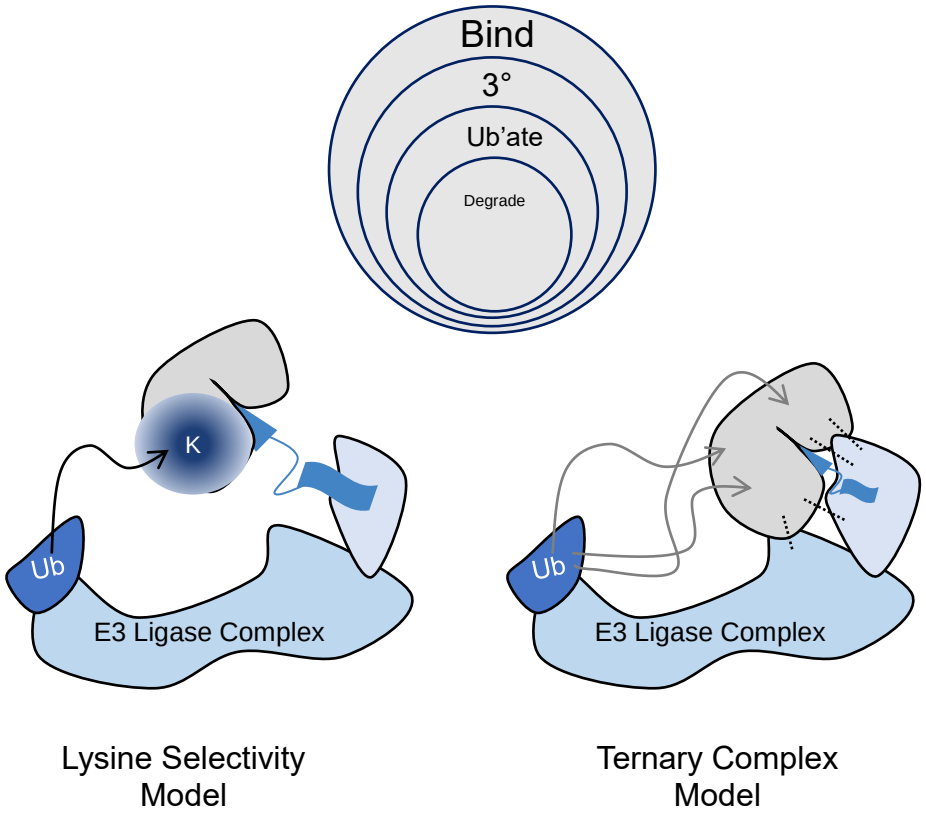

Figure 3.1 Models for PROTAC function and the differences between PROTACs of related geometries

Top shows a Venn diagram for various PROTACs that all bind to the target protein. While all compound may bind to the target protein, a subset will form a ternary complex (target:PROTAC:E3 ligase), fewer will ubiquitinate the target, and fewer will degrade the target. This chapter asks at which step is discrimination achieved. Bottom left, a lysine selectivity model of PROTAC function. The target protein only loosely associates with the E3 ligase, but the PROTAC orients the target in such a way that a lysine residue falls within the "ubiquitination zone" of the E3 ligase. Bottom Right, the ternary complex model of PROTAC function. PROTACs function by orienting the target in such a way that protein:protein interactions between substrate and E3 ligase stabilize the ternary complex. The "ubiquitination zone" is broad in this model. A hybrid to these models is also possible (not shown).

And of course, a hybrid of the two models is also possible. Perhaps the protein:protein interactions between substrate and ligase are important for stabilizing the ternary complex so that only one lysine is ubiquitinated rather than many: poly-monoubiquitination might be unproductive but mono-polyubiquitination leads to a recognizable degron. Many such permutations are imaginable.

Section 3.2: HaloTag is Degraded Within a "Sweet Spot" of Linker Length

To investigate the discriminating biochemical step of PROTAC function, we used the simplest system in which a linkerology effect has been observed: the HaloPROTACs. HaloTag is a modified bacterial dehalogenase that has been used in our and other labs in many contexts[184,251,265,266]. By mutating away critical residues in the active site, the HaloTag protein is unable to complete its typical catalytic cycle – dehalogenating an alklyl chloride – and thus the alkyl chloride covalently labels an internal aspartate residue in HaloTag. Such compounds have been used to chemically incorporate fluorescent labels, immobilization tags, and degradation tags onto HaloTag.

In developing the VHL ligand to be used in all small molecule PROTACs, the alkyl chloride moiety could be appended to generate a new panel of HaloTag modifying ligand that would induce its VHL-mediated degradation[166]. The goal of this initial project was two-fold: generating a chemical biology toolbox in which a protein of interest can be fused to HaloTag and then degraded by the HaloPROTAC, and, secondly, examining the importance of linker length by generating and testing a panel of compounds.

HaloPROTACs are ideal for investigating linkerology for several reasons. First, because the protein covalently binds the PROTAC, it simplifies the system from a ternary complex equilibrium to a pseudo-binary problem. Second, HaloTag is a very stable protein and easy to purify which can aid protein-demanding biophysical studies. And third, the HaloPROTAC panel was chosen was because it provides a concise and clear illustration

of the linkerology effect (Figure 3.2). The three HaloPROTACs, compounds **8-10**, have increasing linker lengths by one polyethylene-glycol unit, or three atoms. HaloPROTAC **8**, with a 6-atom linker shows almost no degradation, while the longest linker of 12 atoms shows modest degradation (PROTAC **10**). The best compound, PROTAC **9** lies in between these two extremes, at 9 atoms, and degrades the GFP-HaloTag fusion protein with a DC_{50} of ~20 nM and D_{Max} of ~90%.

Section 3.3: Does Lysine selectivity explain HaloPROTAC efficiency?

First, a lysine selectivity model was examined. This model implies that the E3 ligase's zone of ubiquitination is rather small and therefore PROTACs of different linker lengths would induce different ubiquitination patterns on the substrate. To evaluate this, the same HA-eGFP-HaloTag7 protein used in the degradation studies was cloned into a bacterial expression vector and purified. Then, this protein was mixed with PROTAC, VHL complex, E1 and E2 enzymes, and Ubiquitin. The proteins were then denatured and analyzed by western blot. As seen in Figure 3.3, the optimal HaloPROTAC, **9,** caused the formation of higher order species, whereas less potent compounds did not. Overall, the degradation efficiency of a PROTAC matched quite well with the ubiquitination efficiency observed, especially in the relative ordering of the different compounds. If anything, the lack of activity for HaloPROTAC **10** would predict that this compound degrades far worse than **9**, whereas the two compounds in cells are fairly similar. The fact that these compounds induce such different ubiquitination patterns rules out the possibility that degradation is solely determined at the stage of proteasome recognition but does not provide evidence against any other model.

The precise sites of ubiquitination were then evaluated. Ubiquitinated HaloTag was prepared using HaloPROTAC **9** and then subjected to trypsin digestion and tandem LC/MS/MS analysis (Keck Mass Spectrometry Facility, Yale University). The C-terminus

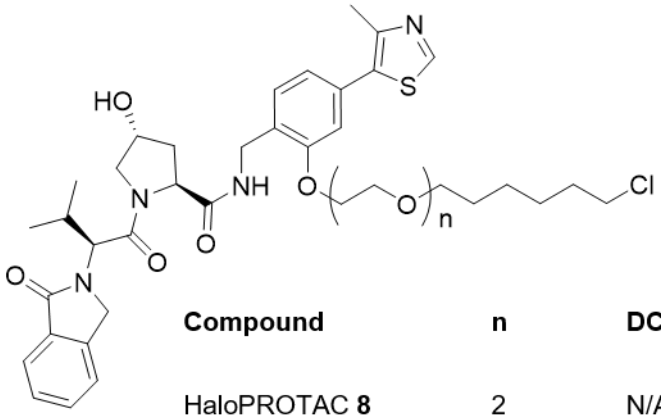

Compound	n	DC_{50}	DC_{max}
HaloPROTAC **8**	2	N/A	N/A
HaloPROTAC **9**	3	20 nM	90
HaloPROTAC **10**	4	20 nM	65

Figure 3.2 - Summary of HaloPROTAC panel of compounds

All three compounds share a similar attachment point to the “right-hand” side of the VHL ligand. Degradation data were determined by flow cytometry of a HA-GFP-HaloTag construct. DC_{50} refers to the concentration at which half-maximal degradation occurs, while D_{max} is the maximal reduction of protein levels observed. Degradation data are previously published results[166].

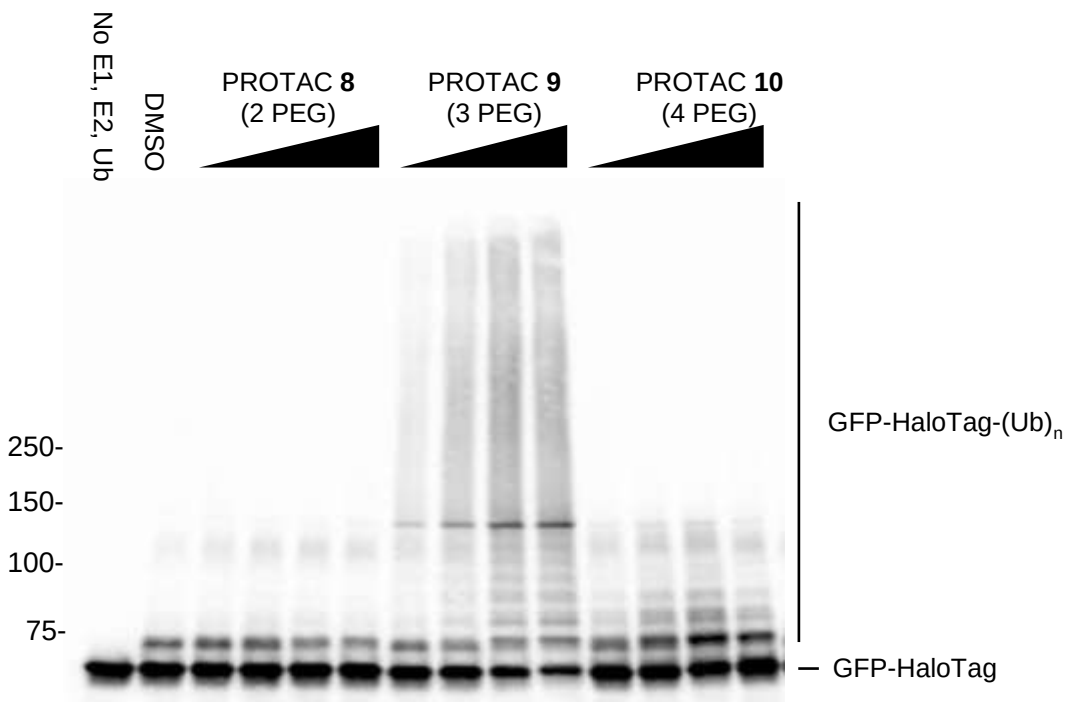

Figure 3.3 Ubiquitination of GFP-HaloTag with HaloPROTACs

Ubiquitination reactions were carried out as described in Figure 2.6A. Compound concentrations are 100, 250, 500, and 1,000 nM. After an overnight reaction, the samples were quenched with SDS and analyzed by western blot with an antibody against the HA epitope of the GFP-HaloTag protein. Molecular weight markers are shown on the left side of the blot.

of ubiquitin is the attachment point on substrate lysine residues, and the final residues of ubiquitin are Arginine-Glycine-Glycine. As trypsin cleavages after lysine and arginine residues, only the DiGly motif is left on lysine residues. Furthermore, the addition of this DiGly motif blocks the recognition of that lysine residue by trypsin, resulting in a missed cleavage. Thus, missed cleavage and DiGly addition are indicative that a particular lysine residue had received a ubiquitination mark[267].

The GFP-HA HaloTag protein contains 27 lysine residues and of these, 12 were found to be ubiquitinated (Figure 3.4). Most impressively, lysine residues which were ubiquitinated are found throughout the protein, spread throughout both the GFP and HaloTag fusion portions, both in primary sequence and tertiary structure. This argues against any model in which the availability of lysine residues is the limiting factor for PROTAC-mediated degradation.

Data from *in vitro* systems can often be misleading, and there are several possibilities for why this initial profiling of ubiquitinated lysine residues should be doubted. First, the cognate E2 enzyme for the VHL complex is not known. That is, although the enzyme seems to be functional with a variety of E2 enzymes *in vitro* (see, for example, Figure 2.6C in chapter two), it is not known whether these E2 enzymes cooperate with VHL in cells[208] and this is a rather hard question to answer[268]. Furthermore, in an *in vitro* context devoid of degradation and deubiquitination machinery, it is also possible that the substrate is ubiquitinated on irrelevant lysine residues that would never be recognized for degradation. For these reasons, we sought to determine the sites ubiquitinated in cells after treatment with HaloPROTAC **9**. The time at which 50% degradation occurs is approximately 8 hours, and so we choose a time slightly earlier than this time as a snapshot of protein ubiquitination, assuming that most of the protein is in an equilibrium

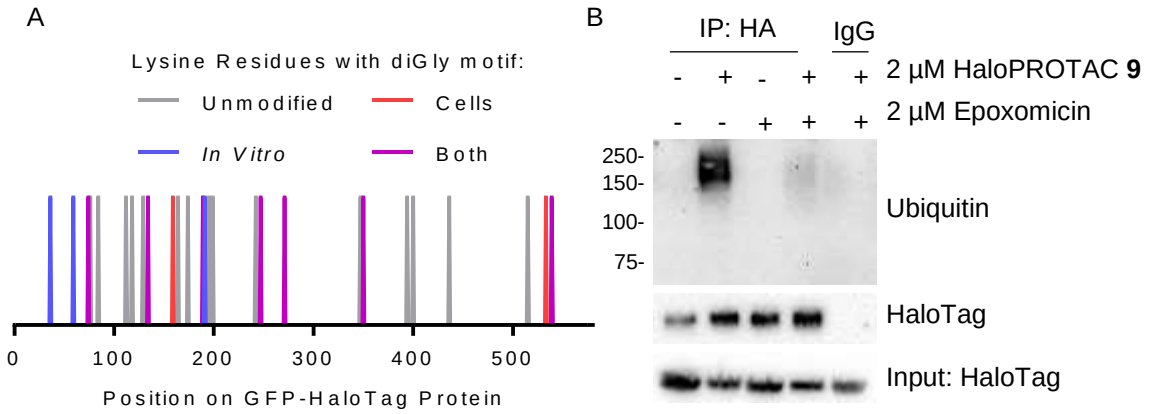

Figure 3.4 Mapping of HaloTag lysine residues ubiquitinated by HaloPROTAC **9**

(A) Mass Spectrometry profiling of trypsin digested peptides identifies many different ubiquitinated lysines. In gray are lysine residues that were never identified as being ubiquitinated, while blue and red lines indicate lysine residues identified from and *in vitro* or cellular context, respectively. Residues identified with magenta were identified in both experiments. GFP fusion is residues 1-278, while HaloTag is 279-576. (B) Immunoprecipitation of HaloTag protein from cells after treatment with HaloPROTAC **9**. HEK-293 cells stably expressing the HA-GFP-HaloTag were treated for six hours with PROTAC and/or epoxomicin, followed by immunoprecipitation of the HaloTag protein with an HA antibody:sepharose conjugate overnight. The beads were washed extensively in lysis buffer and proteins were eluted with SDS. IP is immunoprecipitated sample; WCE is whole cell extract.

between ubiquitination and degradation. By treating the cells for 6 hours and then lysing in a denaturing buffer with inhibitors against deubiquitinating enzymes and proteases[269], we were able to immunoprecipitate the protein and detect ubiquitin marks at higher molecular weights (Figure 3.4B). Although proteasome inhibition moderately rescued GFP-HaloTag levels, there was some toxicity associated with this which likely decreased the amount of ubiquitinated protein observed. Furthermore, an isotype matched IgG was also used as an immunoprecipitation control, which was unable to isolate any GFP-HaloTag protein nor any higher molecular weight ubiquitin-reactive species. Given this, we conclude that the sample is enriched for ubiquitinated GFP-HaloTag proteins.

This sample was then run on a polyacrylamide gel, and the region above the unmodified HaloTag was excised, subjected to in gel trypsin digestion and then DiGly containing peptides were analyzed as before. Satisfyingly, although a different array of Lysine residues was identified as being ubiquitinated, it was still a large swath of residues distributed throughout the protein's surface, further discrediting a model in which lysine selection is the limiting factor in PROTAC-mediated degradation (Figure 3.4A). Satisfyingly, many of the ubiquitinated lysine residues were mapped by both *in vitro* and *ex cellula* techniques.

Section 3.4: Optimal HaloPROTACs induce Protein:Protein Interactions

While PROTACs of different linker lengths show drastically different degradation and *in vitro* ubiquitination profiles, it is unlikely that this phenomenon is due to a limited availability of lysine residues (at least for HaloTag and the HaloPROTACs). Having ruled out that hypothesis, we next turned to a model in which the limiting factor is engagement within the ternary complex.

To test this hypothesis, we first developed a simple pulldown assay in which VHL protein was immobilized on sepharose and then incubated with constant concentrations

of HaloTag protein and varying HaloPROTAC. As the VHL purification procedure involves immobilization via a Glutathione S-transferase (GST) tag, the GST-VHL reagent was readily prepared by omitting the tag cleavage step. As shown in Figure 3.5A, upon incubation with different the HaloPROTAC compounds, certain conditions allowed association of HaloTag with the immobilized VHL. HaloPROTAC **9** was able to precipitate HaloTag protein whereas the shorter HaloPROTAC **8** was able to. The longer HaloPROTAC **10**, which shows degradation, slightly precipitated HaloTag but far less than HaloPROTAC **9**. Thus, this pulldown assay seems to provide a compelling picture for the difference between the three HaloPROTAC compounds.

While the results from the pulldown assay are compelling, we sought to validate this results through an orthogonal, more quantitative assay. Importantly, we sought to address whether any of the compounds were exhibiting positive or negative cooperativity[261]. Cooperativity, in this case, describes interactions between the two proteins bridged by PROTACs. Positive cooperativity, would refer to favorable protein:protein interactions, such as hydrogen bonding networks or hydrophobic interactions, whereas negative cooperativity would refer to unfavorable interactions such as steric clashes. The data from Figure 3.4A could be interpreted in multiple ways using this language of cooperativity. It could be that the precipitation seen with HaloPROTAC **9** is a non-cooperative interaction: exactly what we would expect from the affinity of the PROTAC for HaloTag and VHL, with no protein-protein interactions involved. In this case, HaloPROTAC **8** and **10** would show negative cooperativity: steric clashes between the two proteins. Alternatively, it could be that the results for HaloPROTAC **8** and **10** are examples of non-cooperative ternary complexes, and HaloPROTAC **9** is actually engendering protein:protein interactions which explain the enhanced precipitation.

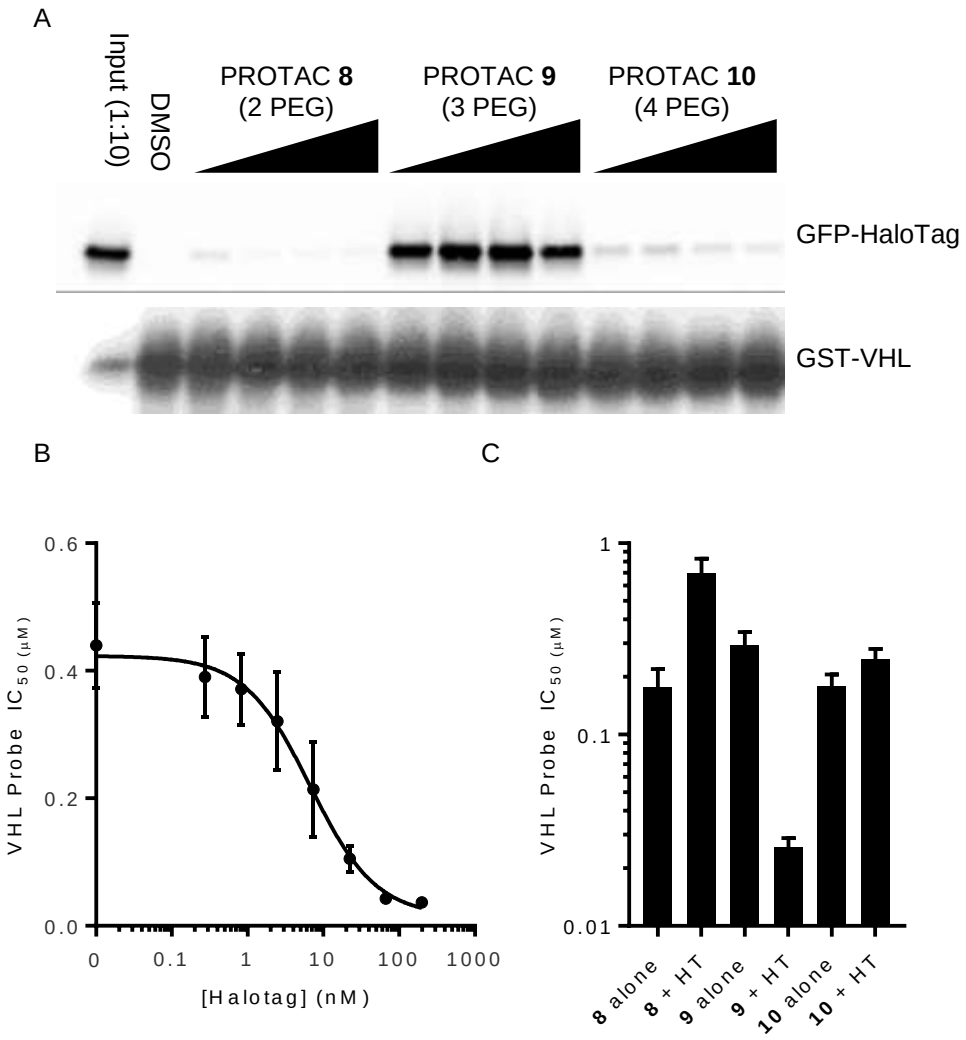

Figure 3.5 HaloPROTAC compounds form the ternary complex with different efficacies

(A) GFP-HaloTag protein was incubated with the various HaloPROTAC compounds and immobilized GST-VHL. After a two-hour incubation, the beads were washed extensively, proteins were eluted with SDS, and analyzed by western blot. The far-left lane is 10% of the total HaloTag protein included in all other reactions. (B) A high-throughput assay for determining ternary complex affinities. An ALPHALisa assay was developed using GST-VHL, a biotinylated VHL ligand, glutathione donor beads, and streptavidin acceptor beads. The biotinylated ligand can be competed away with HaloPROTAC **9**, and the IC_{50} for this reaction is shown on the Y-axis. Upon addition of HaloTag protein, the observed IC_{50} decreases. (C) The different HaloPROTAC compounds have different ternary complex affinities. The IC50 for VHL probe competition for compounds **8**, **9**, and **10** were measured either alone or in the presence of 2 μM HaloTag protein. Error bars in this figure represent Standard error of the mean of duplicate measurements.

To test between these hypotheses, we turned to an assay to measure the VHL affinity for the HaloPROTAC compounds. We hypothesized that the addition of HaloTag protein would make the HaloPROTACs increase or decrease the observed affinity if there was positive or negative cooperativity, respectively. To measure the affinity of the HaloPROTACs in the past, our lab has previously used a fluorescent polarization assay in which a labeled HIF-1α peptide was displaced by VHL ligands[213,214]. This assay is based on a high affinity peptide (with a K_D of ~180-500 nM[214]) and requires high concentrations of the peptide, which limits the ability of this assay to detect high affinity interactions.

For these reasons, we generated a biotinylated VHL ligand probe to perform an amplified luminescent proximity homogeneous assay (ALPHA). This probe bound to VHL with a K_D ~ 1 µM (data not shown). ALPHA is a proximity-based assay and, in this context, makes use of a donor-glutathione beads which immobilizes the GST-VHL, and a streptavidin acceptor bead, which immobilizes the biotinylated probe. When these components are mixed, the GST-VHL and bound biotinylated VHL ligand will cause the two beads to be brought into proximity[270]. Then, when the donor bead is stimulated with 680nm light, singlet oxygen will be generated which can diffuse in its limited lifetime from the donor to the acceptor bead. The singlet oxygen then reacts with chemical in the acceptor bead, eventually giving of light in the 500-600 nm range. When a competitive ligand is added to the reaction which binds competitively to the same site as the biotinylated ligand, the beads will not be brought into proximity, and the signal will drop. Because of the high sensitivity of ALPHA, protein and probe concentrations can be kept far below the K_D of the probe: an ideal situation for accurately determining affinities in competitive binding assays. With VHL and the probe at 30 nM, the ALPHA resulted in a signal to noise ratio >100, providing excellent sensitivity.

Competition of the probe with the HaloPROTAC **9** in the absence of any HaloTag protein yielded an IC_{50} of 290 nM, a value similar to that obtained previously[166]. Addition of HaloTag protein into the assay enhanced the ability of PROTAC **9** to compete with the probe (Figure 3.5B). At 200 nM HaloTag protein, the measured IC_{50} was 37 nM, an ~8-fold enhancement of affinity. These data clearly demonstrate positive cooperativity: HaloPROTAC **9** is orienting VHL and HaloTag in such a way as to engender favorable protein:protein interactions between the two proteins.

Next, the other HaloPROTAC compounds were analyzed with or without excess HaloTag. In order to ensure that negative cooperativity could be measured, a higher excess of HaloTag (2 µM) was used. In contrast to the positive cooperativity observed with HaloPROTAC **9**, the longer HaloPROTAC **10** showed little cooperativity: the affinity of the compound alone is 180 nM and in the presence of HaloTag it is 250 nM. In contrast, HaloPROTAC **8** displayed a high degree of negative cooperativity. Alone, **8** bound with an IC_{50} of 180 nM and with excess HaloTag it bound with a IC_{50} of 700 nM.

Based on these data, it seems that the differences between these compounds in cellular degradation assays are due to a difference in a ternary affinity. This affinity is distinct from the binary affinity of PROTAC:HaloTag or of PROTAC:VHL, as each of these compounds have nearly identical binary affinities. Despite this, the short linker of HaloPROTAC **8** disfavors formation of the ternary complex, likely because upon engagement of the alkyl chloride with HaloTag, the VHL ligand is insufficiently exposed for VHL to successfully bind. Indeed, it is possible that the forced high local concentrations of the VHL ligand and HaloTag actually cause the ligand to “stick” to the surface of HaloTag, enforcing energetic penalties to unbind and then engage VHL.

HaloPROTAC **9**, containing a linker of moderate length, orients the HaloTag protein with respect to VHL in such a way that interactions between the two proteins

stabilizes the ternary complex with respect to the individual binary species. This phenomena, positive cooperativity, leads to a heightening and widening of the bell-shaped association curve[261], and this is indeed seen in the lack of a hook effect in degradation assays[166]. Lengthening the linker, however, does not further increase the ternary affinity: rather it seems the longer linker positions the two proteins far enough away that no interactions exist. It is also feasible that the same conformation and protein:protein interactions present in HaloPROTAC **9** could exist for HaloPROTAC **10**, but that the longer linker must fold in on itself, enforcing an entropic cost. In this situation, perhaps the energetic gains of protein:protein interactions balances the entropic costs of ordering the linker, leading to an observed zero cooperative ternary complex.

These two assays for studying ternary complexes, the GST-VHL pulldown assay and the enhancement of competition via ternary complex, provide results that qualitatively match the degradation data: the best ternary complex leads to the best degradation, the worst ternary complex leads to the worst degradation, etc. However, it is surprising that a 12-fold decrease in ternary complex affinity between HaloPROTAC **9** and **10** (Figure 3.5C) and a near lack of association with VHL in the pulldown assay (Figure 3.5B) results in a very small change in degradation efficacy. The most dramatic change in degradation efficiency between these two compounds is an obvious hook effect with **10** but almost no increase in protein levels with increasing **9** (likely up to the limits of solubility; there should be a hook effect if concentrations increase far enough)[166]. The lack of a hook effect further supports the notion of protein:protein interactions broadening the ternary complex formation curve[261]. Although unlikely, perhaps the difference in activity between PROTAC **9** and **10** *in* vitro is unnecessary for additional *in cellula* activity. Additionally, perhaps the ubiquitin chains built by HaloPROTAC 10 are different and more efficiently recognized for degradation. Finally, the differences in the physicochemical properties of the two

compounds might also offset the ternary affinity gains (e.g. the higher affinity compound has poorer cell permeability). Incorporating these nuances into our understanding of PROTAC-induced ternary complex equilibria is an important future research goal.

Section 3.5: A structural analysis of the VHL:PROTAC:HaloTag Complex

Having shown that HaloPROTAC 2 forms a ternary complex in which favorable protein:protein interactions exist between VHL and HaloTag, we next sought to discover the residue-level detail of some of these interactions. Despite the high affinity of this ternary complex this complex was not amenable to crystallization across hundreds of conditions.

Because of this, we instead chose to pursue computational approach towards understanding these protein:protein interactions. To identify candidate interactions, we combined manual docking of the ternary complex and short molecular dynamics simulations to relax the model to a low energy state. Residues identified in this way were then mutagenized and the mutant protein was assessed for its ternary complex affinity. Because the initial docking is performed manually, several starting orientations were used to orient a hydrophobic patch on VHL with different hydrophobic patches on HaloTag. After MD simulations of these different starting conformations, the resulting ternary complex model was examined by eye as well as using the Protein Interfaces, Surfaces and Assemblies (PISA) web server[271]. This web service used an algorithm originally developed to analyze PDB files of protein complexes, distinguishing between genuine complex from crystallographic artifacts by assessing predicted thermodynamics of association for the complex. Using PISA, only two of the five conformations tested seemed reasonable and were further investigated (Figure 3.6A). These are referred to as conformer 1 and conformer 2. Both conformers 1 and 2 show extended buried surface areas of 1970 and 1822 $Å^2$ respectively.

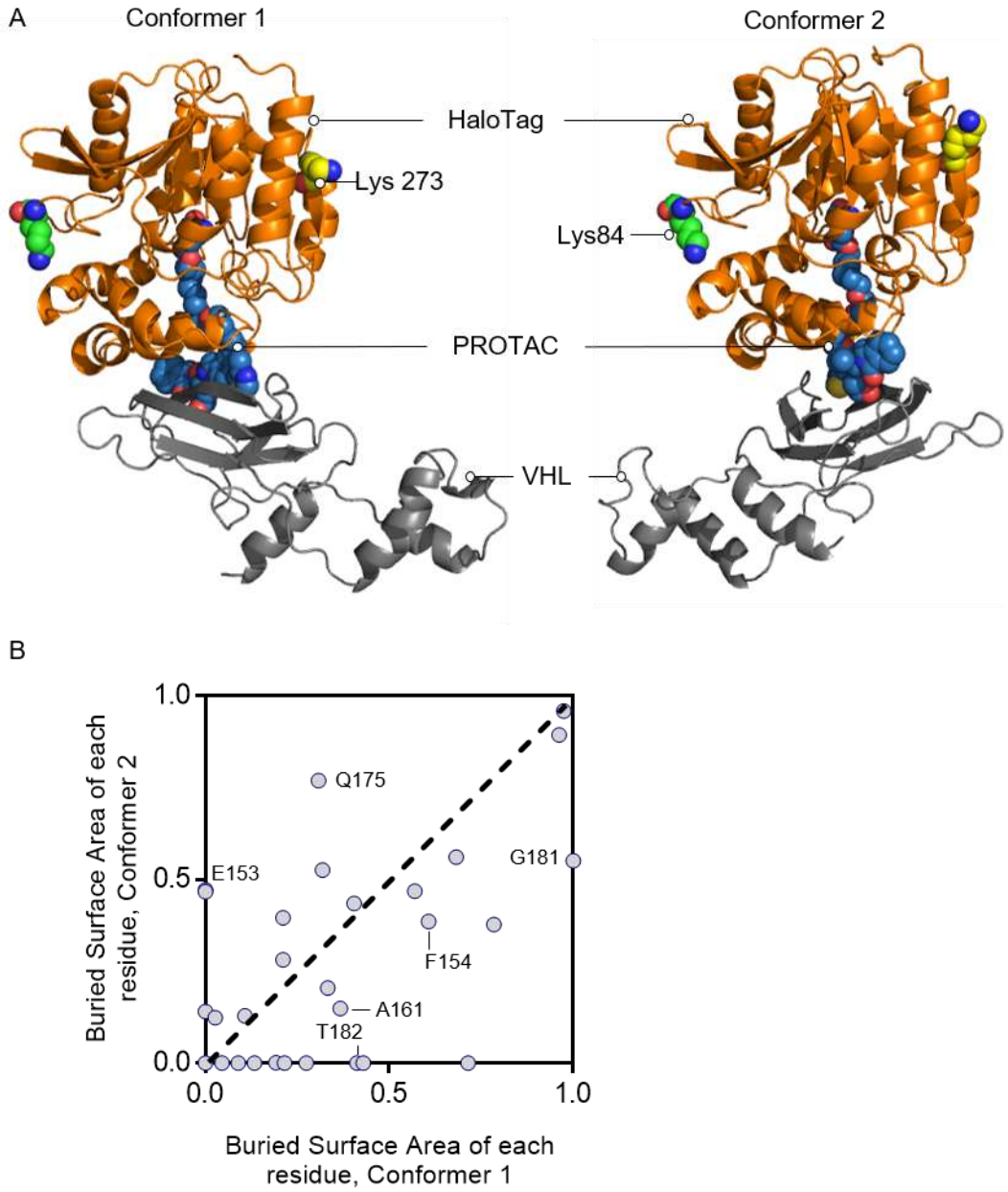

Figure 3.6 Molecular modeling of the ternary complex reveals potential interactions between VHL and HaloTag

(A) After manually docking the HaloTag and VHL proteins (PDBs 4KAF and 4W9H, respectively), short molecular dynamics simulations relaxed the structure into low energy conformations. Two such conformations seemed reasonable by manual inspection and analysis by the PISA web server (see text). HaloTag is shown in orange, VHL in gray, and HaloPROTAC 9 as blue spheres. The ubiquitinated lysine residues on HaloTag (273 and 84) are shown as spheres. The two conformations differ by a 180° rotation of the VHL protein relative to HaloTag. (B) PISA analysis of the buried surface area for each residue in the two conformers. For each residue in the interface, the percentage of available surface area for that particular residue is shown. The two conformers use distinct populations of residues for their interfaces, and residues selected for mutagenesis are labeled (see Figure 3.7 for mutagenesis results)

The most intriguing aspect of these two conformers is the relative orientation of HaloTag with respect to VHL and ubiquitinated lysine residues. While the GFP-HaloTag protein was ubiquitinated on many different residues, only two ubiquitinated residues were identified on HaloTag. Interestingly, these residues were on opposite faces of the protein and are shown as green (Lys84) and yellow (Lys273) spheres in Figure 3.5A. By orienting oneself to these two lysine residues, it is clear that VHL is rotated 180° between the different conformers and in each conformer exactly one of these residues is on the face of HaloTag most accessible to the E3 ligase. While it is unclear how much of the HaloTag surface might be accessible for ubiquitination in any given conformation, these two conformations might give access to different faces and increase the likelihood that both opposing lysines are ubiquitinated. This gave us an initial confidence that perhaps both conformers are relevant structures.

We next analyzed how similar the two conformers were relative to each other. Again, using the PISA web server, we were able to estimate how important each residue was to the different conformers. By calculating an available surface area for each residue and the percentage of that surface area which is buried in the interface, a residue-by-reside comparison between the different conformers was performed (Figure 3.6B). We hoped that this analysis would enable the design of mutants that would inhibit one conformer but not the other.

To test whether both conformations exist in solution, we sought to generate three different sets of mutants. The first set of mutants was designed to bias against conformer 1 without changing the binding properties of conformer 2 (Figure 3.7A). In conformer 1, threonine 182 of HaloTag forms a hydrogen bond with histidine 110 of VHL, and so this threonine was mutated to valine to disrupt hydrogen bonding while maintaining the size because the residue occupies a pocket in conformer 2. Additionally, phenylalanine 154 of

HaloTag interacts via pi-pi stacking with tyrosine 68 of VHL in conformer 1, whereas in conformer 2 Phe154 only interacts with other residues on HaloTag. This residue was mutated to Arginine to inhibit this pi-pi stacking and introduce bulk in the pocket only present in conformer 1.

A second set of mutants was generated to bias against conformer 2 (Figure 3.7B). Glutamate 153 of HaloTag makes a pair of hydrogen bonds with arginine 108 of VHL in conformer 2, but this residue is not making any contacts in conformer 1. We hypothesized that inverting the charge of this residue would inhibit this interaction and so the E153Q mutation was made. In a similar fashion, glutamine 175 of HaloTag forms hydrogen bonding contacts with the backbone of VHL around residues 98 and 99. Changing the charge was again employed with the Q175E mutation.

The third set of mutants were designed to target residues that are involved in both conformers (Figure 2.7C). Both alanine 161 and glycine 181 of HaloTag are buried in the interface between HaloTag, PROTAC **9**, and VHL in both conformers. Mutating either of these residues to arginine would introduce bulk that would likely not be accommodated by either conformer.

These six mutations were introduced by site directed mutagenesis, and the corresponding HaloTag protein was expressed and purified. To assess the ability of these mutant proteins to form the ternary complex, PROTAC **9** was again used to compete the VHL probe compound in the presence of 2 μM mutant proteins (Figure 2.7D). As before, HaloPROTAC **9** binds VHL with an IC50 of 290 nM which is decreased to roughly 40 nM

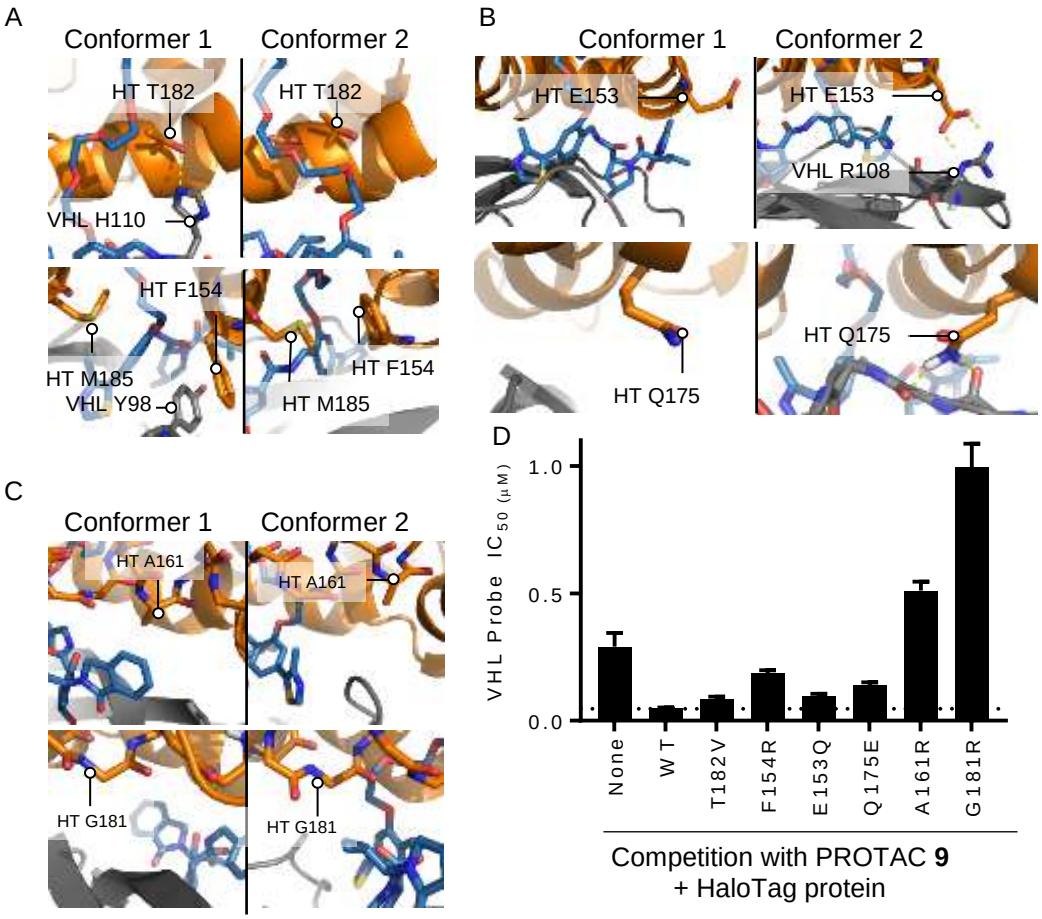

Figure 3.7 Mutagenesis of HaloTag protein disrupts the positive cooperativity seen with VHL and HaloPROTAC **9**

(A) Residues selectively involved in conformer 1. See text for a description of these interactions. (B) Same as A, but for conformer 2 selective residues. (C) Residues predicted to disrupt drastically disrupt both conformers. (D) Competition of VHL probe with HaloPROTAC 9 and wildtype (WT) or mutant proteins. GST-VHL and the biotinylated VHL ligand were incubated with 2 μM HaloTag protein (wildtype or mutants) and varying concentration of HaloPROTAC 9 for one hour, followed by developing the reaction with ALPHA beads specific to GST or biotin. Values represent the IC_{50} fitted to the data, and error bars represent the standard error for this fit.

in the presence of HaloTag protein. Both of the conformer-biasing sets of mutations modestly decreased the enhancement of **9** affinity, indicating that these residues were involved in the ternary complex but none of them were absolutely necessary. This is to be expected if multiple conformers are involved and each uses many multiple interacting residues. In contrast to these modest changes in affinity, the trimer null mutations (A161R and G181R) drastically changed the affinity of the ternary complex, raising the IC_{50} of HaloPROTAC **9** almost to the micromolar range. These values are higher than HaloPROTAC **9** alone, indicating negative cooperativity.

This mutational data provides further evidence that protein:protein interactions between VHL and HaloTag stabilize the ternary complex. Furthermore, as might be expected, the majority of the affinity for this complex arises from the PROTAC itself, and so multiple conformations for the ternary complex are possible. The conformer biasing mutants tested here seem to indicate that both conformers are present in solution, but it must be remembered that these conformers are generated via modeling and MD simulations. It is possible that a third conformation might exist which better explains the mutational data, as well as a third conformer in addition to the two explored here. Additional HaloTag mutants could also be generated, such as the union of the four conformer biasing mutants, to further explore the intricacies of this complex.

To summarize the first half of this chapter, the HaloPROTAC model system was used to ask a relatively simple question and have provided data towards a relatively simple answer. Question: what is the discriminating factor in the HaloPROTAC panel of compounds that explains why linker length is important for degradation? Answer: the compound of optimal linker length engenders protein:protein interactions between the HaloTag and VHL proteins. Using evidence from ubiquitination site mapping and novel

biophysical assays, the formation of the ternary complex is discriminating as opposed to a lysine selection model.

Section 3.6: Selective Protein Degradation with a Promiscuous Warhead

The first half of this chapter focused on a relatively small sample of PROTAC compounds but illustrated a powerful concept. At first glance, PROTACs may seem to be extremely simple: take a ligand for your target protein, a ligand for an E3 ligase, “linker” them together and the protein will be degraded. However, countless groups have found this not to be the case. Optimizing the linker step is non-trivial and often requires extensive time and resources. Upwards of dozens of non-functional PROTACs (and so perhaps a misnomer) are often generated before an effective compound degrades the protein of interest.

The idea that linker length control of protein degradation is due to protein:protein interactions also leads to an obvious hypothesis that different proteins would require different protein:protein interactions for degradation. Furthermore, if a PROTAC were capable of binding multiple substrates, it seems likely that they would not all be degraded, and those non-degraded would perhaps be unable to enter the ternary complex.

The second half of this chapter focuses on this question: if a PROTAC were designed to potentially degrade many different substrates, how many would actually be degraded, and would they all be capable of entering the ternary complex? To address this question, let us first examine the literature to understand what PROTACs may have already begun to address this question.

An initial observation that must be taken into account is the broad use of two different E3 ligases for PROTAC development. Von Hippel Lindau (VHL) is the substrate adapter for the Cullin 2 E3 ligase complex, inducing the potent and rapid degradation of its substrate HIF-1α[272,273]. As already discussed, our lab and others developed high affinity

ligands for VHL[213–215]. A second E3 ubiquitin ligase commonly used in PROTAC design is Cereblon (CRBN), which is the substrate adapter for the Cullin 4a ligase complex whose endogenous substrates have not been fully characterized, but likely include MEIS2 and glutamine synthetase[179,274]. The IMiD thalidomide and its analogs have been shown to bind to CRBN and induce degradation of several neosubstrate proteins [174,175,178].

Many PROTAC molecules have been developed to recruit these E3 ubiquitin ligases to a variety of substrates using high-affinity ligands for the protein of interest. Both VHL and CRBN have been employed to target a wide array of different protein classes. Kinases (RIPK2, BCR/Abl and Abl, Cdk9), Bromodomain proteins (BRD2, 4 and 9), nuclear hormone receptors (Era and ERRα), a transcription factor (pirin), and most recently receptor tyrosine kinases (EGFR, Her2, and c-Met) have all been effectively degraded by PROTACs[246–248,250,252,259,275–281]. In the majority of these cases, the PROTAC was designed with a single target in mind, and the degradation of that target alone was reported.

Based on these literature examples, one could assume that PROTACs developed from high-affinity ligands will induce efficient target degradation. Few literature examples, however, counter this assumption and perhaps change the scope of these questions. Previously, our lab investigated the ability of PROTAC molecules to degrade the endogenous kinase c-Abl and its oncogenic fusion form BCR/Abl[250]. Using several different kinase inhibitors conjugated to either VHL or CRBN ligands, we highlighted differences between these different E3 ligases and showed that target engagement alone was not sufficient for degradation. While the VHL-recruiting PROTACs were unable to degrade BCR/Abl, these compounds could reduce the amount of c-Abl protein levels. At the time we hypothesized the fusion protein was too large to engage with the ternary complex: that there was some cut-off for molecular weight or size above which VHL was

unable to degrade the target protein. In contrast to VHL's limited ability, CRBN was capable of degrading both c-Abl and BCR/Abl, possibly due to differences in the flexibility of the different Cullin-based E3 ligase complexes, though this largely remains to be tested[282–285].

A second set of examples are PROTACs designed to degrade bromodomain-containing proteins (BRD proteins) and illustrates a similar principle. Only one study has investigated VHL-recruiting and BRD-protein-degrading PROTACs, but this study revealed selective degradation of BRD4 over BRD2 and BRD3[279,280]. Another study used a very similar compound, with only a slightly shorter linker, and showed promiscuous degradation of all three proteins[259]. Again in contrast to VHL, CRBN-recruiting PROTACs seem to have a simpler relationship with BRD family proteins: if the PROTACs bind to it, it will be degraded[246–248]. No CRBN-recruiting PROTAC has been reported that degrade BRD-containing proteins with enhanced selectivity over the targeting ligand.

Based on these literature examples, the following questions were addressed more directly. What is the correlation, if any, between the affinity of a PROTAC for a target protein and the degradation of that target? To what degree are PROTACs (VHL- and CRBN-recruiting) capable of selective degradation with respect to the targeting warhead's binding profile? And, lastly, are VHL and CRBN equivalent in their degradation selectivity?

To address these questions, we sought to generate as large a dataset as possible by employing a promiscuous kinase inhibitor as the targeting warhead for PROTACs. Using whole cell proteomics, we indeed show selective degradation and that degradation of a protein is not predicted by the affinity of the PROTAC for that protein. Both VHL and CRBN share this lack of trend. Furthermore, we show that even proteins bound with low affinity can be potently degraded, and that protein:protein interactions within the E3:PROTAC:Target protein ternary complex explain this phenomena.

Section 3.7: Foretinib PROTACs Only Degrade a Subset of Bound Kinases

During our development of receptor tyrosine kinase PROTACs, we synthesized PROTACs based on the c-Met tyrosine kinase inhibitor foretinib[277,286]. Based on the crystal structure of foretinib bound to the c-Met kinase domain[287], we reasoned that the disordered and solvent-exposed morpholine of foretinib was dispensable for affinity, and so we used that phenyl ether as a linker attachment point for E3 ubiquitin ligase recruiting molecules. Both a VHL-recruiting PROTAC (compound **11**, Figure 3.8A) and a CRBN-recruiting PROTAC (compound **12**) were generated based on the foretinib warhead.

We first tested the ability of these compounds to degrade c-Met, the clinically relevant target of foretinib, in the triple negative breast-cancer cell line MDA-MB-231. Since triple-negative breast cancer cells have been shown to express ~75% of the kinome[288], they provide an excellent system to study the selectivity of PROTAC-induced degradation. Treatment of MDA-MB-231 cells for 24 hours with compounds **11** and **12** showed a decrease in the levels of c-Met protein as assessed by western blot (Figure 3.8B). To ensure that the degradation of c-Met was due to the induced ternary complex between the PROTAC, E3 ubiquitin ligase and c-Met, we generated negative control analogs of PROTACs **11** and **12** (Figure 3.8A): by inversion of the stereocenter on the hydroxyproline moiety of the VHL ligand or by methylation of the nitrogen on the glutarimide ring of pomalidomide, we synthesized compounds **13** and **14**, respectively. Neither of these compounds decreased c-Met levels across all concentrations tested.

Given foretinib's relatively promiscuous inhibition of multiple kinases, we sought to explore other potential targets of our compounds. First, using a high-throughput competitive binding assay (DiscoverX KinomeScan), we found that 10 μM foretinib binds to 133 different kinases with a percent of control (a value with inverse relationship to

A

11 - * = R Stereocenter - Active VHL PROTAC

13 - * = S Stereocenter - Inactive VHL Control

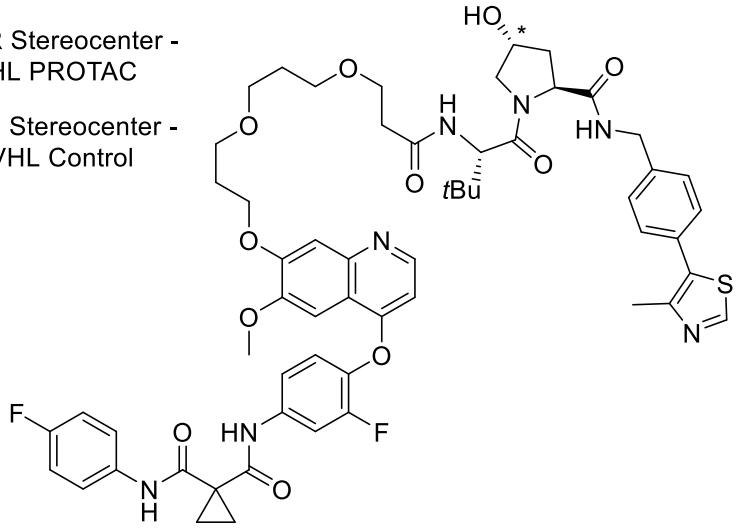

12 - R = H - Active CRBN PROTAC

14 - R = Me - Inactive CRBN Control

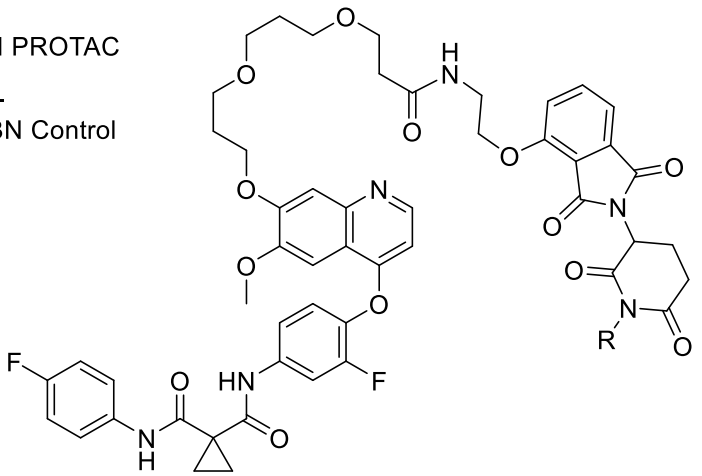

B

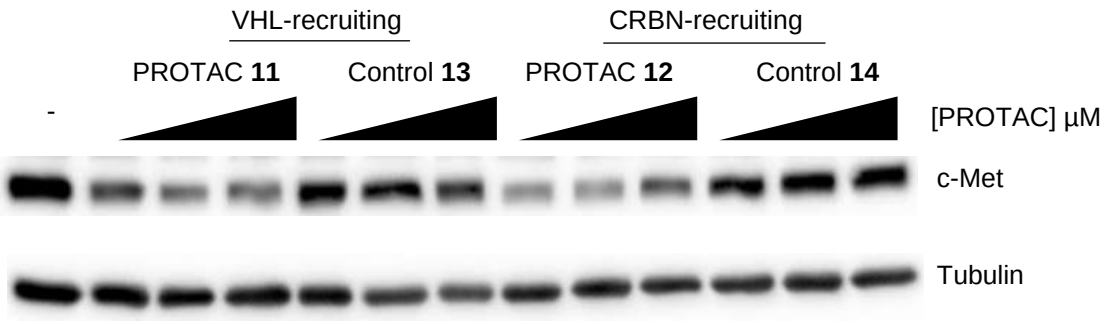

(from previous page)

Figure 3.8 CRBN- and VHL-recruiting PROTACs based on foretinib degrade c-Met.

(A) Structures of the foretinib-based PROTACs used in this study. Top is the VHL-recruiting PROTAC compound **11**. The stereocenter of the hydroxyproline VHL-binding element is R for the active PROTAC while it is S for the inactive control compound **13**. Bottom, the Cereblon-recruiting PROTAC compound **12**. The nitrogen atom of the glutarimide ring is non-methylated in the active PROTAC, while in the inactive control compound **14** it is methylated. (B) MDA-MB-231 cells were treated with the 100 nM, 1 µM, or 10 µM of compounds **11**-**14** for 24 hours, and c-Met and tubulin protein levels were analyzed by immunoblot.

affinity) value of 35 or less – the recommended cut-off to avoid false-positives for kinase-inhibitor pairs (Figure 3.9A)[289,290].

We first sought to address potential changes in binding affinity that result from the addition of a linker and E3 ubiquitin ligase-recruiting molecule to foretinib. Using a competitive binding assay (DiscoverX, KinomeScan), we tested the selectivity of compounds **11** and **12** at 10 μM across the human kinome and compared their binding profiles to foretinib (Figure 3.9B). We found that the addition of a linker and E3-recruiting moiety significantly changed the binding profile of the compounds. Compound **11** retained binding to 52 kinases while compound **12** bound 62 kinases (Figure 3.9B). Interestingly, the binding profiles of compounds **11** and **12** were not identical: even though the aspects of these compounds most proximal to the pocket (i.e. the linker attachment point and linker) are the same, the addition of a different E3-recruiting moiety changed the binding profile of each PROTAC (Figure 3.9C). For example, compound **12** retains binding to p38δ, but the VHL-recruiting PROTAC **11** does not. While conjugation of a linker and an E3-ligase recruiting element raises the selectivity of the PROTACs, both compounds retained binding affinity to a common set of 51 kinases, offering a large set of proteins with which to compare compounds **11** and **12** for their ability to degrade common target proteins.

Given that these PROTACs possess degradation capacity and retain promiscuous kinase-binding ability, we next sought to quantitatively assess their effect on the entire MDA-MB-231 proteome. We chose eight different treatment groups: a vehicle control, two concentrations of each PROTAC, and a high concentration of foretinib and each of the negative control PROTACs (Figure 3.10A). We used two concentrations of each PROTAC in an attempt to eliminate false-negatives due to the hook effect[261]. Negative control compounds were used in this experiment in order to eliminate proteins whose quantitation

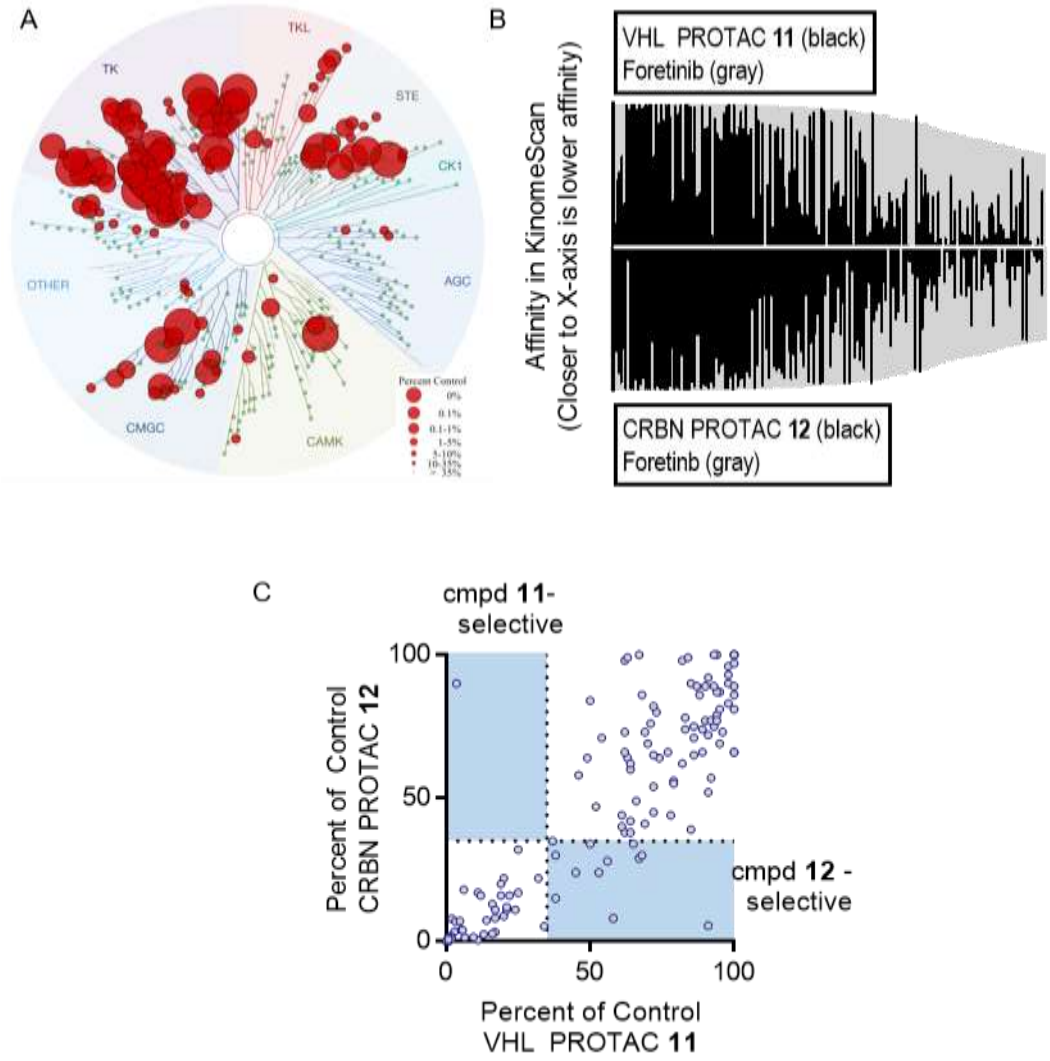

Figure 3.9 Foretinib-based PROTACs bind many protein kinases

(A) KinomeScan binding profile of foretinib. The competitive binding assay uses phage-displayed kinases bound to immobilized ATP-mimetics. The size of the red circles, overlaid on the kinase dendrogram, represent the percent bound of each kinase after competition with 10 μM foretinib, compared to untreated control. (B) The affinity for most kinases changes upon addition of the linker and E3-ligase recruiting element. Along the X-axis are the 133 kinases that are considered hits for foretinib (i.e. having a percent control value of 35 or less in KinomeScan data) sorted in order of decreasing affinity for foretinib. The values for foretinib are plotted in grey on both the positive and negative Y-axes. On the positive Y-axis, the values for compound **11** are plotted in black, while the negative X-axis has the values for compound **12**. (C) Comparison of the binding profile for the CRBN- and VHL-recruiting PROTACs. Percent of control for the VHL PROTAC **11** and the CRBN PROTAC **12** are shown on the X- and Y-axes, respectively. Dotted lines represent percent of control of 35, values below which constitute true kinase:inhibitor binding pairs.

is decreased due to transcriptional changes or destabilization by the inhibitor alone[222,291]. After a 24-hour incubation with each treatment condition, the cells were harvested, lysed under denaturing conditions, and proteins tagged for multiplexed isobaric labeling coupled to tandem LC/MS/MS[292,293]. 7,826 unique proteins were identified in parallel with a false discovery rate of less than one percent (Figure 3.10).

Based on the control compounds (foretinib, compounds **13** and **14**), we chose a protein abundance fold-change cut-off value of 0.8 when normalized to DMSO. That is, a protein must have been reduced by 20% or greater in order to be considered a *bona fide* degradation target. Using this cut-off and compiling the union of both concentrations of each PROTAC, we found that on a proteomic level, compounds **11** and **12** caused the down-regulation of 123 and 204 proteins, respectively (Figure 3.10B). If, however, the proteins which are also down-regulated by the respective negative controls (foretinib and/or the epimer control **13** for VHL PROTAC **11**; foretinib and N-methyl control **14** for CRBN PROTAC **12**) by more than 10% were filtered out, then only 36 proteins are degraded by compound **11** and 62 proteins are degraded by compound **12**. This more conservatively filtered set represents downregulation most likely to be caused through a *bona fide* PROTAC-induced mechanism of degradation. In total, 86 proteins were degraded by one or the other PROTAC, and only 12 were degraded by both.

To date, all published PROTAC molecules have been generated using ligands that have high affinity and fairly high selectivity for the protein to be degraded. Since a correlation between affinity and the extent of degradation might be assumed, we focused on those 54 kinases which are both foretinib targets and for which we had quantitative proteomics data (Figure 3.10B). These selected kinases possess a range of affinities for the two PROTACs and provide a large test-set of possibly degraded proteins. Surprisingly,

A

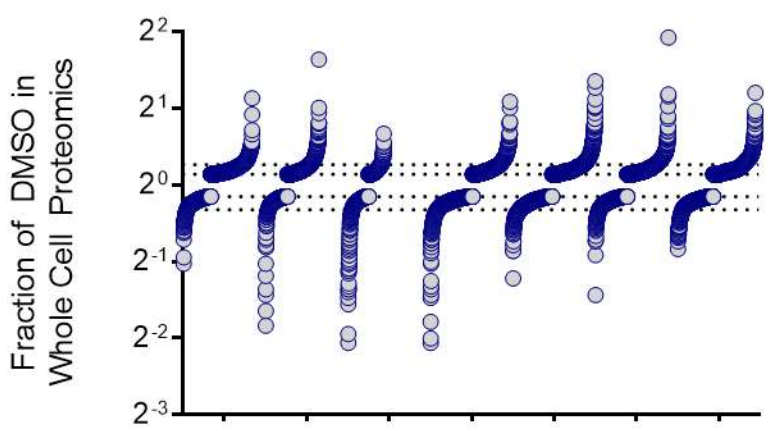

Compound	**11**	**11**	**12**	**12**	**for**	**13**	**14**
Concentration	.1 μM	1 μM	.1 μM	1 μM	1 μM	1 μM	1 μM
Proteins <0.9	500	394	380	774	719	571	638
Proteins <0.8	72	53	83	145	141	79	93

B

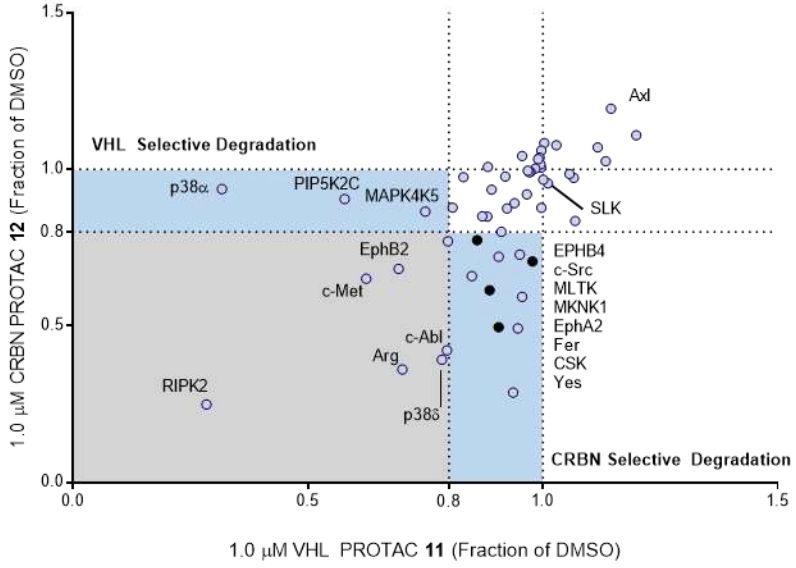

(from previous page)

Figure 3.10 Global proteomic changes caused by foretinib-based PROTACs

(A) Multiplexed tandem mass spectrometry was used to assess global changes in the proteome of MDA-MB-231 cells after treatment with foretinib-based PROTACs. After 24 hours with the indicated compounds, the cells were lysed and proteins levels were quantified. Among each treatment condition, the 7,000 quantified proteins are sorted in ascending order and dotted lines indicate changes ± 10 or 20%. (B) Comparison of proteomic changes after treatment with compounds **11** or **12**. Fraction of DMSO after treatment with 1 μM VHL PROTAC **11** (X-Axis) or CRBN PROTAC **12** (Y-axis) are compared for each of the 54 foretinib-binding kinases. Dotted lines indicate the 80% cutoff for degradation, and areas of selectivity for **11** or **12** are highlighted. The light blue dots indicate proteins that are degraded in PROTAC treatment and in the control compounds, and so are not classified as bona fide PROTAC targets.

we found that the degradation profile of each PROTAC was far more selective than the binding profile of foretinib. Of these 54 kinases, 9 were degraded by VHL PROTAC **11** and 14 were degraded by CRBN PROTAC **12,** with 6 of these kinases in common (Figure 3.10B).

Interestingly, for the 54 kinases tested, there was no correlation between the affinity of either compound **11** or **12** and the extent of PROTAC-induced degradation (Figure 3.11). Evident from this analysis are high-affinity pairs (SLK, Axl) that are not degraded by either PROTAC. Additionally, there are several pairs for which the kinase affinity is far above the percent of control cut-off for a *bona fide* binder, yet the kinase is still efficiently degraded. The most dramatic example of this is p38α, which has a percent of control of 78, yet is efficiently degraded by PROTAC **11** (Figure 3.11A). Based on these observations, we conclude that the extent of degradation of a target by a PROTAC does not necessarily correlate with the PROTAC's affinity for that target. In our dataset, a compound-kinase pair with a higher affinity interaction was no more potently degraded than one with lower affinity.

To confirm this relationship, or lack thereof, we more carefully analyzed the affinity and degradation profiles of 12 different kinases, sampling kinases that were degraded as well as kinases that despite high affinity for either PROTAC were not degraded in our quantitative proteomics dataset. To confirm the proteomics dataset, western blotting was performed on each of the 12 kinases against a dose response of each compound. The DC_{50} and D_{max} were calculated by densitometry. In most cases, the western blot data confirmed the proteomics dataset (Figure 3.12A and B). C-Abl and Arg were decreased by 30% by compound **11** in the proteomics dataset, but showed no degradation by this compound by western blot. Despite this, both proteins were degraded by compound **12**

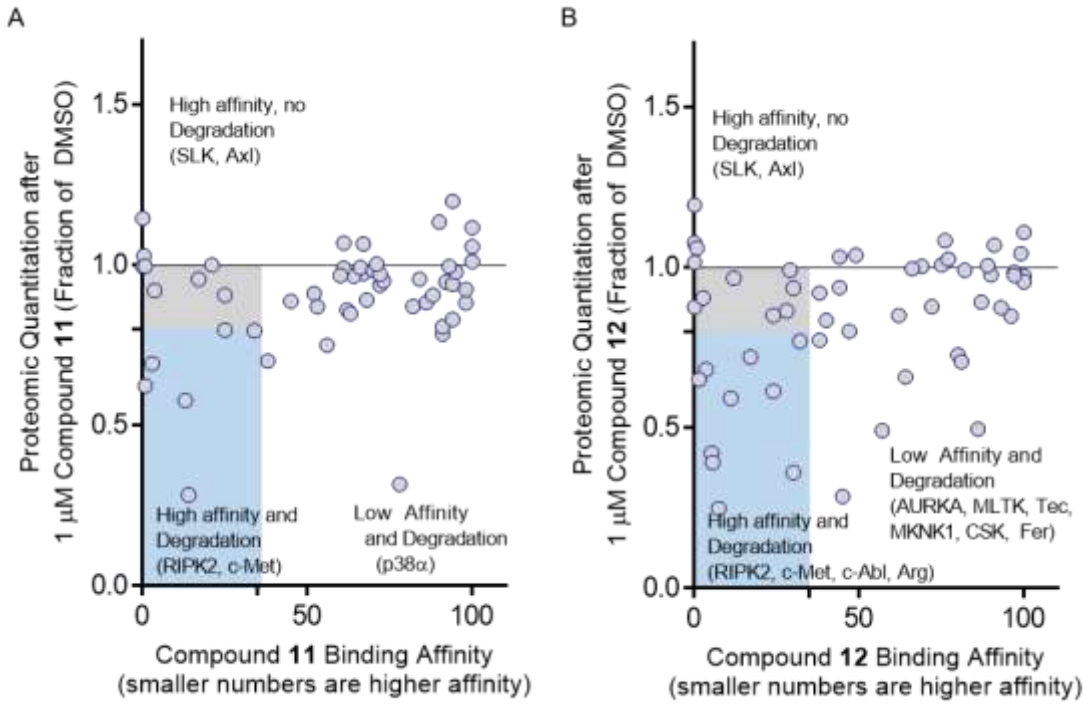

Figure 3.11 Degradation efficiency and PROTAC affinity do not correlate

(A) Comparison of the binding affinity and degradation efficiency of VHL PROTAC **11**. The X-axis shows the percent of control of phage-displayed kinases after incubation with 10 µM PROTAC **11**; lower numbers represent high affinity binding. The Y-axis shows the protein levels of each kinase after treatment with 1 µM PROTAC **11** normalized to DMSO. The light blue box highlights proteins which bind foretinib (percent of control < 35) and are degraded (percent of DMSO < 80). (B) Same as in (A), except for CRBN-PROTAC **12.**

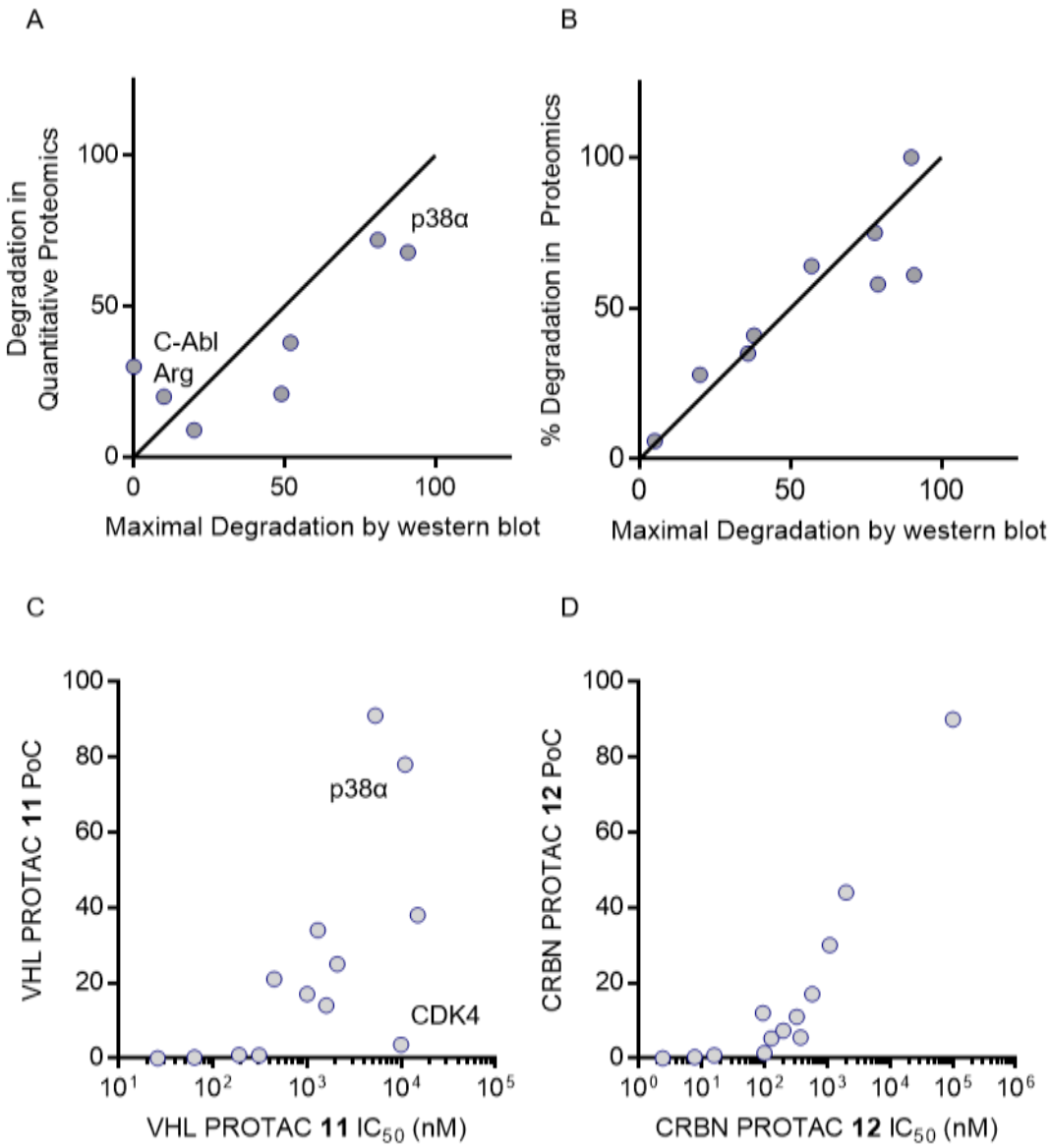

Figure 3.12 More robust characterization of the degradation and affinity of twelve foretinib-PROTAC targets

(A) Comparison of degradation methods. The X-axis is the D_{Max} of VHL PROTAC 11 for various kinases, as assessed by western blot over several concentrations. The Y-axis shows the extent of degradation observed in quantitative proteomics after treatment with 1 μM **11**, normalized to DMSO. (B) Same as in (A), except for CRBN PROTAC **12**. (C) Comparison of affinity determined between single- and multi-point competitive binding analyses. The X-axis shows the concentration at which 50% of the kinase is still bound. The Y-axis shows the percent of bound kinase after treatment with 10 μM **11**, compared to control. Lower numbers on both axes represent higher binding affinity. (D) as in (C) but for the CRBN PROTAC **12.**

using both techniques, illustrating the importance of secondary confirmation of proteomic datasets. To more accurately determine the affinity for each kinase, a dissociation constant (K_D) was determined using multi-point, competitive binding (KinomeScan). The K_D for almost all cases correlated well with that determined from the single point percent of control measurement discussed above (Figure 3.12C and D). The only exception is CDK4: this kinase bound to VHL PROTAC **11** with 100% inhibition in the single-point experiment yet had a K_D of 10 µM (compare this to c-Met with 100% and K_D of 310 nM).

Using these more robust degradation and affinity measurements, the dose responsive changes in protein levels varied for each kinase-PROTAC pair and did not correlate with the affinity of the kinase for the PROTAC. With high affinity for both PROTACs **11** and **12,** MerTK and RIPK2 reached more than half-maximal degradation at the lowest concentration tested (30 nM) and demonstrated a hook effect at higher concentrations. Strikingly, the VHL- and CRBN-recruiting PROTACs show differential selectivity towards the p38-MAPK family. While p38α and p38δ homologs share 61% sequence identity, they were differentially degraded by the VHL- and CRBN-recruiting PROTACs. p38δ was slightly degraded (~30%) by VHL PROTAC **11**, while it was almost completely degraded by the CRBN PROTAC **12** (DC_{50}=27nM, D_{max}=91%). Contrary to this, the VHL-recruiting PROTAC **11** degraded p38α potently (DC_{50}=210nM, D_{max}=91%), yet compound **12** was unable to degrade p38α.

Section 3.8: A stable ternary complex between VHL and a potential substrate is required for degradation

We were surprised to see p38α efficiently degraded by VHL PROTAC **11** with a DC_{50} value (210 nM) that is far lower than its binding affinity (K_D = 11 µM). Furthermore, additional experiments support a *bona fide* PROTAC-based mechanism, despite low binding capacity: 1) proteasome inhibition rescues PROTAC-induced p38α degradation, 2) p38α

protein is degraded rapidly within 12 hours of PROTAC treatment, 3) PROTAC **11** rapidly accelerates the basal half-life of p38α from an hour to a minute timescale, and 4) p38α mRNA levels do not change after 24 hours of PROTAC **11** treatment (Figure 3.13 and data not shown).

Based on the previous results studying HaloTag, we next hypothesized that favorable protein:protein interactions between a target protein and a recruited E3 ligase could compensate for a weak target:PROTAC affinity and thus drive target degradation. Conversely, unfavorable protein:protein interactions might impede target protein degradation and might explain why the high-affinity kinase-PROTAC pairs we observed were not degraded.

To assess the contribution of ternary complex formation, we first used GST-tagged VHL as bait to trap potential ternary complex members in the presence of PROTAC. We elected to use excess VHL as bait, rather than co-immunoprecipitation with endogenous VHL, to avoid false negatives due to competition between potential substrates. When a whole cell lysate from MDA-MB-231 cells was incubated with different concentrations of compounds **11** or **13** and the immobilized VHL bait, interactions for several kinases were detected (Figure 3.14). Endogenous Cullin 2 was precipitated equivalently across all samples. Encouragingly, we found a strong correlation between those proteins that stably interacted with VHL and those that are degraded. Kinase:PROTAC pairs that are not degraded, such as SLK and CDK4 (K_D's of 450 nM and 10 μM), show no detectable enrichment in the presence of PROTAC, indicating that these kinases are not able to form a ternary complex likely due to steric clashes. In contrast, proteins that are degraded (c-Met, RIPK2, p38α with K_D's of 310 nM, 1.6 μM, and 11 μM, respectively) are capable of forming a stable complex with VHL only in the presence of the active PROTAC**11** and not in the presence of control **13**.

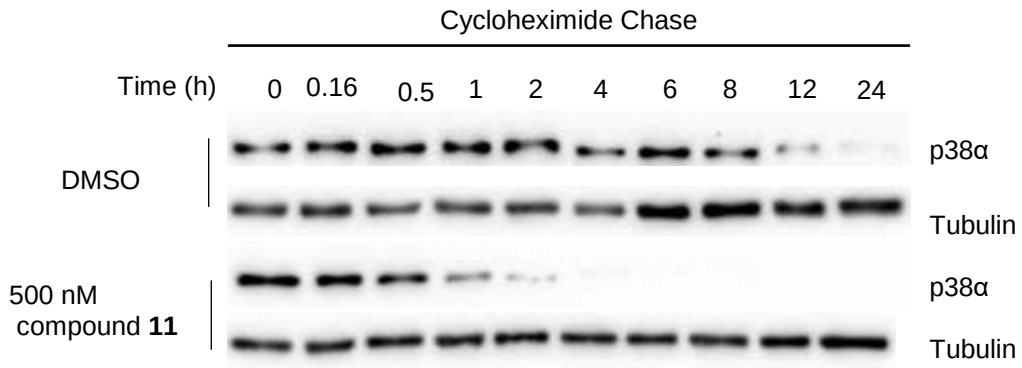

Figure 3.13 p38α protein levels are decreased post-translationally by PROTAC **11**

After a one-hour treatment with 100 µg/mL cycloheximide to block translational activity, MDA-MB-231 cells were treated with DMSO or PROTAC **11** at 500 nM. Cells were harvested at the indicated times, and protein levels of p38α and tubulin were analyzed by western blot.

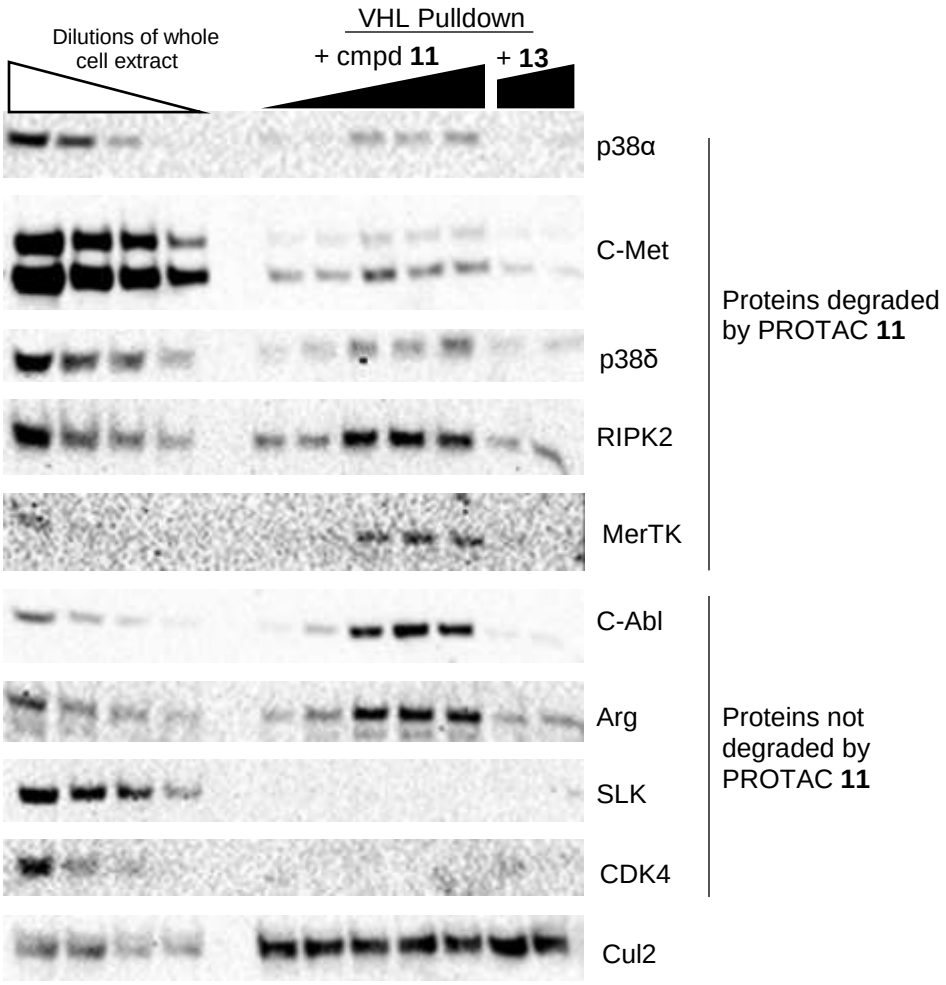

Figure 3.14 Immobilization of PROTAC induced ternary complexes

MDA-MB-231 cell extracts were incubated with the indicated compounds and GST-VHL immobilized on sepharose beads. The beads were then washed extensively, and precipitated proteins were eluted with SDS and analyzed by western blot. Concentrations of compound **11** employed are 300 nM, 1 µM, 3 µM, and 10 µM; compound **13** was used at 1 and 10 µM.

Intriguingly, VHL-recruiting PROTACs do not induce degradation of either c-Abl or Arg despite a stable interaction in the presence of PROTAC **11**. This corresponds to our previous work on PROTACs targeting c-Abl[250]. In that study, we found that VHL-recruiting PROTACs that incorporated imatinib or bosutinib were unable to degrade c-Abl despite robust target engagement, whereas dasatinib-based PROTACs degraded c-Abl well. Regardless, the added results here that non-degrading PROTACs are still capable of inducing a stable ternary complex is surprising. The biophysical basis for these results require further study, and possible hypotheses are discussed below.

Given the paradoxical ability of PROTAC **11** to bind weakly to p38α yet induce a high affinity interaction between p38α and VHL, we sought a molecular understanding for how p38α forms a high-affinity PROTAC-induced ternary complex with VHL. To do this, we used a similar strategy as HaloTag, docking previously published structures of p38α and VHL with the PROTAC **12** and using short molecular dynamics simulations to relax the structure into a low energy conformation. This model revealed a vast protein-protein (800 $Å^2$) interaction surface between p38α and VHL.

According to the model, the linker region of VHL PROTAC **11** must adopt a kinked conformation in order to accommodate protein-protein interactions between VHL and p38α. Arginine 69 of VHL provides close, hydrophobic contacts to the linker region while alanine 40 of p38α is poised to accommodate both Arg69 of VHL and the kinked linker of the PROTAC (Figure 3.15A). To experimentally validate this model, we mutated Ala40 to either lysine or valine, predicting that the former would abrogate any favorable protein-protein interactions while the latter would not. Using purified p38α protein in either a luminescent proximity assay (ALPHALisa) or the VHL pulldown assay, we found that the

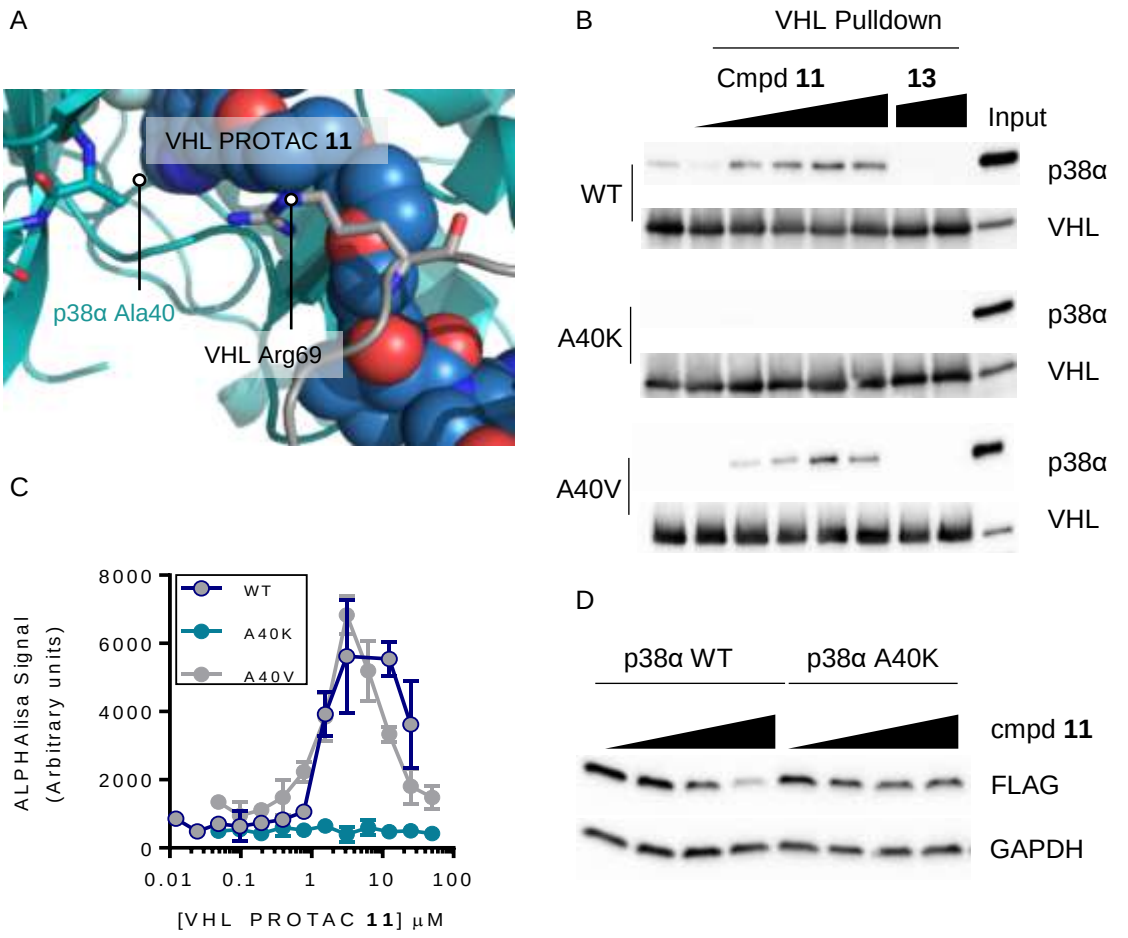

Figure 3.15 Initial characterization of the p38α:PROTAC **11**:VHL complex.

(A) A crystal structure of p38α (PDB code 1W82) and VHL (PDB code 4W9H) were manually docked and relaxed using a short molecular dynamics simulation. In this structure, the linker of PROTAC **11** kinks and forms a small cavity into which alanine 40 of p38α fits. Large substitutions at position 40 would be expected to disrupt the ternary complex. (B) A VHL pulldown assay was performed using purified p38α (wildtype (WT), A40K, and A40V mutants) and GST-VHL. Compound **11** was used at 100 nM, 250 nM, 500 nM, 1 μM, or 5 μM. Compound **13** was used at 1 or 5 μM. (C) ALPHA-based assessment of the ternary complex. p38α and GST-VHL were incubated with various concentrations of PROTAC **11**, followed by developing the reaction with glutathione donor and anti-His_6 acceptor beads. Data shown represent standard error for the mean of triplicate measurements. (D) FLAG-tagged p38α (wildtype (WT) or A40K mutant) were overexpressed in HeLa cells, followed by a 24-hour incubation with PROTAC **11**. After incubation, cells were lysed and protein levels of FLAG-p38α and GAPDH were analyzed by western blot. Concentrations used are 30 nM, 300 nM, or 3 μM.

A40K mutant has no ability to form a stable ternary complex, while the A40V mutant has roughly equivalent ternary complex formation as wildtype underscoring the highly specific interactions that occur within PROTAC-induced ternary complexes (Figure 3.15A and B). Each of these mutations do not greatly decrease the protein's stability or kinase activity, nor does the A40K mutation abrogate binding to VHL PROTAC **11** (data not shown). Finally, when p38α is overexpressed in HeLa cells, the wildtype protein is efficiently degraded by VHL PROTAC **11**, whereas the A40K mutant shows no degradation (Figure 3.15D). This indicates that ternary complex formation is necessary for PROTAC-induced degradation of p38α.

Section 3.9: Discussion

The goal of this chapter has been to explain a phenomenon that has delayed and frustrated many medicinal chemistry efforts to generate PROTACs. Why do some PROTAC molecules – containing a binding portion for an E3 ligase and a substrate protein connected by a flexible linker – not degrade their target proteins? Two systems were used to address this question. The first asked why the HaloTag protein was differentially degraded by three HaloPROTAC compounds of different inker length. The second system used a promiscuous kinase inhibitor-based PROTAC and asked why it was unable to degrade every protein that it bound to.

Initial hypotheses focused on a lysine selectivity model. Under this theory, a PROTAC positions a substrate protein so that lysine residues on the protein are positioned in a three-dimensional volume in which the E3 ligase complex is capable of ubiquitinating. Linker length control, then, would imply extremely precise lysine selectivity of the E3 ligase: if a difference of three atoms is capable of completely changing the degradation profile in a pair of PROTACs, then the ligase has a tightly defined ubiquitination zone. An unsettling suggestion from this idea would be that some proteins would not have a lysine

that *could* be positioned in this zone, and so would be undruggable by even PROTAC technologies.

The actual answer to the question of linkerology, however, likely expands the classes of proteins that can be degraded, rather than limiting it. The data shown indicates that PROTACs are capable of positioning substrate proteins such that residues at the interface of the substrate and E3 ligase begin to interact and stabilize the ternary complex with respect to the binary species. At first, this seems surprising: two random proteins are suddenly forming stabilizing interactions? The idea is less untenable when considering that the majority of the binding interaction would be due to the PROTAC forming interactions, with a relatively minor contribution from the protein:protein interactions. From the HaloPROTAC **9**:HaloTag:VHL ternary complex, the HaloTag protein reduces the K_D of HaloPROTAC **9** for VHL from 290 nM to 30 nM. This amounts to a change in the free energy of binding from -37.3 kJ/mol to -42.9 kJ/mol. This 5.5 kJ/mol of energy is roughly the energy of a hydrogen bond, or dozens of square angstroms of hydrophobic interactions.

Changing one's thinking on PROTACs to include protein:protein interactions moves PROTAC molecules into an already existing class of small molecules. While the concept of using protein:protein interactions has been employed in other contexts[262,294,295], the most closely related class would be Immunomodulatory Imide Drugs (IMiDs) such as thalidomide and its derivatives. These compounds bind to CRBN, but function by remodeling the surface of the protein to then bind and ubiquitinate additional protein targets[174–176,181,296]. The key distinction between these compounds and PROTACs is that IMiDs would have no detectable binding to the protein to be degraded in the absence of CRBN. The finding that PROTAC **11** binds only weakly to, but potently degrades, p38α is surprising. Additionally, like the targets degraded by IMiDs (transcription factors, kinases,

and translational termination factors), the p38α example opens the door to new classes of PROTAC targets: those with only weak ligands available.

Many potential drugs fail clinically or even earlier due to a lack of potency. And even larger pool of failed chemical probes failed to garner interest because of modest or weak affinity to their targets. Here, PROTACs may reignite interest in these near-misses, if PROTACs could be designed to engender protein:protein interaction which would stabilize the ternary complex. Key to this approach would be the development of high throughput assays to study the ternary complex[297]. In this chapter, three techniques for studying the ternary complex are presented. The pulldown assay, which can be used with either purified proteins or a whole cell extract as an input, is useful for qualitatively determining what proteins form the ternary complex, and could likely be adapted for a proteomic-level study of selectivity. Competition of the VHL probe compound by PROTACs, and corresponding enhancement with a ternary complex, provides a quantitative measure of protein:protein interactions and can be used to determine cooperativities. ITC has also been used to this effect, but at much lower throughput[280,298]. Lastly, the ALPHA-based proximity measurement provides sensitive and direct detection of the ternary complex without the washing steps of the pulldown assay. Furthermore, this assay is easily run in 384-well plates, and so can likely be used for screening large panels of compounds for their ability to form the ternary complex[248].

While these assays can be used as high-throughput readouts of the ternary complex, design principles also must be generated for synthesizing PROTACs that stabilize the ternary complex. Likely the most useful data for this would be structural and atomic-level understanding of the ternary complex. Recently, a crystal structure of a VHL:PROTAC:Brd4 ternary complex was solved, which revealed protein:protein interactions similar to those discussed here[280]. The authors took this further and used this

information to design a new molecule with a novel linker geometry and enhanced degradation selectivity towards the desired target protein over closely related isoforms.

With these structural studies deepen our understanding of PROTAC-induced ternary complexes, it is possible to envision that future PROTACs may not look much like current PROTACs at all. For example, it is clear that the VHL-binding moiety of HaloPROTAC **9** actually interacts with HaloTag itself: one can envision modifying the VHL ligand portion of the molecule to specifically enhance the HaloTag ternary complex. The linker could similarly be modified. Under this thinking, a PROTAC is no longer made of distinct binding entities, but rather the entire molecule is designed to stabilize a particular ternary complex.

It must be noted, however, that the exact necessity and sufficiency of the ternary complex is not fully understood. This is highlighted most notably by the fact that c-Abl and Arg form a ternary complex quite well with VHL and PROTAC **11**, and yet are not degraded (Figures 3.12 and 3.14). The reasons for this are not entirely clear, but several hypotheses can be proposed. First, these examples could illustrate the importance of lysine selectivity, if the ternary complex that forms has no lysine residues in an accessible ubiquitination zone. As discussed above several times, this seems unlikely. Second, perhaps the ternary complex is *too* stable: to be degraded, the target protein needs to dissociate from the E3 ligase for threading into the proteasome and degradation and perhaps a *too stable* ternary complex inhibits this. Again unlikely, but possible, especially given c-Al and Arg were the most enriched in the pulldown experiment. The most likely hypothesis, given our lab's difficulty in degrading c-Abl[250], is that something inherent to the protein is manipulating the ubiquitin proteasome pathway. Phenomena inherent to c-Abl require further study, and will be more fully discussed in chapter 4.

Overall, this chapter aids in our understanding of how PROTACs work and give clear principles for making more potent PROTACs. There are still open areas of investigation in terms of the understanding of PROTAC biochemistry, and answers to these questions will provide even greater insight into the design and application of PROTAC molecules. This chapter provides a compelling reason to understand basic biochemical and biophysical processes in order to optimize and apply therapeutic modalities.

Chapter 4

Drugging the Undruggable:

Broadening the Applications of Targeted Protein Degradation

Preface

The work in this chapter is unpublished and performed largely by me. Dr. George Burslem and Hervé de Laborde synthesized all of the ROR2 ligands. Dr. George Burslem also synthesized the BCR/Abl PROTACs. The RPPA data was collected by the MD Anderson RPPA core facility. Data generated from patient Leukemic Stem Cells was collected by members of the laboratory of Dr. Brian Druker (Oregon Health and Science University).

The preceding two chapters introduced major technical and conceptual advances in proteolysis targeting chimera or PROTACs. Whereas previous iterations of these compounds were limited by potency and cell permeability, these next generation PROTACs are relatively small, highly specific, and capable of degrading their target proteins at nanomolar concentrations. Furthermore, the driving factor for determining degradation for many PROTACs seems to be their ability to form a ternary complex with the E3 ligase and the target protein.

However important technological advancements are, these advancements have thus far only produced tool compounds. The deepened understanding is of, in some sense, an artificial system. This chapter, aims to go further than just looking at PROTACs but instead to questions that PROTACs can help answer. Chapter one introduced two of these questions. The first deals with BCR/Abl and possible kinase independent roles of the protein that maintain leukemic stem cells. More generally, are PROTACs advantageous in their ability to degrade the entire protein rather than inhibiting one single domain of a protein? The second question for this chapter deals with ligand development for pseudokinases. These proteins have interesting roles in disease, but few have been druggable. Though small molecule ligands for pseudokinases may be ineffective in their own right, they can yet provide targeting warheads for PROTACs. This section will focus on the pseudokinase ROR2 as well as a new platform for the development of pseudokinase ligands.

In that this chapter asks more questions than it answers, it provides a framework for moving forward with PROTAC compounds. This new and improved tool allows researchers to ask more questions that might not have been explored fully in the past.

Section 4.1: Targeting BCR/Abl Kinase Independent Roles

As summarized in chapter one, the BCR/Abl tyrosine kinase has been an exemplar of the benefits and drawbacks of the “kinase-only” paradigm. First described in the late 1980s as a tyrosine kinase resulting from the Philadelphia chromosomal translocation of chromosomes 9 and 22, BCR/Abl is the causative agent for >95% of all cases of chronic myelogenous leukemia (CML). At the time, CML was a deadly disease where the only treatments available were cytotoxic chemotherapy or autologous bone marrow transplants. In 2002, the tyrosine kinase inhibitor imatinib was approved by the FDA for the treatment of CML and has shown remarkable clinical efficacy. This was the first example of an inhibitor selective enough to halt cancer’s progression without inhibiting the entire kinome leading to deleterious side effects. CML is now a lifelong, manageable disease[299].

Despite the success of tyrosine kinase inhibitors, imatinib and related drugs are not curative in CML. Very few patients ever reach complete molecular response in which no BCR/Abl mRNA can be quantified in the patient’s blood. Thus, most patients have some residual disease and withdrawal of imatinib or TKI treatment from these patients often leads to rapid relapse of the disease[87]. Current thinking attributes this relapse to the presence of BCR/Abl-expressing hematopoietic stem cells (leukemic stem cells or LSCs) which despite complete inhibition of BCR/Abl kinase activity are kept in a quiescent state but are not killed[88]. There is currently much debate on whether these LSCs are entirely independent of BCR/Abl, or if there are non-kinase roles of BCR/Abl which drive the persistence of these cells. Possible molecular explanations for this are discussed in chapter one.

In this section, several chemical tools to study non-kinase roles of BCR/Abl will be discussed. Briefly, compound **5**, the thiazolidinedione compound used to target ERRα for

degradation in chapter two, will be discussed in more detail. PROTACs based on **5** showed the strange off-target degradation of BCR, and so their effect on BCR/Abl activity is explored further. Next, more potent BCR/Abl PROTACs are introduced, their ability to inhibit non-kinase functions of BCR/Abl are discussed, and preliminary results from patient-derived LSCs are presented.

Section 4.2: Targeting BCR/Abl by Direct Inhibition of BCR

In chapter two, the ERRα-degrading PROTAC **6** was assessed for its selectivity across MCF7 proteomes. The only protein degraded beside ERRα was BCR. This selectivity was encouraging, but the off-target of BCR was surprising given that no binding to this protein had been investigated before and there doesn't seem to be sequence or domain homologies between the two proteins. Because no chemical probes exist to target the BCR portion of BCR/Abl, we sought to validate and investigate the effects of this compound on BCR/Abl-driven leukemias. Almost all experiments in this section are performed in the K562 cells line, which are p210 BCR/Abl expressing cells taken from a 53-year old woman in CML blast crisis in 1970[300].

Confirming the whole cell proteomics experiment, PROTAC **6** decreased levels of a ~150 kDa band immunoreactive with a BCR antibody, while the control **7** had no effect (Figure 4.1A). There was a slight decrease in BCR/Abl levels with the PROTAC, but, surprisingly both compounds **6** and **7** decreased pSTAT5 levels. This is surprising given that the c-Abl kinase domain is typically attributed with the ability to phosphorylate STAT5 and no data has implicated BCR in this process. Regardless, it has been hypothesized that the BCR fusion increases this repertoire to include additional proteins crucial to oncogenesis, STAT5 included[85,301,302].

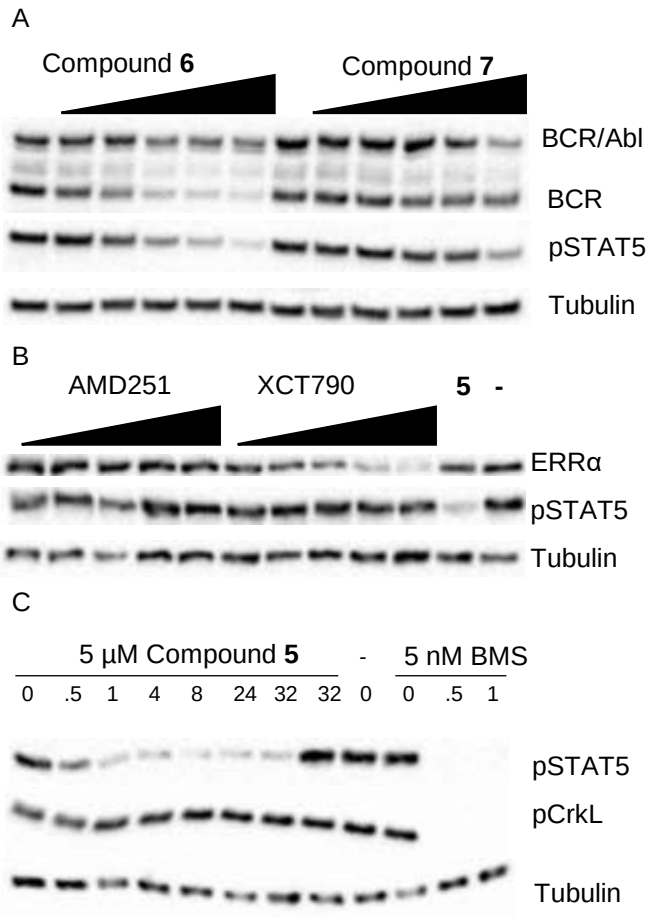

Figure 4.1 Compound **5** inhibits pStat5 through an unknown mechanism

(A) The ERRα-targeting PROTACs decrease BCR/Abl levels. The ERRα-targeting PROTAC **6** and negative control **7** were incubated with K562 cells for 16 hours, followed by analysis of the indicated proteins by western blot. (B) ERRα antagonism is not sufficient for pSTAT5 antagonism. The ERRα antagonists XCT790 and AMD251 and compound **5** were incubated with K562 cells for 16 hours. ERRα levels were decreased with XCT790, but this is not sufficient for pSTAT5 inhibition. Concentrations used were 5 μM for **5**, and a three-fold dilution series starting at 10 μM for XCT790 and AMD251 (C) Compound 5 decreases pSTAT5 levels rapidly without affecting pCrkL levels. 5 nM dasatinib (BMS) or 5 μM compound **5** were incubated with K562 cells for the indicated times, followed by analysis of the indicated proteins by western blot.

Given that control compound **7** was capable of decreasing pSTAT5 levels, we sought to determine if the parent ligand also had this ability. Indeed, treatment of K562 cells with 5 μM **5** decreased pSTAT5 levels by 80% (Figure 4.1B). In contrast, structurally dissimilar ERRα antagonists (XCT790 or AMD251) do not decrease pSTAT5 levels, indicating that this effect is not owing to ERRα degradation or antagonisn[303]. Furthermore, the decrease in pSTAT5 is rapid, occurring on roughly the same time scale as Dasatinib treatment (Figure 4.1C), and is not concomitant with a decrease in pCrkL levels. This indicates that it isn't a general BCR/Abl kinase inhibitor and that the effect is not via destabilization of total STAT5 as has been observed for the structurally related thiazolidinedione pioglitazone[92].

From these data, several conclusions can be drawn about the mechanism for the decrease in pSTAT5 levels by Compound **5.** First, this compound is not a general BCR/Abl kinase inhibitor. Given that pCrkL and pERK levels are not affected, the BCR/Abl kinase is still active. Second, the effect is not dependent on the ERRα-binding ability of **5**, given that structurally dissimilar compounds that are even capable of degrading ERRα do not affect levels of pSTAT5. Third, while a structurally similar compound (pioglitazone, another thiazolidinedione) has been shown to decrease total STAT5 levels on a day time-scale, compound **5** reduces pSTAT5 levels within one hour, indicating a distinct mechanism of action.

Much more cannot be said at this time about the actual mechanism for how compound **5** decreases pSTAT5 levels. As a result of the fusion to BCR, the c-Abl gains the additional substrate STAT5, and different BCR/Abl isoforms (differing only in the BCR portion) have different kinase activities and phosphoproteomic outcomes[102,103]. Thus, the BCR portion of the fusion protein may act a as a recruitment element for new substrate, bringing proteins such as STAT5 into proximity of the hyperactive c-Abl kinase. Compound

5, which can be assumed to bind the BCR portion (as assessed by degradation, Figure 4.1A), may therefore bind to the BCR portion and block recruitment of STAT5. This is an intriguing hypothesis, but lies outside the scope of this discussion and would require biophysical characterization of the binding between compound **5** and BCR as well as the interaction between STAT5 and BCR.

Section 4.3: Degrading BCR/Abl with Allosteric Site PROTACs

While targeting the BCR portion of BCR/Abl through traditional inhibitors may provide interesting insights into its molecular functions, the most direct way to inhibit all functions of BCR/Abl would be through PROTAC-induced degradation. Our lab has previously published a series of compounds with differing abilities to degrade BCR/Abl and was one of the first and most comprehensive studies on the importance of choosing a proper E3 ligase, targeting warhead, and linker[250].

This study highlighted how the chemical design of PROTACs had drastic outcomes on degradation of BCR/Abl. This is most striking with respect to the choice of targeting warhead. Three different warheads were used: imatinib, dasatinib, and bosutinib. No imatinib-based PROTACs were capable of degrading either c-Abl or BCR/Abl, despite modest degradation with geometrically similar PROTACs based on the dasatinib or bosutinib. The best dasatinib-based, VHL- or CRBN-recruiting PROTACs are summarized in Figure 4.2. We reasoned that these dasatinib-based PROTACs were not potent enough to study BCR/Abl kinase independent roles, and preliminary studies suggested that these PROTACs were similar to their negative control analogs in stem cell proliferation assays (data not shown).

The working hypothesis for the difference between imatinib and dasatinib/bosutinib was that the former is a type II inhibitor whereas the latter are type I inhibitors. Because

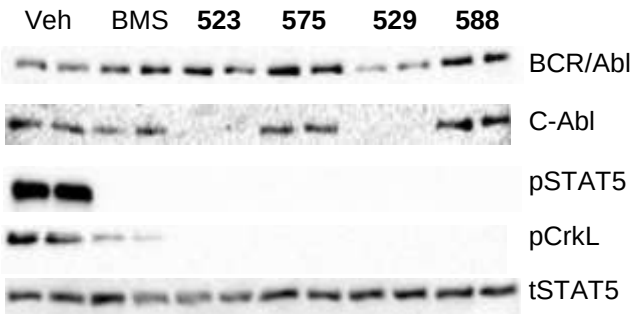

Figure 4.2 Modest degradation of c-Abl and BCR/Abl by dasatinib based PROTACs

K562 were treated with the indicated compounds for 16 hours. Vehicle (Veh); 5 nM dasatinib (BMS); 250 nM VHL-dasatinib PROTAC (**523**); 250 nM VHL negative control (**575**); 1 µM CRBN-dasatinib PROTAC (**529**); 1 µM CRBN negative control (**588**). These compounds have previously been published[250].

the conformation of the kinase domain is different between these two types of inhibitors[73], perhaps this altered conformation inhibits the ability of the kinase to associate with the ternary complex (similar to the findings of chapter three) or the ability of the E3 ligase to ubiquitinate accessible lysine residues. This naturally led to the search for different targeting warheads that might afford more potent degradation of BCR/Abl.

In 2006, allosteric inhibitors of BCR/Abl were reported. In c-Abl, an N-terminal myristoyl group binds to an allosteric pocket near the catalytic cleft of the kinase domain and auto-inhibits the protein kinase activity[304,305]. Upon activation of c-Abl, the myristoyl group is liberated and the kinase becomes active. This auto-inhibitory mechanism is absent in BCR/Abl, but the allosteric pocket remains. In a high-throughput screen for cellular toxicity, the GNF-series of compounds discovered. This compounds bind competitively with a myristoylated peptide but non-competitively with imatinib or ATP[306]. Further biochemical and structural data indicating that the most potent allosteric inhibitor, GNF-5 (Figure 4.3), bound in the myristoyl-binding pocket of c-Abl and stabilized the inactive state of c-Abl[307]. GNF-5 inhibits BCR/Abl dependent phosphorylation of STAT5 with an IC50 ~250 nM.

We first synthesized the GNF-5-targeting, VHL-recruiting compound **15** and found that this compound showed modest degradation of BCR/Abl or c-Abl in K562 cells, despite inhibition of BCR/Abl indicating that the compound was able to diffuse into cells and engage the target (Figure 4.4A). Changing to an ether-based linkage to the GN-5 moiety and reducing the length of the linker by 1 atom (compound **16**), a 5-fold increase in potency was observed (Figure 4.4B). Next, by moving the linker attachment point from the meta to the para position (compound **17**, Figure 4.4C), a 50-fold increase in potency was observed, yielding a DC50 of ~100 nM and near complete degradation at 1 µM. This is a

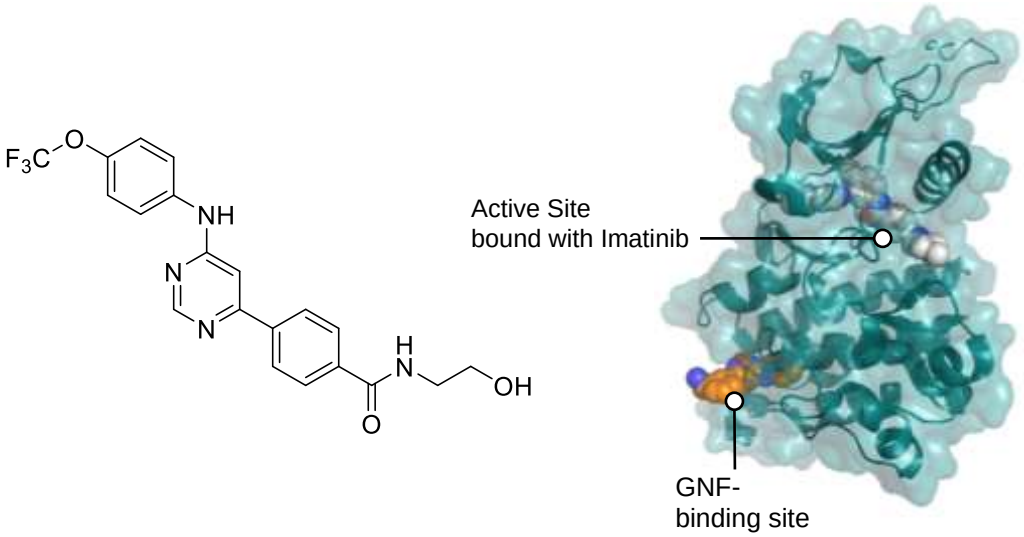

Figure 4.3 The BCR/Abl inhibitor GNF-5 binds in an allosteric pocket

The chemical structure of the BCR/Abl allosteric inhibitor GNF-5 is shown to the left, while the crystal structure of bound imatinib and GNF5 reveal that the allosteric site is on the opposite face of c-Abl kinase domain (PDB 3K5V).

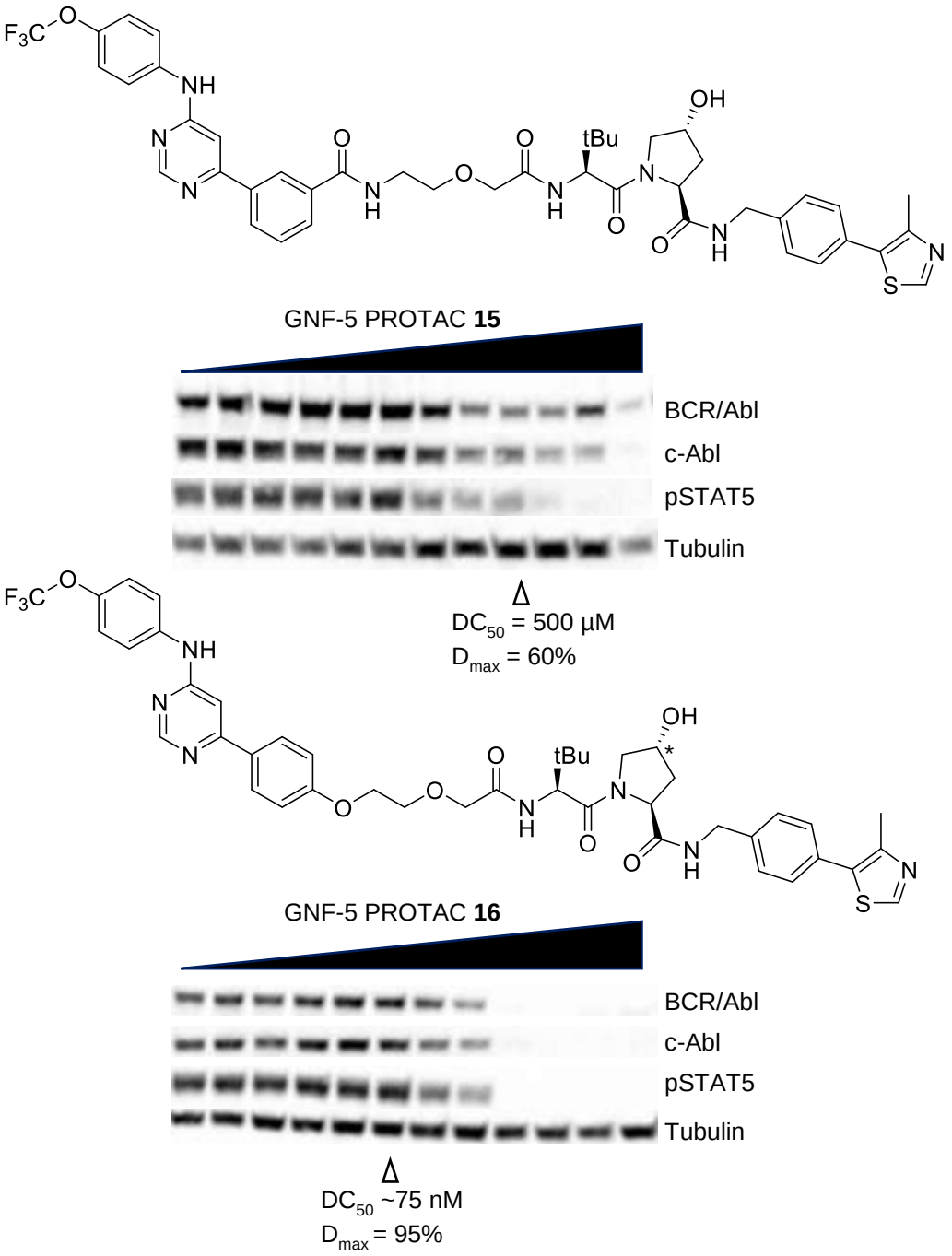

Figure 4.4 Optimization of GNF-5 based PROTACs for BCR/Abl

Top, PROTAC **15** designed to recruit VHL to the allosteric site of BCR/Abl. After a 16-hour treatment with **15**, levels of the indicated protein were assessed by western blot. Bottom, the improved allosteric-targeting PROTAC **16**, tested in the same way. PROTAC **17** is the negative control designed by inverting the indicated stereocenter on **16**. Concentrations of compound used are 0, 1 nM, 3 nM, 10 nM, 30 nM, 100 nM, 300 nM, 1 µM, 3 µM, 10 µM, and 30 µM.

vast improvement on previously reported BCR/Abl degrading compounds[250]. The control **18** was also synthesized by inversion of the stereocenter in the VHL moiety: this compound does not degrade BCR/Abl across any concentration tested (data not shown).

Section 4.4: Why are allosteric PROTACs more potent at degrading BCR/Abl

Next, we sought to understand why allosterically targeting PROTACs were so much more potent than the dasatinib series published previously. Because VHL was unable to degrade BCR/Abl, despite target engagement and concomitant degradation of c-Abl, we assumed that VHL was unable to accommodate the added bulk of BCR/Abl: perhaps the protein was just too big to fit into the E3 ligase complex. Recruiting VHL to BCR/Abl via the allosteric site might change the orientation in which BCR/Abl associates with the complex, and so allows for degradation.

To assess this hypothesis, we performed a ternary complex experiment akin to that used in chapter three. A whole cell extract of K562 cells was incubated with immobilized VHL and different concentrations of the best dasatinib-based, VHL-recruiting compounds from our previous manuscript, as well as the new allosteric compounds **17** and **18**. As seen in Figure 4.5, the dasatinib PROTAC **523** was capable of efficiently forming the ternary complex, whereas the negative control compound **575** had little ability to do so. In contrast, the GNF-5 PROTAC **17** had far less ability to precipitate BCR/Abl or c-Abl, although the signal of BCR/Abl relative to input is consistent with previous potent PROTACs (see for example, Figure 3.14 in chapter three). In summary, these results indicate that the ability of these PROTACs to form a ternary complex is not predictive of degradation.

Why are dasatinib-based PROTACs unable to degrade BCR/Abl? With the surprise that ternary complex formation isn't sufficient for degradation, new explanations

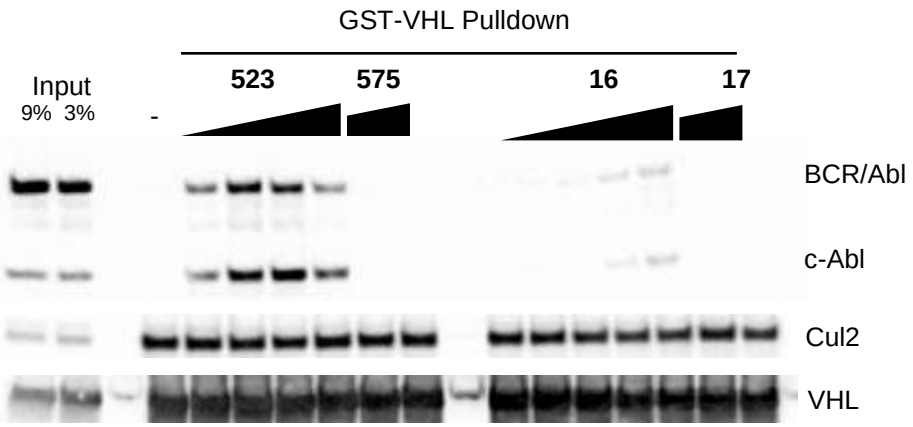

Figure 4.5 Allosteric PROTACs do not form the ternary complex better than dasatinib-based PROTACs

K562 cell extracts were incubated with the indicated compounds and GST-VHL immobilized on sepharose beads. Precipitated proteins were washed extensively and eluted with SDS. Concentrations of compound were 30 nM, 100 nM, 300 nM, and 1 µM for **523** and **16**; 100 nM and 1 µM for **575** and **17**. VHL-dasatinib PROTAC (**523**); VHL negative control (**575**) are compounds published previously[250].

are required. A first hypothesis might indicate the ternary complex is too stable: that perhaps BCR/Abl is being ubiquitinated but it's association with the E3 ligase inhibits its association with and threading into the proteasome. However, a deeper look at the data indicates this is not the case: if one compares the relative amount of protein precipitated in Figure 4.5 with the input, it appears that c-Abl actually associates more strongly with VHL in the presence of **523** than does BCR/Abl. c-Abl is the protein degraded. It therefore appears that excessive stability is not an answer.

A second hypothesis would, again, revolve around the accessibility of lysine residues to the E3 ligase. As discussed and evidenced in chapter two, this seems a surprising hypothesis given the promiscuity of lysine residues typically ubiquitinated by E3 ligases and the relatively small linker differences in PROTAC structures. In this context, however, the differences in PROTAC geometries could be quite stark: the ATP-binding cleft and allosteric site lay on different faces of the c-Abl kinase domain and so might allow entirely different faces of BCR/Abl to be ubiquitinated. Furthermore, it has been shown that BCR/Abl associates with different E3 ligases and de-ubiquitinating enzyme or DUBs[264,308,309]. Thus, it is possible that BCR/Abl exists in a dynamic ubiquitination state equilibrium, in which chains are constantly being added and removed. Perhaps the allosteric PROTAC allows ubiquitination on a face of the protein which is inaccessible by DUBs and so the ubiquitin chain builds rapidly in contrast to chains built by active site PROTACs. Conversely, perhaps the allosteric PROTAC builds on pre-existing chains placed by previous E3 ligases.

Overall, the potent degradation of BCR/Abl by GNF-5-based PROTACs is mysterious, and the prevailing theory of ternary complex formation does not offer a satisfactory explanation. Other examples in which ternary complex formation is not sufficient have been demonstrated in the lab, and these provide interesting avenues for

further research. Not only will these examples shed light on PROTAC biochemistry, but they might reveal underappreciated aspects of endogenous biology.

Section 4.5: Investigating Kinase Independent Functions of BCR/Abl

With more potent, GNF-5-based PROTACs against BCR/Abl in hand, we next sought to generate hypotheses for what non-kinase functions might be inhibited with these PROTACs. To do this, we sought a low-cost assay in which multiple signaling pathways could be assess simultaneously. Such an assay could perhaps identify pathways which are changed in the presence of PROTAC **17** treatment but not in the presence of the negative control **18**.

Reverse Phase Protein Array (RPPA) fulfills some of these requirements and has been used in the context of CML before[310]. This system is fundamentally a multiplexed western dot blot. Cellular extracts are printed onto separate nitrocellulose blots which are then probed with hundreds of different antibodies. The cost of the analysis is kept low because hundreds of extracts can be screened in parallel. A prior study used this technique with LSCs and found candidate genes upregulated in the different stages of CML progression[310].

We prepared K562 cells treated for 8 hours with PROTAC, as this time point gives almost complete degradation (Figure 4.6A). Furthermore, this early timepoint is likely to limit discovery to primary effects of BCR/Abl degradation rather than secondary or tertiary effects. Samples were then sent to the MD Anderson Cancer Center for RPPA analysis with 304 different monoclonal and the signal was quantified. Figure 4.6B shows a comparison of the fold change for PROTAC **17** treatment on the X-axis and fold change for the inactive control **18** treatment on the Y-axis.

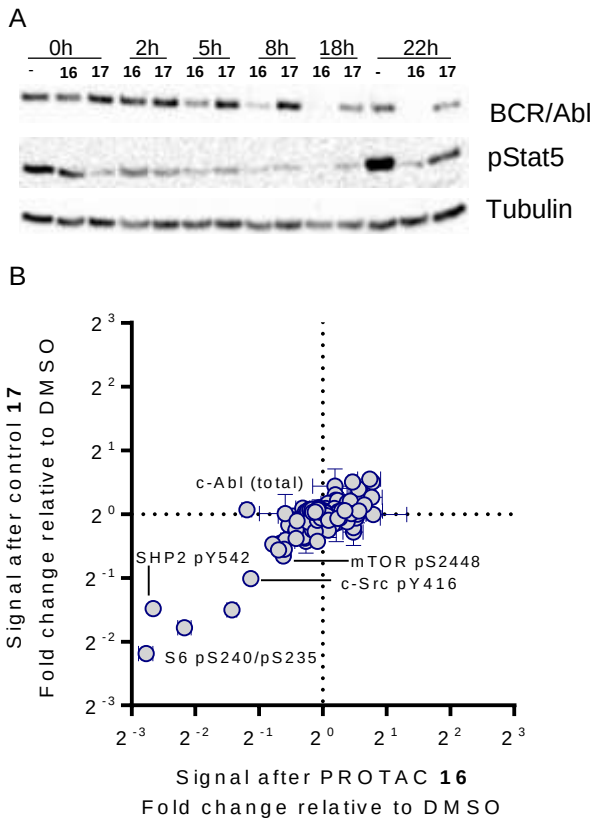

Figure 4.6 Unbiased analysis of effects caused by BCR/Abl degradation and inhibition

(A) Time Course of BCR/Abl Degradation. K562 cells were treated for the indicated times with vehicle or VHL PROTAC **16** or VHL control **17** at 5 µM. Cells were lysed and protein levels were analyzed by western blot. (B) Reverse Phase Peptide Analysis after BCR/Abl degradation or inhibition. After an 8-hour treatment with vehicle and 5 µM of PROTAC **16** or control **17,** cells were lysed and submitted to the RPPA facility at the MD Anderson Cancer Center. The comparative binding of 304 antibodies to the whole cell extracts was assessed, and the change relative to DMSO for compounds **16** and **17** are shown on the X- and Y-axes, respectively. Analytes of interest are labeled. Error Bars represent standard error of duplicate samples.

Analytes that fall on Y=1 would be those that are unchanged by control **17** treatment. Importantly, c-Abl is decreased by 50% upon treatment with PROTAC **16**, indicating that very few off-target proteins are degraded by the PROTAC. Another set of analytes were increased slightly by **16** but unchanged with **17**. Cell cycle regulators such as total p21 and total CDK1 were both increased, as has been reported before[311]. STAT3 and STAT5 proteins were also increased upon BCR/Abl degradation. Both of these proteins are selectively phosphorylated by BCR/Abl p210 relative to p185, and so functions other than the kinase domain of BCR/Abl are certainly relevant to these STAT proteins[101].

Several signaling pathways were affected by both compounds, indicating that these effects are due to inhibition of BCR/Abl kinase activity. For example, mTOR, PDCD4 and pS6 levels were all decreased by both compounds and have been previously described as being part of the same BCR/Abl signaling axis[312–314]. Interestingly, the effects on mTOR have been reported to be secondary: inhibition of BCR/Abl kinase activity stimulate AKT signaling, leading to an upregulation of mTOR levels which in turn affects pS6 and PDCD4. Even though these early time points were chosen to see degradation-dependent effects, inhibition occurs within 2 hours (Figure 4.6A) and so secondary effects of this sort are possible. However, the relative signs of these changes were inconsistent between literature reports and the RPPA data, and there was also no change in pAKT levels. Another profoundly decreased analyte was the phosphatase SHP-2, which is phosphorylated by BCR/Abl and is an important transforming factor in the progression of CML[315]. Finally, pSrc Tyr416, on the activation loop of c-Src, was also decreased by both compounds **16** and **17**. BCR/Abl has not been reported to phosphorylate c-Src on this site before, indicating this is perhaps an interesting new interaction.

Overall, a clear picture does not emerge from this data. Certain of these pathways should be investigated more carefully to see if the changes observed here are *bona fide* and relevant to the mechanisms of BCR/Abl leukemogenesis. Furthermore, two drawbacks are inherent to this strategy. First, whereas non-kinase roles of BCR/Abl are contested in LSCs, there is no doubt that inhibition of BCR/Abl is able to efficiently induce apoptosis in blast phase cells such as K562. For that reason, it is possible that inhibition of BCR/Abl kinase activity would activate pathways in these cells that would mask more subtle changes that might be associated with relevant non-kinase roles. Second, the sampling of antibodies in the RPPA set is rather limited and unlikely to be representative of the entire phosphoproteome. Another approach to survey transcriptional changes after perturbation (e.g. degradation of BCR/Abl) uses 1,000 different RNA transcripts and faithfully represents 81% of the transcriptome[4]. This approach of the "connectivity map" may yield deeper information and connections between BCR/Abl degradation and specific signaling pathways.

Section 4.6: BCR/Abl degradation in Leukemic Stem Cells

To address whether degradation of BCR/Abl by Compound **16** was able to eliminate LSCs, we initiated a collaboration with Brian Druker, a renowned leader in the understanding and treatment of CML. The Druker lab has access to samples of freshly CML cells from freshly diagnosed patients. In the experiments that follow, bone marrow from a patient with newly diagnosed CML in blast phase was used to isolate LSCs.

Previous studies have indicated that the CML stem cell population resides in the CD34+CD38- fraction of cells, and so we isolated this population of cells and first evaluated the ability of PROTACs to degrade BCR/Abl and inhibit downstream signaling. As seen in Figure 4.7A, compound **16** degraded BCR/Abl and c-Abl with similar efficacy

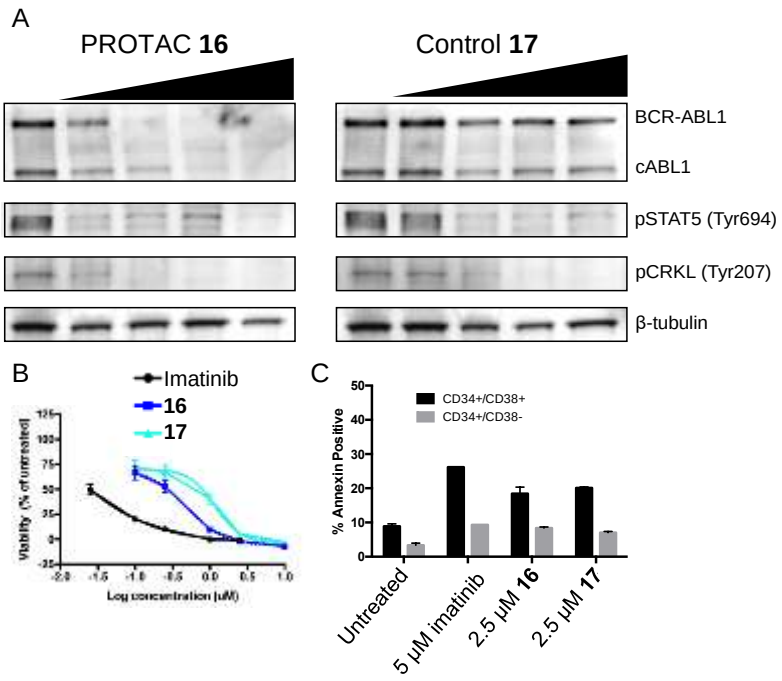

Figure 4.7 PROTACs degrade BCR/Abl in leukemic stem cells and cause apoptosis

(A) From a newly diagnosed patient with chronic myelogenous leukemia, leukemic stem cells ($CD34^+CD38^-$) were isolated and treated with the indicated compounds overnight. Both compounds were used at 250 nM, 1 µM, 2.5 µM, or 10 µM. The indicated protein levels were then assessed by immunoblot. (B) Bulk $CD34^+$ (Stem and progenitor populations) were treated with various concentrations of imatinib, PROTAC **16**, or control **17**. After 72 hours, cell viability was assessed by MTS assay according to manufacturer's instruction. Data shown are the mean of quadruplicate measurements. (C) Induction of apoptosis by PROTACs. Leukemic stem and progenitor cells were isolated and treated with the indicated concentrations of compounds. After 72 hours, the cells were stained with Annexin V and sorted to determine the percent of cells undergoing apoptosis. These data were generated by members of the Druker Lab.

as in K562 cells. The negative control **17** had no effect (especially if the signal is normalized to the tubulin loading control). Encouragingly, both compounds were able to inhibit the kinase activity of BCR/Abl as assessed by pSTAT5 and pCrkL.

We next assessed the ability of imatinib and these compounds to inhibit cell viability and induce cell apoptosis. To assess viability, cells were incubated in full serum for 72 hours with increasing concentrations of imatinib or compounds **16** and **17**. After 72 hours, the cell viability was measured using a colorimetric MTS assay. All compounds were capable of inhibiting cell viability: imatinib as the most potent (IC_{50} ~60 nM) and PROTAC **16** and the negative control **17** displayed milder potency (IC_{50}'s of 600 nM and 1 µM, respectively). In a parallel experiment, cells were cultured for 72 hours in serum free conditions with 5 µM imatinib or 2.5 µM PROTAC **16** or negative control **17**. After the incubation, the cells were stained for markers of apoptosis (Figure 4.7C). All compounds were capable of inducing apoptosis to similar degrees. Imatinib had slightly enhanced apoptotic markers, but this might be due to the higher concentrations of compound used in the assay.

These experiments in patient cells are encouraging, as the compounds are capable of degrading BCR/Abl similarly to cultured cells. Tissue distribution or variable expression levels of VHL can be a concern in these types of experiments but does not seem to be an issue here. The viability and apoptotic experiments are also encouraging, as in these conditions, the signaling of BCR/Abl is thought to drive survival through phosphorylation of STAT5[302]. However, these conditions do not mimic the *in vivo* niche in which LSCs persist[86,90]. In that context of cytokine signaling leukemic cells persist in a quiescent state resistant to cell cycling, and so the inhibition of BCR/Abl kinase activity has no effect. It is in this context of enhanced cytokine signaling in which imatinib would not induce apoptosis and non-kinase roles of BCR/Abl should be investigated. Further

experiments can focus on using bone marrow stromal cells or cytokine cocktails to mimic the bone marrow niche and to assess PROTAC function in that context.

Section 4.7: Are Non-Kinase Roles of Protein Kinases Underappreciated?

In summary, targeting the allosteric site of BCR/Abl allowed for far greater potency of degradation, but the reasons for this are unknown. Unbiased analysis of signaling pathways affected by BCR/Abl degradation suggests interesting phenomena, but these are neither validated nor mechanistically clear. And, finally, the ability of BCR/Abl degradation to clear leukemic stem cells *in vivo* remains to be illustrated.

Non-kinase roles in general should be explored more fully. Looking beyond BCR/Abl, non-catalytic roles of protein kinases have been implicated in varieties of diseases, yet reviews and other articles highlighting these findings go relatively unnoticed[11]. Furthermore, the literature is replete with poorly articulated discoveries about kinases. For example, if kinase inhibition or expression of a kinase dead mutant do not phenocopy the expected results, often authors will say that the protein itself is not involved in the phenonema. It would be far more accurate to say that the *kinase activity* was not involved: such distinctions are usually not made, further confusing potential non-kinase roles of kinases domain-containing proteins.

Future efforts should focus on developing robust standard practices for defining non-kinase roles of protein kinases. Some studies rely on expression of catalytically dead kinases, typically by mutating the ATP-binding lysine to an arginine or alanine: this result implicates non-kinase roles of Brk in promoting breast cancer proliferation[316]. However, occupation of the ATP-binding site typically changes the conformation of a protein kinase which can have drastic effects on downstream signaling[128,317]. An alternative approach might be the bump-hole system introduced by Kevan Shokat and colleagues, in which a mutation is introduced into the active site of kinases that enable the selective use of an

ATP analogue to inhibit the kinase[318]. This method obviates the laborious need of a selective chemical inhibitor and can quickly probe whether the function of the gene is kinase-dependent or -independent.

A recently published case study illustrates the potential danger in pursuing kinase-independent functions. TANK Binding Kinase 1 was identified as synthetic lethal vulnerability in KRas mutant cells, but kinase inhibitors for the protein did not phenocopy the original RNAi-based screen[319,320]. This seemed to be an ideal scenario in which PROTACs may confer an advantage over inhibition, but potent PROTACs (DC_{50} = 9 nM; D_{max} = 96%) had a very modest effect in KRas mutant cell lines[321]. In this context, two possibilities are readily apparent. First, because RNAi target a gene at the mRNA-level, whereas PROTACs target the protein level, perhaps RNA structural or regulatory functions are relevant. Second, and seemingly much more likely, off-target effects of the RNAi knockdown could account for the observed phenotype.

To summarize this section, degradation of BCR/Abl remains to be demonstrated as a novel and beneficial therapeutic strategy. Although many reports hint at kinase-independent roles of this protein, such roles need to be elucidated and defined more clearly. PROTACs, and especially the more potent compounds outlined here, provide a useful chemical probe to study these effects. Rather than relying on RNAi methods, which are slow in their effects, PROTAC allow for rapid and highly specific depletion of the protein of interest. This is especially important in precious material such as leukemic stem cells isolated from patients. Widening the scope, PROTACs provide a valuable platform for studying and treating protein functions that cannot be directly inhibited by small molecules.

Section 4.8: Techniques to Develop Ligands for "Undruggable" Proteins

As discussed in chapter one, ROR2 is a pseudokinase implicated in the maintenance of several cancers. It is normally not expressed in adults, but re-expression of this protein in cancers is associated with activation of Wnt signaling and metastasis. The exact mechanisms for ROR2's implication in cancer is unclear: further investigation is required. Developing a PROTAC for ROR2 would be highly informative for clarifying such roles. Having such a PROTAC would also allow screening dozens or hundreds of cancer cell lines to identify cancers where proliferation, viability or metastasis is inhibited by ROR2 degradation.

Obviously, the first step towards a ROR2 PROTAC would be the discovery of a ligand with reasonable affinity and selectivity towards ROR2. As has been seen with various pseudokinases in the past, this ligand might have therapeutic applications in and of itself[130]. Although the inactive state of ROR2 seems very stable, perhaps ligands directed to its "ATP-binding site" may further stabilize the active site. Probes that stabilize the active state would also be interesting chemical probes for understanding the function of ROR2.

Pseudokinases provide a compelling proof-of-concept for using PROTACs to degrade undruggable targets. While ligands for these targets may not inhibit the protein's function, derivatization of the ligand into a PROTAC would degrade the protein and thereby inhibit it. The problem with this strategy is the difficulty in finding a suitable targeting ligand. Two reasons for this. First, when no enzymatic pocket it present, finding a start point for medicinal chemistry efforts is difficult. Pseudokinases perhaps solve this issue. Although some features of the ATP-binding pocket in pseudokinases are mutated, the general shape of the pocket should be intact, and so screening kinase inhibitor libraries could provide a suitable starting point.

A second problem with developing ligands for pseudokinases, and "undruggable" proteins more broadly, is a lack of robust technologies for high-throughput screening (HTS). This is not an issue for kinases or other enzymes. A variety of techniques have been developed to detect the accumulation of the product of an enzymatic reaction, many of which allow sensitive detection in 384- or even 1526-well formats. This facilitates the screening of tens or hundreds of thousands of compounds per day. The presence of multiple different assays with different underlying biochemistries, and therefore different biases or false positives, also facilitates secondary screening and further triage. For an excellent review, please see reference[322].

Proteins lacking enzymatic activity have a bit harder time in developing and screening ligands. Fundamentally, an assay for these targets must be able to detect a binding interaction rather than an enzymatic product. Several assays have been developed but most simply do not rise to the level of throughput available for, say, *bona fide* kinases.

A commonly used type of screening involves affinity enrichment. In this situation, prospective ligands are selected by precipitating the protein of interest after incubation with a small molecule library. Ligands that bind to the protein of interest will co-precipitate with the protein and the affinity of the interaction should be correlated with the amount of small molecule pulled down. A main difficulty of these technique has been the sensitivity of detection because early efforts focused on using mass spectrometry to detect ligands[323]. The use of DNA-encoded libraries, in which small molecule are identified by means of a DNA barcode covalently linked to the small molecule, allows for more sensitive detection. DNA-encoded libraries have come a long way since their conceptual introduction in 1992, and now provide inexpensive and deep coverage of chemical space[324,325]. Furthermore, with advances in deep DNA sequencing methods, sensitive

detection of ligands co-precipitated with a protein of interest is far more feasible[326]. A recent technique involves the self-ligation of DNA barcodes from the small molecule *and* the protein target, yielding one strand of DNA which encodes the protein target and the potential ligand[327]. This technique could allow for libraries of proteins to be screened against a library of small molecules in one pot[328]. The potential for DNA-encoded libraries to transform modern HTS is beginning to be realized[324].

NMR is another commonly used platform for identifying ligands which bind to any protein of interest[329]. A main advantage to this technique is that neither protein nor small molecules require any modification or barcoding, likely decreases false positives or negatives due to these modifications. Many NMR methods are available for HTS[330,331]. Although NMR provides biophysical information from the interaction (particularly the site of binding of the ligand in small proteins), it is severely limited by low throughput, and screens are usually conducted in pools and require deconvolution.

Another commonly used technique is the thermal shift assay (TSA). This technique capitalizes on the stabilization of a protein that occurs upon ligand binding. As a ligand binds to the folded state of a protein, it should shift the equilibrium of that protein's unfolding towards the folded state: this often leads to an increase in the protein's melting temperature[332–334]. The use of fluorescent dyes for detecting the folded state of a protein allow miniaturization of this technique and high-throughput screening. Importantly for this discussion, TSA has been used with kinases, and especially to characterize the ATP-binding potential of pseudokinases and for identifying ligands of pseudokinases[335–337]. This technique's main advantages are its throughput, low cost, lack of specialized equipment (it can be performed on almost any qPCR instrument) and use of small amounts of modified protein and ligand. A main drawback of this technique is that the degree of stabilization is not always correlated to the affinity or other biophysical parameters of the

interaction. This technique is also prone to false negatives, as not all proteins are amenable to ligand-induced stabilization[338,339].

Section 4.9: Identification of ROR2 Ligands by a Thermal Shift Screen

To discover ligands for the pseudokinase ROR2, we choose a small library of published kinase inhibitors: the published kinase inhibitor set (PKIS)[340,341]. This set of 900 compounds consists of FDA-approved and preclinical small molecules which bind kinases competitively with ATP. Given ROR2 has the overall structure of a kinase[124], we reasoned that a small set lacking diversity but focused towards the kinase fold might afford ligand discovery.

As a screening platform, we choose TSA because of its prior use with pseudokinases. The first step was to determine an appropriate condition for screening ROR2 that would give reproducible melting curves: 5 µM protein was sufficient for this. Based on this, we screened the 950-compound library at 20 µM in duplicate.

In Figure 4.8A, the results for each of six plates were sorted by decreasing change in melting curve. Unfortunately, replicate plates showed very little agreement (R^2 of 0.14, 0.02, and 0.06) which inhibited any statistical analysis of the results. This poor reproducibility amounts from either poor-quality protein, poor quality DMSO stocks on the plates, or differences in how each plate was handled.

Regardless, rather than determining hits from the replicate results, the compounds which induced the largest positive shifts in melting temperature were picked from the plates, and multiple doses were screened against the protein. Compounds which gave melting temperature shifts in this secondary screen were then selected for surface plasmon resonance analysis. 26 compounds were chosen for this secondary validation.

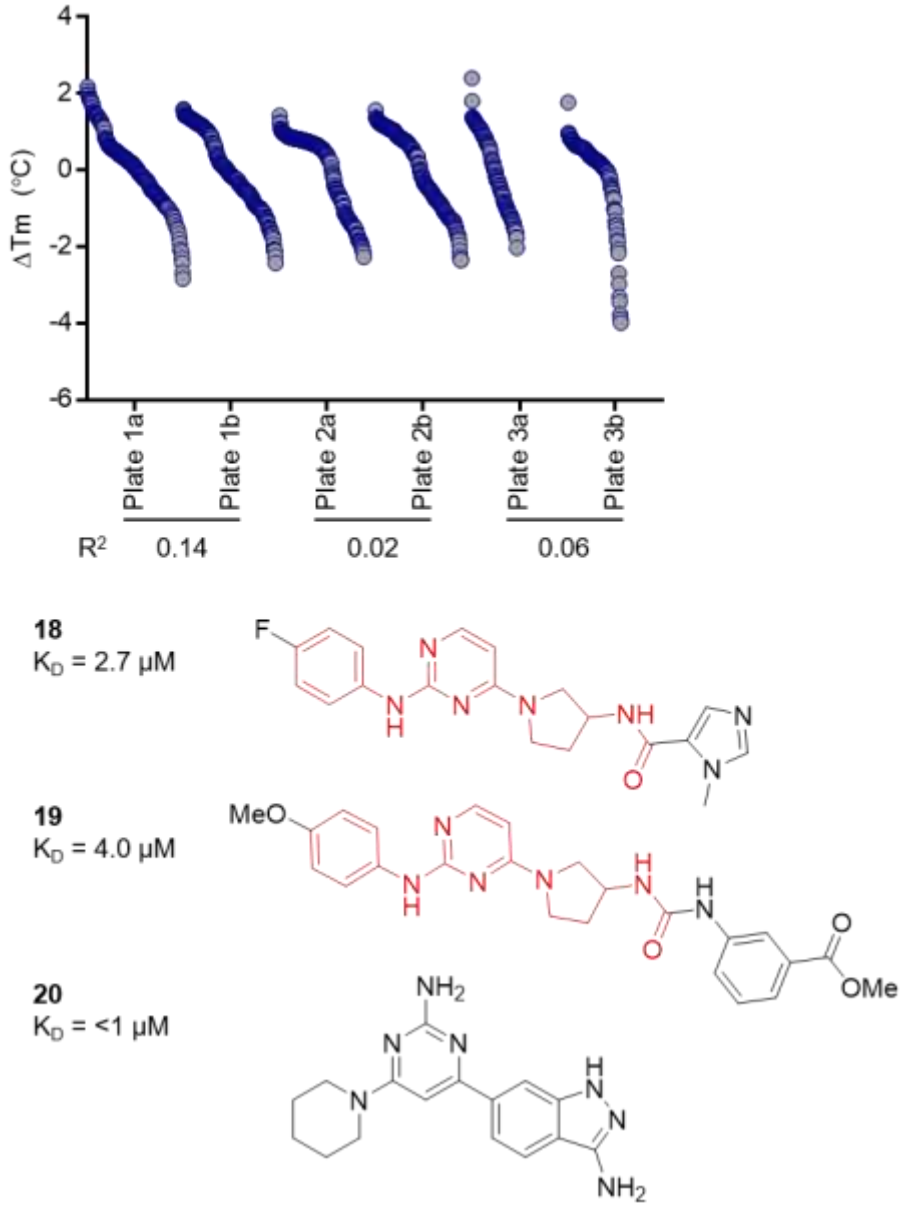

Figure 4.8 A thermal Shift Screen Identifies ligands for ROR2

(A)The published kinase inhibitor set (PKIS) was screened in duplicate against purified ROR2 protein. Because of poor reproducibility between replicate plates (the Pearson product correlation coefficients are shown at the bottom of the chart), each of the six plates were analyzed for compounds which raised the melting temperature above the mean for that plate. Base on this, 26 compounds were selected for secondary screening. (B) Three compounds bound to ROR2 by SPR. Using surface plasmon resonance (SPR), compounds from (A) were tested at multiple doses for their ability to bind immobilized His_6-ROR2. The chemical structures and affinities for the three hits are shown. The common scaffold of compound **18** and **19** is highlighted in red.

Surface plasmon resonance (SPR) uses immobilized protein on a gold chip. A laser is shone at the chip, and at a particular angle the light couples with plasmon waves within the chip. This angle, the plasmon resonance angle, varies with the electronic properties of the chips, and therefore the mass of immobilized analytes. A solution of potential ligands can be passed over the immobilized protein, and as the ligand binds, this is indicated by a small change in the resonance angle, and this response over time can be used to determine binding kinetics and affinity for the analyte and protein.

With immobilized ROR2, the 26 potential ligands were tested in multiple doses to assess their binding affinity. Of these, three compounds were found to bind to ROR2 with dissociation constants in the low micromolar range (Figure 4.8C). Gratifyingly, compounds **18** and **19** bound with similar affinity and share a common pharmacophore.

With these encouraging results in hand, we next sought to derivatize the compounds. This first round of medicinal chemistry was designed to identify a binding mode for the compounds. If modification of the ligand in a particular site inhibits all binding, that is likely to be an important site of interaction. Other sites that have little effect on binding might not be involved in interacting with the protein or are solvent exposed (and thus likely to be a good linker attachment point for a PROTAC). Roughly 40 compounds have been synthesized with this goal in mind and have been tested via SPR. Disappointingly, re-synthesis of compound **18-20** did not reproduce the binding affinities reported in Figure 4.8. This is a common issue in HTS: compounds in the stock plates are stored for months or years and likely undergo many freeze-thaw cycles. While most compounds should be stable in these conditions, some degeneration may occur. A second issue is that no clear model for how the binding mode of these compounds arise from the structure-activity relationship. Based on these data, new compounds were not synthesized, since no logical path forward could be envisioned.

Rather, crystallography efforts were made. Generating a co-crystal structure of ROR2 in complex with some of the higher affinity ligands would provide valuable evidence for and information about the binding of these compounds. Because the previously published ROR2 crystal structure would seem to occlude compound binding, soak-able crystals were not expected to be attainable through those means. Rather, co-crystallization was attempted, but thousands of conditions across two labs have not yielded crystals that diffract.

In summary, these ligands for ROR2 appear to be binding with modest affinity, but the development of more potent ligands has been halted. Medicinal chemistry is difficult without a structural guide to how these ligands bind further attempts should be pursued. Because of the difficult access to SPR or other binding techniques, a more robust and high-throughput binding assay would also speed the testing of already and newly synthesized compounds. The possible development of such an assay is discussed below.

Section 4.10: New probes for ROR2 and other pseudokinases

As highlighted in the previous sections, ligand development for undruggable proteins suffers because of a lack of robust HTS assays. This is true of pseudokinases; their active site similarity to true kinases might allow access to already developed assays. One particular type of binding assay for kinases uses competition of an ATP-mimetic rather than enzymatic assay to generate signal. Perhaps the most widespread use of a platform like this is the KinomeScan service by DiscoverX (see Figure 3.9 in chapter three). Here, immobilized ATP-mimetics are incubated with phage-displayed kinase domains along with potential ligands[289,290,342]. Unbound kinases are washed away, and bound kinases are eluted and the phage DNA is used to assess the amount of kinase bound by the competitor. This is relatively inexpensive platform that can, in parallel, assess binding of a competitor ligand to almost the entire kinome.

Another commonly used platform is LanthaScreen, marketed by ThermoFisher[343]. This technique is available to any researcher with a time resolved Förster resonance energy transfer (trFRET)-equipped plate reader. In Lanthascreen, a kinase is incubated with a Europium-labeled antibody (likely bound to a fusion tag used for purification of the kinase such as His_6 or GST) and an AlexaFluor 647-conjugated "kinase tracer" which binds in the active site of the kinase. Without any competition, excitation of the europium antibody allows for non-radiative energy transfer to the fluorescent tracer, which then emits light at a different wavelength if the antibody:tracer pair is close enough. Competition by a potential ligand decreases this signal. This platform offers excellent assay windows and sensitivity for protein kinases, and has been used to screen ligands for the pseudokinase Her3[187]. Unfortunately, none of the commercially available kinase tracers were capable of engaging ROR2 to any appreciable amount, likely indicating that these compounds did not bind to ROR2 (data not shown).

While screening compounds for ROR2 using SPR, we also found that a promiscuous kinase inhibitor, compound **21**, bound to ROR2 with a dissociation constant of 13 μM. This compound has been previously reported to bind to the pseudokinase KSR and roughly 85% of the kinome[128,344]. Akin to the competitive binding assays outlined above, we next sought to determine if this compound could be used as a probe for pseudokinase ligand development, and so the biotinylated probe **22** was synthesized (Figure 4.9A). This compound binds with a similar affinity by SPR.

A first assay was designed to test the ability of this probe to bind multiple kinases[345]. A plasmid encoding an epitope-tagged ROR2 kinase domain (ROR2_KD) was overexpressed in HeLa cells, and cell extracts were incubated with compound **22** with or without competition of the free ligand **21**. The biotinylated probe was then precipitated with

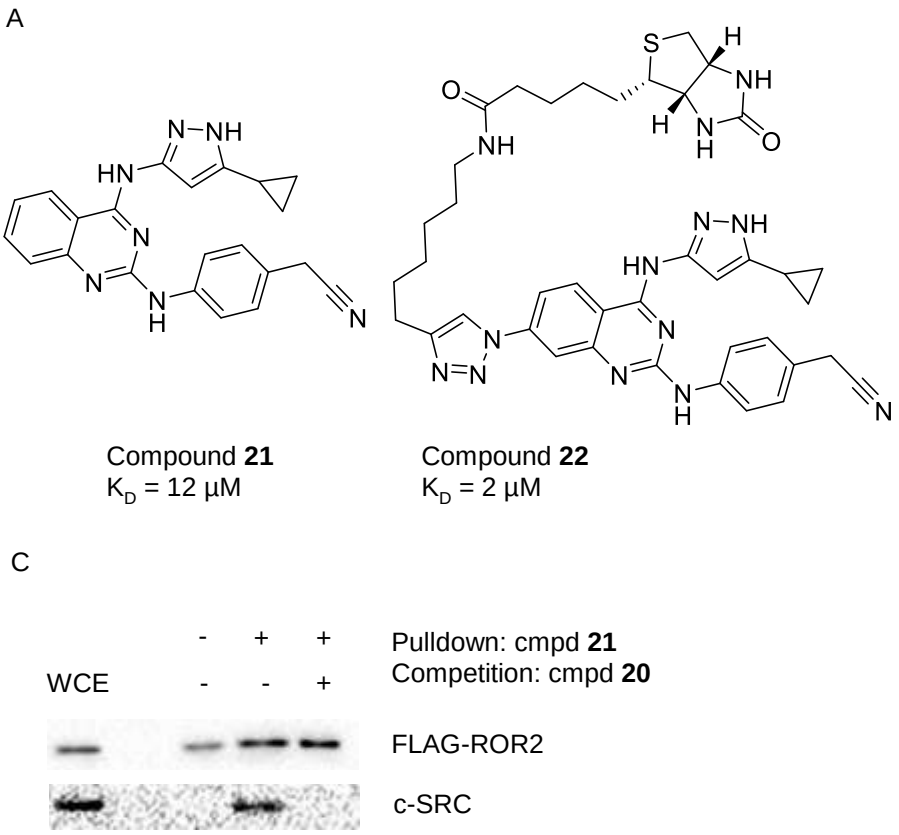

Figure 4.9 Discovery of a biotinylated probe which binds ROR2

(A) Structures of the promiscuous kinase inhibitor which binds ROR2. To the left is a kinase inhibitor, **21**, which binds ~85% of kinases. It is derivatized with a biotin pulldown handle in the structure to the right, compound **22**. (B) A pulldown assay for assessing ROR2 association with the biotinylated probe. FLAG-ROR2 was overexpressed in HeLa cells, and cell extracts were incubated with the indicated compounds, followed by incubation with neutravidin-coated beads. After extensive washing, precipitated proteins were eluted with SDS and analyzed by western blot.

neutravidin beads, and proteins were eluted by SDS and analyzed by western. As seen in Figure 4.9B, endogenous c-Src was efficiently precipitated by the compound **22**, and this interaction was inhibited by the free ligand **21**. This indicates that the addition of linker still enables this compound to bind kinases (although likely a subset of kinases bound by the parent ligand, see Figure 3.9 of chapter three). Unfortunately, no binding of these compound was detected for the overexpressed ROR2 construct, likely due to high background binding of the protein to the beads. Additional optimization of this pulldown experiment would be required to determine if the probe can bind and precipitate ROR2. If this assay could be optimized, the ability of other compounds to compete with binding of ROR2 and **22** could also be assessed (e.g. for compound **18-20** identified in the thermal shift).

Biotinylated compounds such as **22** offer a potential platform for developing HTS assays for pseudokinases. One can imagine overexpressing a pseudokinase of interest in cells and precipitating the protein with several different promiscuous ligands, ideally affording at least one probe which binds to the protein. The protein can then be purified, and a HTS assay, similar to LanthaScreen, can then be developed. This platform would ideally de-risk ligand development for pseudokinases.

Section 4.11: Discussion

This chapter highlights some of the prospects and challenges in broadening the scope of PROTACs. Two specific examples are highlighted, both of which require far more study to truly appreciate the potential of PROTACs.

In the first example, a protein which is efficiently targeted by a traditional small molecule likely has additional functions. Degradation of the protein can be achieved through PROTACs and, hopefully, inhibit these additional functions for therapeutic benefit.

However, these functions are relatively understudied and also apply only in particular cellular contexts.

In the second example, a pseudokinases which lacks enzymatic activity would likely be considered undruggable by traditional inhibitors. However, through the development of binding assays and through high throughput screening, ligands for this pseudokinases may be developed. These ligands may inhibit the protein on their own. Regardless, degradation of the pseudokinase via PROTACs would certainly inhibit the protein.

Although these two examples are clearly at an early stage of research, they serve as useful examples for the most exciting applications of PROTACs. Although the literature is replete with excellent manuscripts describing incremental benefits of protein degradation, it is when highly oncogenic proteins such as KRas or c-Myc are degraded by PROTACs that even the definition of undruggable will continue to shrink.

Summary and Significance

This thesis began, in the first chapter, with a brief description of seminal works that have solidified our understanding of protein kinases. These proteins are integral regulators of diverse cellular processes: their mis-regulation causes many diseases. Inhibition of protein kinases is a valuable therapeutic strategy, but it is limited in its application. This chapter explored two such examples of these limitations. BCR/Abl non-kinase roles may permit leukemic stem cells to persist despite inhibition of BCR/Abl kinase inhibition. Secondly, the ROR2 pseudokinase has no kinase activity, but its implication in cancers make it a valuable therapeutic target. This chapter also outlined several possible alternatives to conventional inhibitors and how these strategies are yet to be realized.

The second chapter outlined advances in proteolysis targeting chimera, or PROTACs. These advances offer an alternative and generalizable strategy by degrading proteins rather than inhibiting them. By using a small molecule ligand for an E3 ubiquitin ligase, these PROTAC molecules potently, selectively, and catalytically degrade their proteins of interest. Two examples of PROTACs are presented: for the serine/threonine kinase RIPK2 and for the nuclear hormone receptor ERRα.

Chapter three broadens the biophysical understanding of PROTAC molecules. Whereas conceptual thinking about these compounds initially involved two proteins only connected by the “PROTAC bridge”, data presented in this chapter clearly show that the most PROTAC molecules align the substrate and E3 ligase to make protein:protein interactions. These interactions enhance the potency of PROTAC molecules. The most dramatic example of this is a protein which is degraded by a PROTAC at concentrations ~100-fold lower than its binding affinity.

Although chapter three provides a basis for understanding the structure:activity relationship of many PROTACs, further study is still required on the biochemistry of PROTACs. That c-Abl and Arg (and BCR/Abl in chapter four) form a stable ternary complex but are resistant to degradation is an exciting and puzzling anomaly. Robust techniques for determining the physiological ubiquitin modifications of these proteins is a priority.

Chapter four returns to the applications of PROTACs highlighted in the first chapter. Potent PROTACs for BCR/Abl are developed and are capable of degradation in leukemic stem cell models. However, their ability to inhibit functions crucial to leukemic stem cell survival is still unclear. Initial efforts towards developing ligands for a pseudokinase are pursued, and some lead compounds are discovered. These ligands require further optimization.

Chapter four provides a sort of “road map” for the future of PROTAC molecules. Current examples in the literature of small molecule PROTACs show that degradation can overcome some limitations of inhibitors, but their value will be demonstrated when truly undruggable protein functions are targeted. Whether it be additional, non-kinase roles of protein kinases or non-enzymatic proteins such as pseudokinases, transcription factors, or scaffolds, future work should focus on developing PROTACs for these targets. These efforts will be greatly helped by new screening methodologies to identify ligands that merely bind to undruggable targets.

Overall, this study provides justification for the broader adoption of the PROTAC technology. The techniques and principles presented here allows targeted protein degradation by small molecules to become a more widespread tool used in research laboratories, as well as a therapeutic modality used in the clinic.

Materials and Methods

VHL Ligand Selectivity proteomics experiment (Figure 2.1C)

In order to generate a probe matrix of the active and inactive VHL ligand, an amine-functionalized derivative of the VHL ligand was immobilized on NHS-activated Sepharose 4 Fast Flow beads (Amersham Biosciences) at a ligand density of 0.5 mM. Derivatized beads were incubated over- night at room temperature in darkness on an end-over-end shaker and unreacted NHS groups were blocked by incubation with aminoethanol at room temperature on the end-over-end shaker, overnight. Beads were washed with 10 ml of DMSO and were stored in isopropanol at –20 °C. Prior to use, beads were washed three times with 5–10 volumes of DP buffer (50 mM Tris-HCl, 0.8% (v/v) NP40, 5% (v/v) glycerol, 150 mM NaCl, 1.5 mM $MgCl_2$, 25 mM NaF, 1 mM sodium vanadate, 1 mM dithiothreitol, Complete EDTA-free protease inhibitor tablet (Roche), pH 7.5), collected by centrifugation for 1 min at 300g and finally re-suspended in DP buffer to prepare a 5% beads slurry. Affinity profiling assays were carried out as described previously with minor modifications[346]. MCF-7 lysate was diluted with DP buffer to a protein concentration of 5 mg/mL and cleared by centrifugation at 145,000g. Aliquots of cell extracts (1 ml) were incubated with test compounds (5 µM active VHL ligand **1**, inactive VHL ligand or vehicle) for 45 min, then 35 µL derivatized Sepharose beads were added per sample and incubated on an end-over-end shaker for 1 h at 4 °C. Beads were transferred to disposable columns (MoBiTec), washed with DP buffer containing 0.2% NP40 and eluted with 50 µL 2× SDS sample buffer. Proteins were alkylated with 200 mg/ml iodoacetamide for 30 min, partially separated on 4–12% NuPAGE (Invitrogen), and stained with colloidal Coomassie before trypsin digestion and mass spectrometric analysis.

RIPK2 Ligand Kinobeads assay (Figure 2.2C)

Competition binding assays were performed as described previously[346].

VHL CoIP Proteomics (Figure 2.4)

THP-1 cells were harvested and lysed in lysis buffer (50 mM Tris-HCl, 5% Glycerol, 1.5 mM $MgCl_2$, 150 mM NaCl, 1 mM Na_3VO_4, 0.008% NP40 with Complete EDTA-free protease inhibitor cocktail). Mouse anti- VHL antibody (IgG1k, BD Biosciences) was immobilized at 0.125 µg antibody per µl agarose beads (AminoLink Plus, Thermo Fisher Scientific), and separately, mouse IgG1κ at 0.125 µg antibody per µl agarose beads was immobilized as control antibody. Comopund **2**, **3**, or **4** prepared in DMSO at 200 times the final assay concentration. THP-1 lysate was diluted to 5 mg/mL total protein concentration with lysis buffer, and 10 mg total protein was incubated with the indicated concentrations of compounds at 4 °C for 2 h. AminoLinked agarose beads were washed and equilibrated in lysis buffer, and incubated with lysate compound mixture at 4 °C for 2h. The beads were settled and supernatant was removed. The beads were washed twice with 30 times bed volume of lysis buffer and once with 30 times bed volume of lysis buffer without detergent. Bound protein was eluted from the agarose beads with 2x SDS sample buffer and heated at 95 °C for 10 min. The eluate was subjected to Immunoblotting and LC-MS analysis.

VHL Ubiquitination and Neddylation assays (Figures 2.5, 2.6, and 2.7)

Ubiquitination reactions were performed in three stages. In the first stage, RIPK2 (final 500 nM) was incubated for 10 min at room temperature with ^{32}PγATP in kinase buffer (25 mM Tris pH 7.5, 50 mM KCl, 2 mM $Mg(CH_3CO_2)_2$, 2 mM $MnCl_2$, 2 mM DTT) to radiolabel RIPK2 through auto-phosphorylation. In the second stage, ubiquitination buffer (25 mM Tris pH 7.5, 5 mM $MgCl_2$, 100 mM NaCl, 2 mM ATP, 0.1 mg/ml BSA, and 2 mM DTT) was added to complete auto-phosphorylation, and then VHL (final 250 nM) and indicated

PROTACs (various concentrations) were added to the mixture to allow ternary complex formation. In parallel, UbE1 (final 25 nM), Ubc4 (final 5 μM), and ubiquitin (final 116 μM) were mixed in ubiquitination buffer to allow charging of the E2 enzyme with activated ubiquitin. In stage three of the reaction, the RIPK2-PROTAC-VHL and UbE1-Ubc4~Ub mixtures were combined, and incubated at room temperature for various times before being quenched with 2x sample buffer, followed by separation by 4-15% SDS-PAGE and imaging using a PhosphoImager Screen.

Profiling of Phosphorylated Sites on RIPK2 (Figure 2.5)

RIPK2 protein was incubated with ATP in kinase buffer as above, and then digested with trypsin. Peptides were extracted with 0.5% trifluoroacetic acid, dried, resuspended, and applied to a TiO_2 TopTip micro-spin column (Glygen Corp.). Unbound peptides were washed off and bound peptides were eluted with a 1:33 solution of saturated ammonia. Peptide mixtures were fractionated by HPLC interfacing an electrospray ionisation quadrupole time-of-flight mass spectrometer, as described previously[347]. All MS/MS spectra were searched using the Mascot algorithm. For ubiquitination site mapping, di-glycine modification of lysine was also allowed as a variable modification.

Tissue Culture

Cells were provided by the American Type Culture Collection (ATCC) and were cultured according to recommended conditions. THP-1 cells were cultured in RPMI 1640 with 10% fetal bovine serum (FBS), 1% pen-strep (PS), and 50 μM β-mercaptoethanol. NIH 3T3-L1, HEK 293, and HeLa cells were cultured in DMEM with 10% FBS and 1% PS. K562 cells were cultured in IMDM with 10% FBS and 1% PS. MDA-MB-231 cells were cultured in RPMI 1640 with 10% FBS and 1% PS.

Treatment of cells and immunoblotting from cell extracts (various figures)

In general, compounds were delivered by preparing a 1,000x stock of the compound in DMSO, addition of the compound to warm culture media followed by vortexing, and then adding the media:compound mixture to cells. After the indicated times, cells were harvested by scraping or centrifugation and washed in ice cold tris buffer saline (TBS). The cell pellet was then resuspended in lysis buffer (1% Triton X-100, 50 mM Tris pH 7.5, 1 mM Na_3VO_4, 10mM NaF, 20mM β-glycerophosphate, and 1x protease inhibitor cocktail from Roche.) and incubated on ice for 10 minutes. Cellular debris was then cleared by centrifugation and 4x SDS sample buffer was added. Proteins were separated by SDS-PAGE and transferred to nitrocellulose using wet transfer. Blots were blocked in 5% Milk in TBS + 0.04% Tween 20 and then incubated with the indicated antibodies overnight. Blots were then rinsed and an appropriate secondary antibody was added for one hour at room temperature. The blots were washed thrice and then imaged using ECL prime (GE healthcare).

List of Antibodies		
c-Abl	SantaCruz	23
Actin	Abcam	ab6276
Arg	SantaCruz	81154
BCR	SantaCruz	sc-885
CDK4	Cell Signaling	12790
pCrkL (phospho Tyr221)	Cell Signaling	3491S
ERRα	Millipore	EPR46Y
FLAG M2	Sigma	F1804
GAPDH	Cell Signaling	2118

HA Tag	Cell Signaling	C29F4
HA Tag (Bead Conjugate)	Cell Signaling	3956
HaloTag	Promega	G921A
p38α	Cell Signaling	9218
RIPK2	Cell Signaling	4142
c-MET	Cell Signaling	8198
SLK	Cell Signaling	41255
Src	Cell Signaling	2123
STAT5 (total)	Santa Cruz	sc-1656
STAT5 (phospho Tyr694)	Cell Signaling	4322S
CUL2	Invitrogen	700179
VHL	Cell Signaling	68547
Tubulin	Sigma	T9026
Ubiquitin	P4D1	Millipore
HRP linked Mouse IgG	GE Life Sciences	NA931
HRP Linked Rabbit IgG	GE Life Sciences	NA934
Anti-Rb IgG (Bead Conjugate)	Cell Signaling	6990

Whole Cell Expression Proteomics (Figure 2.8D, 2.10C, 3.10, and 3.11)

Lysates were prepared per usual. Samples were sent to the Thermo Fisher Center for Multiplexed Proteomics at Harvard Medical School (TCMP@HMS) for quantitative whole proteome analysis. Samples were prepared as previously described with the following modification[348]. A micro-BCA assay (Pierce) was used to determine the final protein concentration in the cell lysate. Proteins were reduced and alkylated as previously described. Proteins were precipitated using methanol/chloroform. In brief, four volumes of

methanol were added to the cell lysate, followed by one volume of chloroform, and finally three volumes of water. The mixture was vortexed and centrifuged to separate the chloroform phase from the aqueous phase. The precipitated protein was washed with one volume of ice cold methanol. The washed precipitated protein was allowed to air dry. Precipitated protein was resuspended in 4 M Urea, 50 mM Tris pH 8.5. Proteins were first digested with LysC (1:50; enzyme:protein) for 12 hours at 25 C. The LysC digestion is diluted down to 1 M Urea, 50 mM Tris pH8.5 and then digested with trypsin (1:100; enzyme:protein) for another 8 hours at 25 C. Peptides were desalted using a C18 solid phase extraction cartridges as previously described. Dried peptides were resuspended in 200 mM EPPS, pH 8.0. Peptide quantification was performed using the micro-BCA assay (Pierce). The same amount of peptide from each condition was labeled with tandem mass tag (TMT) reagent (1:4; peptide:TMT label) (Pierce). The 8-plex labeling reactions were performed for 2 hours at 25 C. Modification of tyrosine residue with TMT was reversed by the addition of 5%hydroxyl amine for 15 minutes at 25 C. The reaction was quenched with 0.5% TFA and samples were combined at a 1:1:1:1:1:1:1:1 ratio. Combined samples were desalted and offline fractionated into 24 fractions as previously described.

12 of the 24 peptide fractions from the basic reverse phase step (every other fraction) were analyzed with an LC-MS3 data collection strategy on an Orbitrap Lumos mass spectrometer (Thermo Fisher Scientific) equipped with a Proxeon Easy nLC 1000 for online sample handling and peptide separations[292,293,349]. Approximately 5 µg of peptide resuspended in 5% formic acid + 5% acetonitrile was loaded onto a 100 mm inner diameter fused-silica micro capillary with a needle tip pulled to an internal diameter less than 5 mm. The column was packed in-house to a length of 35 cm with a C18 reverse phase resin (GP118 resin 1.8 mm, 120 A˚, Sepax Technologies). The peptides were separated using a 180 min linear gradient from 3% to 25% buffer B (0.125% formic acid

in acetonitrile) equilibrated with buffer A (3% acetonitrile and 0.125% formic acid) at a flowrate of 600 nL/min across the column. The scan sequence for the Fusion Orbitrap began with an MS1 spectrum (Orbitrap analysis; resolution 120,000; 350-1350 m/z scan range with quadrapole isolation, AGC target $1x10^6$, maximum injection time 100 ms, dynamic exclusion of 60 seconds). “Top N” (the top 10 precursors) was selected for MS2 analysis, which consisted of CID ion trap analysis, AGC $2.5x10^4$, NCE 35, maximum injection time 200 ms). Charge state dependent quadrapole isolation was used for MS scans (1.2 Da for m/z =2, 1.0 Da for m/z = 3, and 0.8 Da for m/z 4-6). The top ten fragment ion precursors from each MS2 scan were selected for MS3 analysis (synchronous precursor selection), in which precursors were fragmented by HCD prior to Orbitrap analysis (NCE 55, max AGC $2.2x10^5$, maximum injection time 300 ms, MS2 quadrapole isolation was set to 2.0 Da, resolution 60,000).

A suite of in-house software tools were used to for .RAW file processing and controlling peptide and protein level false discovery rates, assembling proteins from peptides, and protein quantification from peptides as previously described. MS/MS spectra were searched against a Uniprot human database (February 2014) with both the forward and reverse sequences. Database search criteria are as follows: tryptic with two missed cleavages, a precursor mass tolerance of 50 ppm, fragment ion mass tolerance of 1.0 Da, static alkylation of cysteine (57.02146 Da), static TMT labeling of lysine residues and N-termini of peptides (229.162932 Da), and variable oxidation of methionine (15.99491 Da). TMT reporter ion intensities were measured using a 0.003 Da window around the theoretical m/z for each reporter ion in the MS3 scan. Peptide spectral matches with poor quality MS3 spectra were excluded from quantitation (<200 summed signal-to-noise across 8 channels and <0.5 precursor isolation specificity.

***In vivo* degradation of ERRα (Figure 2.10D)**

Mice were housed in pathogen-free animal facilities at NELS (New Haven, CT). All experiments were conducted under an approved protocol. Female CD-1 mice were obtained from Taconic Laboratories and implanted subcutaneously with 5 million MDA-MB-231 cells in Matrigel (Corning Life Science). After several weeks, mice bearing >100 mm^3 tumors were randomized into two unblended groups with five mice in each group. One group served as a control for dosing vehicle, while the other group was given four administrations of PROTAC **6** (100 mg/kg, intraperitoneal, every eight hours). Mice were sacrificed five hours after final dose. Kidney, heart, liver, and MDA-MB-231 tumors were thawed on ice, chopped into pieces, and placed into microfuge tubes with homogenization buffer (25 mM HEPES, 50 mM NaCl, 1% NP40, 0.1% SDS, pH 7.4; 10 mL/mg tissue). Tissues were disrupted with a Qiagen TissueLyser bead miller (5 mm stainless steel bead; 2 min, 25 Hz), and homogenates were clarified (15,000g, 10 min, 4 °C) and transferred to new tubes. Protein levels were normalized by Bradford and separated by SDS-PAGE.

RT-PCR for mRNA levels (Figures 2.12 and 4.1)

After the indicated treatment, cells were lysed by addition of trizol reagent to the culture dish, and RNA was extracted using the manufacturer's instructions. cDNA was synthesized from 2 μg of total RNA per condition according to the manufacturer's protocol (Applied Biosystems) and real-time PCR was performed with the indicated primers and SYBR Green Reaction Mix (Applied Biosystems). RT-PCR samples were performed and analyzed in triplicate, from two independent experiments. *Beta-Tubulin* was used for normalization.

Analysis of ubiquitinated sites on HaloTag (Figure 3.4)

For samples prepared from *in vitro* ubiquitination, ten parallel reactions with HaloPROTAC **9** were pooled, concentrated ten-fold and digested with trypsin. Peptides were handled as for RIPK2 phosphosite mapping except for omission of the TiO_2 enrichment step. Database searches were performed allowing for one missed trypsin cleavage and the additional DiGly motif.

For isolation of ubiquitinated proteins from cells, one 10cm dish of HEK293 cells stably expressing the KGH7 construct were pretreated with 5 µM epoxomicin for thirty minutes, followed by an eight-hour treatment with 5 µM HaloPROTAC **9**. Cells were then lysed in TGH buffer (150 mM KCl, 2 mM $MgCl_2$, 20 mM HEPES pH 7.2, 10% glycerol, 1 mM dithiothreitol, 1 mM EGTA, 1 mM EDTA, 1 mM Na_3VO_4, 10 mM NaF, 5 mM iodoacetamide, 1% Triton X-100, 1% sodium deoxycholate and 10 mM N-ethyl-maleimide). Cellular debris was cleared by centrifugation, and the whole cell extract was immunoprecipitated with 20 µL of HA-sepharose conjugate or IgG control. After incubation overnight at 4°C, the sepharose beads were washed 4x with 10x bed volume of lysis buffer plus 500 mM NaCl. Bound proteins were eluted with SDS sample buffer. One tenth of the total eluate was used for immunoblotting, while the rest was separated by SDS-PAGE for in-gel tryspin digestion and LC/MS/MS analysis as described for the *in vitro* reaction.

Purification of GST-VHL

For the expression of GST-tagged VHL:Elongin B:Elongin C (herein referred to as GST-VHL), wild-type human VHL, Elongin B, and Elongin C were coexpressed in E. coli. BL21(DE3)RIPL cells were co-transformed with pBB75-Elongin and pGEX4T-2-VHL-rbs-Elongin B and selected in LB medium containing carbenicillin (100 mg/mL) and kanamycin

(25 mg/mL) at 37°C until OD600 = 0.8, at which point the culture was chilled to 16°C and induced with 0.4 mM IPTG for 16 hr. Cells were resuspended and lysed by microfluidization in a lysis buffer containing 30 mM Tris pH 8.0, 200 mM NaCl, 5% glycerol, 5 mM dithiothreitol and 1x protease inhibitor cocktail (Roche). Clarified cell lysate was applied to Glutathione Sepharose 4B beads (GE Life Science) and gently rotated for 2 hr at 4°C. Beads were washed with four column volumes of lysis buffer, followed by four column volumes of elution buffer (50 mM Tris pH 8.0, 200 mM NaCl, 10 mM Glutathione). Eluted protein was assessed for identity and purity via Coomassie staining of sample run on an SDS-PAGE gel and pure elutions were pooled, concentrated, and diluted in ion-exchange buffer A (30mM Tris pH 8.0, 5% glycerol, 1 mM DTT) until the salt concentration was 50 mM, before loading onto a Mono Q 5/50 GL column (GE Life Sciences). The protein was subjected to a linear gradient of NaCl (0-500 mM NaCl) using ion-exchange buffer B (30 mM Tris 8.0, 1 M NaCl, 5% glycerol, 1 mM DTT). Fractions were then assessed for purity via a Coomassie-stained gel, pooled, concentrated, and run on a Superdex-200 column (GE Life Sciences) using size-exclusion buffer (30 mM Tris pH 8.0, 100 mM NaCl, 10% glycerol, 1 mM dithiothreitol). Pure fractions of GST-VHL were pooled, concentrated to 5 mg/mL, aliquoted, and flash-frozen before storing at -80°C.

All other proteins were purified with minor variations on this protocol.

VHL Pulldown assay (Figures 3.5, 3.14, 3.15, and 4.5)

Glutathione Sepharose 4B was washed twice with 1X TBS-T (Tris buffered saline plus 0.02% Tween 20) and then blocked for one hour at room temperature with 10% BSA in TBST. The beads were then washed again twice with TBS-T and once with wash buffer (50mM HEPES pH 7.5, 150mM NaCl, 1mM DTT, 0.01% NP40, 5 mM MgCl2, 10% Glycerol) and then purified GST-VBC was immobilized for two hours at 4°C at 360 pmole per µL of beads. The beads were then washed thrice with wash buffer, resuspended and

p38α protein was added at 500 nM per 50 µL reaction with 5 µL of beads. The bead:p38α mixture was then aliquoted to separate tubes and PROTAC was added at the indicated concentration (PROTACs were intermediately diluted in 10% DMSO and 0.25% CHAPS) and this was incubated at 4°C for two hours. The beads were washed thrice with 10 column volumes of wash buffer and then eluted with SDS loading buffer.

For experiments in which the input substrate is a whole cell lysate, the sample was prepared as follows. Approximately 30 million cells were used per condition. Cells were harvested by scraping or centrifugation, and then washed with TBS. The cells were pelleted, resuspended in wash buffer, and then lysed by sonication (Branson sonicator microtip, power = 7, 50% duty cycle for 3 cycles of two minutes on and two minutes rest). The lysate was cleared by centrifugation and then added to the beads as an input substrate, as above.

ALPHA-based competitive binding assay for VHL (Figures 3.5 and 3.7).

HaloPROTAC compounds were first diluted in DMSO. A 12-point, 3x dilution curve was made with a top concentration of 3 mM. Compounds were then diluted ten-fold into a solution containing HaloTag protein (wildtype or mutants) at 15 µM in ALPHA buffer (50 mM HEPES, 50 mM NaCl, 69 mM BRIJ-35, and 0.1 mg/mL BSA). After incubation for one hour at 4°C, 5 µL of this protein:compound mixture was added to 5 µL of buffer in the assay plate. In parallel, GST-VHL (60 nM) was incubated with the biotinylated ligand (180 nM) for one hour at 4°C, and 5 µL of this was added to assay plate followed by a one-hour incubation at room temperature. 7.5 µL of a 1:100 dilution of glutathione donor beads were added, and this was incubated at room temperature for 15 minutes in the dark. 7.5 µL of a 1:100 streptavidin acceptor beads were then added and this was incubated for a further 15 minutes at room temperature in the dark. Plates were read on a SYNERGY 2

microplate reader (BioTek Instruments) with an excitation wavelength of 680 nm and emission wavelength of 615 nm.

MD Simulations (Figure 3.6 and 3.15)

The starting coordinates for p38α and HaloTag came from crystal structures downloaded from Protein Data Bank (PDB) entries 1W82 and 4KAF. P38α was “bound to foretinib” by overlaying the backbone of PDB entry 5IA4 with that of 1W82, transferring foretinib to the 1W82 structure and replacing the original ligand. The obtained p38α-foretinib complex (and the HaloTag alone structure) was subject to the Protein Preparation Wizard of Maestro 2016-3 program available from Schrodinger Inc. (New York City, NY), with which the hydrogen atoms were added; the missing side chains were built; and the protonation states were assigned assuming a pH of 7.0 for the ionizable groups. An energy minimization of the complex was performed for 500 steps.

The starting coordinates for VHL came from the PDB entry 4W9H. The starting coordinates for ternary complexes were prepared as follows. (1) The electrostatic surface was generated for p38α-ligand, HaloTag, and VHL-ligand complexes. (2) The VHL-ligand complex was set to have different relative dispositions with respect to the p38α-ligand/HaloTag complexes in a way that the hydrophobic patch of the VHL-ligand surface opposed different hydrophobic patches and grooves of the other surface, thus producing different starting modes in terms of the relative dispositions between p38α/HaloTag and VHL. (3) For each starting mode, the appropriate linker was built to form the full PROTAC. And (4) an energy minimization of 500 steps was performed for each starting point of trimer.

OPLS3 force-field was used throughout the calculation steps. The torsional angle parameters were examined with Force Field Builder program and found that the torsional

angles between the amide and cyclopropyl group and between the fluorophenyl group and the oxygen ether atom attached to the quinoline group in foretinib needed corrections; and thus the new torsional profiles were generated to match the profiles given by Jaguar quantum mechanical calculations.

Each starting point of each ternary complex was subject to molecular dynamics (MD) simulation. The system setup was done using System Builder of Maestro program, in which the periodic boundary condition was used; the box shape was orthorhombic with absolute size of 100×100×100 $Å^3$. The explicit waters were added. The system was neutralized using Na^+/Cl^- ions and salted into 0.15 M ionic strength. The MD was done using Desmond Multisim version 3.8.5.19 which was an eight-stage process: task; simulation of 100 picosecond with Brownian dynamics NVT with T at 10 K, small time-steps and restraints on solute heavy atoms; simulation of 12 picosecond, NVT ensemble, T at 10 K, small time-steps and restraints on solute heavy atoms; simulation of 12 picosecond, NPT ensemble, T at 10 K and restraints on solute heavy atoms; solvation of potential unfilled pockets; simulation of 12 picosecond up to the target temperature of 310 K, NPT ensemble and restraints on solute heavy atoms; simulation of 24 picosecond, NPT ensemble without restraints at T of 310 K; and finally, production run of 120 nanosecond. During the production run, coordinate frames were saved at every 10 picosecond. The target pressure was set to 1.01325 bar in the related steps.

The post-simulation analysis after each run was done as follows. The last 20 nanosecond of trajectory frames were extracted. A clustering analysis using hierarchical clustering method was performed. The distance between any two members (frames) was the root-mean-square deviation (RMSD) of the solute heavy atoms between the members after overlaying them. The cutoff distance was 2 Å. Every frame was used. The structure closest to the centroid of each cluster was written out as the representative structure of

that cluster. The representative structure of the largest cluster for each MD simulation was considered as the representative structure of that simulation run. Such a structure can be considered as the most populated conformation of that run.

The MD simulation was performed using the g2.2×large instances of Amazon Web Service cloud machines. The Desmond GPU-enabled code was used and mainly run using GPU.

Cycloheximide chase assay (Figure 3.13)

MDA-MB-231 cells were plated at 3 x 10^5 cells per well in a 6-well dish, allowed to adhere, and switched to serum-free RPMI-1640 media for 16 hr. Cells were then pre-treated with cycloheximide (Sigma) at 100 μg mL^{-1} for 1 hr prior to adding PROTAC (500 nM) or vehicle. At the indicated timepoints, cells were immediately placed on ice, rinsed with PBS, lysed, and boiled.

ALPHA for detection of PROTAC induced ternary complexes (Figure 3.15)

Assays were performed at room temperature and reagents were diluted in buffer containing 50 mM HEPES, 50 mM NaCl, 69 mM BRIJ-35, and 0.1 mg/mL BSA. Recombinant GST-VHL-ElonginB-ElonginC (VBC) was mixed with His6-p38α and PROTAC (diluted from a 6x stock) to a final volume of 15 mL per well in a OptiPlate-384 well microplate (PerkinElmer) and incubated for 30 min. VBC and p38α were kept at a constant concentration of 50 nM and 100 nM, respectively. 7.5 mL of Alpha Glutathione Donor beads (PerkinElmer) were added to each well and plates were incubated for 15 min. 7.5 mL of and Anti-6xHis AlphaLISA Acceptor beads (PerkinElmer) were added to each well and plates were incubated for 45 min. Plates were read on a SYNERGY 2 microplate reader (BioTek Instruments) with an excitation wavelength of 680 nm and emission wavelength of 615 nm.

Transfections (Figure 3.15 and 4.10)

Transfections were carried out using Lipofectamine 2000 (Invitrogen) in HeLa cells seeded at 2.5 x 10^6 cells per 100 mm plate. 10 µg of of FLAG-containing pcDNA5-p38alphaWT or pcDNA5-p38alphaA40K was used per transfection and Opti-MEM media was changed after 6 hours to DMEM (1X).

Thermal Shift Assay (Figure 4.8)

Thermal Shift assays were performed as described previously[335]. Briefly, 20 nL of 10 mM DMSO stocks of the published kinase inhibitor set were transferred to 384-well plates. The ROR2 protein was diluted to 5 µM in TS buffer (150 mM NaCl, 20 mM Tris pH 8.0, 1 mM dithiothreitol, 1 mM $MgCl_2$) and Sypro Orange (Sigma) was added at 1x manufacturer's suggestion. 10 µL of ROR2 protein mixture was then added to each well, and the plate was heated from 25°C to 100°C at 10°C per minute in a Roche LightCycler 480 II. The Protein Melt Analysis software was then used to calculate melting temperatures.

Surface Plasmon Resonance (Figure 4.8 – 4.10)

All SPR experiments were conducted on Bertha, a BiaCore 3000 instrument. A fresh sensor chip NTA was loaded into the instrument, and $NiCl_2$ was flowed over channels 2, 3, and 4. His_6-ROR2 was then flowed over channels 3 and 4 until approximately 4,000 response units remained immobilized on the chip. ROR2 protein was diluted in SPR buffer prior to loading (SPR buffer is 50 mM Tris pH 7.5, 150 mM NaCl, 0.005% Tween 20, 10 mM $MgCl_2$). Compound dilutions curves were prepared in neat DMSO and then diluted 50x into SPR buffer. Compounds were injected into the instrument at a flow rate of 20 µL/minute. Injections were performed over 60 seconds, with 240 seconds between each injection. Data was processed using Scrubber 2.

Pulldown assay using biotinylated ligands (Figure 4.10)

Pulldown assays were performed as described previously[350]. Briefly, probe **22** was immobilized on neutravidin resin (ThermoFisher) at 0.5 pmoles per µL of beads. In parallel, HeLa cells transfected with FLAG-ROR2 were scraped into wash buffer + 0.6% NP40 (wash buffer alone is 50 mM Tris/ HCl pH 7.5, 150 mM NaCl, 0.2% NP40, 5% glycerol, 1.5 mM $MgCl_2$, 1 mM Na_3VO_4, 375 µM NaF, 1 mM dithiothreitol) and cell debris was cleared by centrifugation. The whole cell extract was then incubated for one hour at 4°C with 100 µM free ligand **21**. After competition, cells extracts were added to the beads, and this was incubated for one hour at 4°C. The beads were then washed three times with 10 bed volumes of lysis buffer and bound proteins were eluted with SDS sample buffer.

Literature Cited

1. Lowy, D., Singer, D., DePinho, R., Simon, G. C. & Soon-Shiong, P. Cancer moonshot countdown. *Nat. Biotechnol.* **34,** 596–599 (2016).

2. Singer, D. S., Jacks, T. & Jaffee, E. A U.S. 'Cancer Moonshot' to accelerate cancer research. *Science (80-.).* **353,** 1105–1106 (2016).

3. Kolch, W. & Pitt, A. Functional proteomics to dissect tyrosine kinase signalling pathways in cancer. *Nat. Rev. Cancer* **10,** 618–629 (2010).

4. Subramanian, A. *et al.* A Next Generation Connectivity Map: L1000 Platform and the First 1,000,000 Profiles. *Cell* **171,** 1437–1452.e17 (2017).

5. Tsherniak, A. *et al.* Defining a Cancer Dependency Map. *Cell* **170,** 564–576.e16 (2017).

6. Le, D. T. *et al.* Mismatch repair deficiency predicts response of solid tumors to PD-1 blockade. *Science (80-.).* **357,** 409–413 (2017).

7. Cancer, B. Two Decades After BRCA : Setting Care and Prevention. 1466–1471 (2014). doi:10.1126/science.1251827

8. Cohen, P. Protein kinases--the major drug targets of the twenty-first century? *Nat. Rev. Drug Discov.* **1,** 309–315 (2002).

9. Li, Y. H. *et al.* The human kinome targeted by FDA approved multi-target drugs and combination products: A comparative study from the drug-target interaction network perspective. *PLoS One* **11,** 1–15 (2016).

10. Adjei, A. a. What Is the Right Dose? The Elusive Optimal Biologic Dose in Phase I Clinical Trials. *J. Clin. Oncol.* **24,** 4054–4055 (2006).

11. Kung, J. E. & Jura, N. Structural Basis for the Non-catalytic Functions of Protein Kinases. *Structure* **24,** 7–24 (2016).

12. Meyerhof, O. Über die enzymatische Milchsäurebildung im Muskelextrakt. III. Mitteilung: Die Milchsäurebildung aus den gärfähigen Hexosen. *Biochem. Z.* **183,** 176–215 (1927).

13. Cori, G. T. & Green, A. A. Crystalline Muscle Phosphorylase II. Prosthetic Group. *J. Biol. Chem.* **151,** 31–38 (1943).

14. Cori, G. T. & Green, A. A. Crystalline Muscle Phosphorylase I. Preparation, Properties, and Molecular Weight. *J. Biol. Chem.* **151,** 21–29 (1943).

15. Cori, G. & Cori, C. The enzymatic conversion of phosphorylase a to b. *J. Biol. Chem.* 383–396 (1945).

16. Velick, S. F. & Wicks, L. F. The Amino Acid Composition of Phosphorylase. *J. Biol. Chem.* **190,** 741–751 (1951).

17. Keller, P. J. & Cori, G. T. Enzymic conversion of phosphorylase a to phosphorylase b. *Biochim. Biophys. Acta* **12,** 235–238 (1953).

18. Fischer, E. H. & Krebs, E. G. Conversion of phosphorylase b to phosphorylase a

in muscle extracts. *J. Biol. Chem.* **216,** 121–132 (1955).

19. Krebs, E. G. & Fischer, E. H. The phosphorylase b to a converting enzyme of rabbit skeletal muscle. *Biochim. Biophys. Acta* **20,** 150–157 (1956).

20. Krebs, E. G., Kent, A. B. & Fischer, E. H. The Muscle Phosphorylase b Kinase Reaction. *J. Biol. Chem.* **231,** 73–84 (1958).

21. Linn, T. C., Pettit, F. H. & Reed, L. J. Alpha-keto acid dehydrogenase complexes. X. Regulation of the activity of the pyruvate dehydrogenase complex from beef kidney mitochondria by phosphorylation and dephosphorylation. *Proc. Natl. Acad. Sci. U. S. A.* **62,** 234–241 (1969).

22. Walsh, D. A., Perkins, J. P. & Krebs, E. G. An adenosine 3',5'-monophosphate-dependant protein kinase from rabbit skeletal muscle. *J. Biol. Chem.* **243,** 3763–3765 (1968).

23. Hunter, T. A thousand and One Protein Kinases. *Cell* **50,** 823–829 (1987).

24. Kawai, S. & Hanafusa, H. The effects of reciprocal changes in temperature on the transformed state of cells infected with a Rous sarcoma virus mutant. *Virology* **46,** 470–479 (1971).

25. Brugge, J. S. & Erikson, R. L. Identification of a transformation-specific antigen induced by an avian sarcoma virus. *Nature* **269,** 346–348 (1977).

26. Stehelin, D., Varmus, H. E., Bishop, J. M. & Vogt, P. K. DNA related to the transforming gene(s) of avian sarcoma viruses is present in normal avian DNA. *Nature* **260,** 170–173 (1976).

27. Spector, D. H., Varmus, H. E. & Bishop, J. M. Nucleotide sequences related to the transforming gene of avian sarcoma virus are present in DNA of uninfected vertebrates. *Proc. Natl. Acad. Sci. U. S. A.* **75,** 4102–6 (1978).

28. Collett, M. S. & Erikson, R. L. Protein kinase activity associated with the avian sarcoma virus src gene product. *Proc. Natl. Acad. Sci. U. S. A.* **75,** 2021–2024 (1978).

29. Stoker, A. W., Enrietto, P. J. & Wyke, J. A. Functional domains of the pp60v-src protein as revealed by analysis of temperature-sensitive Rous sarcoma virus mutants. *Mol. Cell. Biol.* **4,** 1508–1514 (1984).

30. Snyder, M. A., Bishop, J. M., McGrath, J. P. & Levinson, A. D. A mutation at the ATP-binding site of pp60v-src abolishes kinase activity, transformation, and tumorigenicity. *Mol. Cell. Biol.* **5,** 1772–1779 (1985).

31. Cooper, J., Gould, K., Cartwright, C. & Hunter, T. Tyr527 is phosphorylated in pp60c-src: implications for regulation. *Science (80-.).* **231,** 1431–1434 (1986).

32. Piwnica-Worms, H., Saunders, K. B., Roberts, T. M., Smith, A. E. & Cheng, S. H. Tyrosine phosphorylation regulates the biochemical and biological properties of pp60c-src. *Cell* **49,** 75–82 (1987).

33. Kmiecik, T. E. & Shalloway, D. Activation and suppression of pp60c-srctransforming ability by mutation of its primary sites of tyrosine phosphorylation. *Cell* **49,** 65–73 (1987).

34. Cartwright, C. A., Eckhart, W., Simon, S. & Kaplan, P. L. Cell transformation by pp60c-src mutated in the carboxy-terminal regulatory domain. *Cell* **49,** 83–91 (1987).

35. Boggon, T. J. & Eck, M. J. Structure and regulation of Src family kinases. *Oncogene* **23,** 7918–7927 (2004).

36. Wheeler, D. L., Iida, M. & Dunn, E. F. The role of src in solid tumors. **14,** 667–678 (2012).

37. Carpenter, G. & Cohen, S. Epidermal growth factor. *Annu. Rev. Biochem.* **48,** 193–216 (1979).

38. CARPENTER, G., KING, L. & COHEN, S. Epidermal growth factor stimulates phosphorylation in membrane preparations in vitro. *Nature* **276,** 409–410 (1978).

39. Downward, J. *et al.* Close similarity of epidermal growth factor receptor and v-erb-B oncogene protein sequences. *Nature* **307,** 521–527 (1984).

40. Gilmore, T. & Martin, G. S. Protein Phosphorylation at Tyrosine Is Induced the v-erbB Gene Product In Vivo and In Vitro. *Cell* **40,** 609–618 (1985).

41. Kris, R. *et al.* Antibodies against a Synthetic Peptide as a Probe for the Kinase Activity of the Avian EGF Receptor and v-erbB Protein. *Cell* **40,** 619–625 (1985).

42. Chen, W. S. *et al.* Requirement for intrinsic protein tyrosine kinase in the immediate and late actions of the EGF receptor. *Nature* **328,** 820 (1987).

43. Honegger, A. M. *et al.* Point mutation at the ATP binding site of EGF receptor abolishes protein-tyrosine kinase activity and alters cellular routing. *Cell* **51,** 199–209 (1987).

44. Gill, G. N. *et al.* Relationship between production of epidermal growth factor receptors, gene amplification, and chromosome 7 translocation in variant A431 cells. *Somat. Cell Mol. Genet.* **11,** 309–318 (1985).

45. Kawamoto, T. *et al.* Relation of epidermal growth factor receptor concentration to growth of human epidermoid carcinoma A431 cells. *J. Biol. Chem.* **259,** 7761–7766 (1984).

46. Ullrich, A. *et al.* Human epidermal growth factor receptor cDNA sequence and aberrant expression of the amplified gene in A431 epidermoid carcinoma cells. *Nature* **309,** 418–425 (1984).

47. Yarden, Y. & Schlessinger, J. Epidermal Growth Factor Induces Rapid, Reversible Aggregation of the Purified Epidermal Growth Factor Receptor. *Biochemistry* **26,** 1443–1451 (1987).

48. Schlessinger, J. Signal transduction by allosteric receptor oligomerization. *Trends Biochem. Sci.* **13,** 443–447 (1988).

49. Honegger, a M., Kris, R. M., Ullrich, a & Schlessinger, J. Evidence that autophosphorylation of solubilized receptors for epidermal growth factor is mediated by intermolecular cross-phosphorylation. *Proc. Natl. Acad. Sci. U. S. A.* **86,** 925–929 (1989).

50. Lemmon, M. a. & Schlessinger, J. Cell signaling by receptor tyrosine kinases. *Cell*

141, 1117–1134 (2010).

51. Freed, D. M. *et al.* EGFR Ligands Differentially Stabilize Receptor Dimers to Specify Signaling Kinetics. *Cell* **171,** 683–695.e18 (2017).

52. Widmann, C., Gibson, S., Jarpe, M. B. & Johnson, G. L. Mitogen-Activated Protein Kinase: Conservation of a Three-Kinase Module From Yeast to Human. *Physiol Rev* **79,** 143–180 (1999).

53. Hanks, S., Quinn, A. & Hunter, T. The protein kinase family: conserved features and deduced phylogeny of the catalytic domains. *Science (80-.).* **241,** 42–52 (1988).

54. Manning, G., Whyte, D. B., Martinez, R., Hunter, T. & Sudarsanam, S. The Protein Kinase Complement of the Human Genome. *Science (80-.).* **298,** 1912–1934 (2002).

55. Knighton, D. R. *et al.* Crystal structure of the catalytic subunit of cyclic adenosine monophosphate-dependent protein kinase. *Science (80-.).* **253,** 407–414 (1991).

56. Endicott, J. A., Noble, M. E. M. & Johnson, L. N. The Structural Basis for Control of Eukaryotic Protein Kinases. *Annu. Rev. Biochem.* **81,** 587–613 (2012).

57. Konopka, J. B., Watanabe, S. M. & Witte, O. N. An alteration of the human c-abl protein in K562 leukemia cells unmasks associated tyrosine kinase activity. *Cell* **37,** 1035–1042 (1984).

58. Shtivelman, E., Lifshitz, B., Gale, R. P. & Canaani, E. Fused transcript of abl and bcr genes in chronic myelogenous leukaemia. *Nature* **315,** 550 (1985).

59. Daley, G., Van Etten, R. & Baltimore, D. Induction of Chronic Myelogenous Leukemia in Mice by the P210 bcr/abl Gene of the Philadelphia Chromosome. *Science (80-.).* **247,** 824–830 (1990).

60. Heisterkamp, N. *et al.* Acute leukaemia in bcr/abl transgenic mice. *Nature* **344,** 251 (1990).

61. Kelliher, M. A., McLaughlin, J., Witte, O. N. & Rosenberg, N. Induction of a chronic myelogenous leukemia-like syndrome in mice with v-abl and BCR/ABL. *Proc. Natl. Acad. Sci. U. S. A.* **87,** 6649–53 (1990).

62. Lugo, T. G., Pendergast, A. M., Muller, A. J. & Witte, O. N. Tyrosine kinase activity and transformation potency of bcr-abl oncogene products. *Science* **247,** 1079–82 (1990).

63. Daley, G. Q. & Baltimore, D. Transformation of an interleukin 3-dependent hematopoietic cell line by the chronic myelogenous leukemia-specific P210bcr/abl protein. *Proc. Natl. Acad. Sci. U. S. A.* **85,** 9312–6 (1988).

64. Szczylik, C. *et al.* Selective inhibition of leukemia cell proliferation by BCR-ABL antisense oligodeoxynucleotides. *Science (80-.).* **253,** 562–565 (1991).

65. Anafi, M., Gazit, A., Zehavi, A., Ben-Neriah, Y. & Levitzki, A. Tyrphostin-Induced Inhibition of p 210bcr-abl Tyrosine Kinase Activity Induces K562 to Differentiate. *Blood* **82,** 38–52 (1993).

66. Okabe, M. *et al.* Effect of Herbimycin A, an Antagonist of Tyrosine Kinase, on.

Blood **80,** 1330–1338 (1992).

67. Zimmermann, J. Phenylamino-pyrimidine (PAP) derivatives: a new class of potent and selective inhibitors of protein kinase C (PKC). *Arch. Pharm. (Weinheim)* **329,** 371–376 (1996).

68. Zimmermann, J. *et al.* Phenylamino-pyrimidine (PAP) - Derivatives: A new class of potent and highly selective PDGF-Receptor autophosphorylation inhibitors. *Bioorganic Med. Chem. Lett.* **6,** 1221–1226 (1996).

69. Druker, B. J. *et al.* Effects of a selective inhibitor of the Abl tyrosine kinase on the growth of Bcr–Abl positive cells. *Nat. Med.* **2,** 561–566 (1996).

70. Schindler, T. *et al.* Structural mechanism for STI-571 inhibition of Abelson tyrosine kinase. *Science (80-.).* **289,** 1938–1942 (2000).

71. Mohammadi, M. Structures of the Tyrosine Kinase Domain of Fibroblast Growth Factor Receptor in Complex with Inhibitors. *Science (80-.).* **276,** 955–960 (1997).

72. Johnson, L. N., Noble, M. E. M. & Owen, D. J. Active and inactive protein kinases: Structural basis for regulation. *Cell* **85,** 149–158 (1996).

73. Zhao, Z., Wu, H., Wang, L., Liu, Y. & Knapp, S. Exploration of Type II Binding Mode: a Privileged Approach for Kinase Inhibitor Focused Drug Discovery? *ACS Chem. …* (2014).

74. Nieborowska-Skorska, M. *et al.* Signal transducer and activator of transcription (STAT)5 activation by BCR/ABL is dependent on intact Src homology (SH)3 and SH2 domains of BCR/ABL and is required for leukemogenesis. *J. Exp. Med.* **189,** 1229–1242 (1999).

75. Horita, M. *et al.* Blockade of the Bcr-Abl Kinase Activity Induces Apoptosis of Chronic Myelogenous Leukemia Cells by Suppressing Signal Transducer and Activator of Transcription 5–Dependent Expression of Bcl-X L. *J. Exp. Med.* **191,** 977–984 (2000).

76. Gesbert, F., Sellers, W. R., Signoretti, S., Loda, M. & Griffin, J. D. BCR/ABL Regulates Expression of the Cyclin-dependent Kinase Inhibitor p27 ^{Kip1} through the Phosphatidylinositol 3-Kinase/AKT Pathway. *J. Biol. Chem.* **275,** 39223–39230 (2000).

77. Druker, B. J. & Lydon, N. B. Lessons learned from the development of an Abl tyrosine kinase inhibitor for chronic myelogenous leukemia. *J. Clin. Invest.* **105,** 3–7 (2000).

78. Druker, B. J. *et al.* Efficacy and Safety of a Specific Inhibitor of the BCR-ABL Tyrosine Kinase in Chronic Myeloid Leukemia. *N. Engl. J. Med.* **344,** 1031–1037 (2001).

79. Capdeville, R., Buchdunger, E., Zimmermann, J. & Matter, A. Glivec (ST1571, imatinib), a rationally developed, targeted anticancer drug. *Nat. Rev. Drug Discov.* **1,** 493–502 (2002).

80. Druker, B., Guilhot, F. & O.'Brien, S. Five-year follow-up of patients receiving imatinib for chronic myeloid leukemia. *N. Engl. J. Med.* **355,** 2408–2417 (2006).

81. Futreal, P. A. *et al.* A census of human cancer genes. *Nat. Rev. Cancer* **4,** 177–183 (2004).

82. Zhang, J., Yang, P. L. & Gray, N. S. Targeting cancer with small molecule kinase inhibitors. *Nat. Rev. Cancer* **9,** 28–39 (2009).

83. Beissert, T. *et al.* Targeting of the N-terminal coiled coil oligomerization interface by a helix-2 peptide inhibits unmutated and imatinib-resistant BCR/ABL. *Int. J. Cancer* **122,** 2744–2752 (2008).

84. Taylor, C. M. & Keating, A. E. Orientation and oligomerization specificity of the Bcr coiled-coil oligomerization domain. *Biochemistry* **44,** 16246–16256 (2005).

85. Wöhrle, F. U. *et al.* Gab2 signaling in chronic myeloid leukemia cells confers resistance to multiple Bcr-Abl inhibitors. *Leukemia* 118–129 (2012). doi:10.1038/leu.2012.222

86. Graham, S. M. *et al.* Primitive, quiescent, Philadelphia-positive stem cells from patients with chronic myeloid leukemia are insensitive to STI571 in vitro. *Blood* **99,** 319–325 (2002).

87. Claude Chomel, J. *et al.* Leukemic stem cell persistence in chronic myeloid leukemia patients in deep molecular response induced by tyrosine kinase inhibitors and the impact of therapy discontinuation. *Oncotarget* **7,** 35293–35301 (2016).

88. Holyoake, T. L. & Vetrie, D. The chronic myeloid leukemia stem cell : stemming the tide of persistence. **129,** 1595–1607 (2017).

89. Ichim, C. V. Kinase-independent mechanisms of resistance of leukemia stem cells to tyrosine kinase inhibitors. *Stem Cells Transl. Med.* **3,** 405–15 (2014).

90. Corbin, A. S. *et al.* Human chronic myeloid leukemia stem cells are insensitive to imatinib despite inhibition of BCR-ABL activity. *J. Clin. Invest.* **121,** 396–409 (2011).

91. Konig, H. *et al.* Enhanced BCR-ABL kinase inhibition does not result in increased inhibition of downstream signaling pathways or increased growth suppression in CML progenitors. *Leukemia* **22,** 748–755 (2008).

92. Prost, S. *et al.* Erosion of the chronic myeloid leukaemia stem cell pool by PPARγ agonists. *Nature* **525,** 380–383 (2015).

93. Okuda, K., Golub, T. R., Gilliland, D. G. & Griffin, J. D. p210BCR/ABL, p190BCR/ABL, and TEL/ABL activate similar signal transduction pathways in hematopoietic cell lines. *Oncogene* **13,** 1147–52 (1996).

94. Voss, J. *et al.* The leukaemic oncoproteins Bcr-Abl and Tel-Abl (ETV6/Abl) have altered substrate preferences and activate similar intracellular signalling pathways. *Oncogene* **19,** 1684–1690 (2000).

95. Golub, T. R. *et al.* Oligomerization of the ABL tyrosine kinase by the Ets protein TEL in human leukemia. *Mol. Cell. Biol.* **16,** 4107–16 (1996).

96. Million, R. P. The Tel-Abl (ETV6-Abl) tyrosine kinase, product of complex (9;12) translocations in human leukemia, induces distinct myeloproliferative disease in

mice. *Blood* **99,** 4568–4577 (2002).

97. Kovacic, B. *et al.* Diverging fates of cells of origin in acute and chronic leukaemia. *EMBO Mol. Med.* **4,** 283–297 (2012).

98. McLaughlin, J., Chianese, E. & Witte, O. N. In vitro transformation of immature hematopoietic cells by the P210 BCR/ABL oncogene product of the Philadelphia chromosome. *Proc Natl Acad Sci U S A* **84,** 6558–6562 (1987).

99. McLaughlin, J., Chianese, E. & Witte, O. N. Alternative forms of the BCR-ABL oncogene have quantitatively different potencies for stimulation of immature lymphoid cells. *Mol. Cell. Biol.* **9,** 1866–74 (1989).

100. Tala, I. *et al.* Contributions of the RhoGEF activity of p210 BCR/ABL to disease progression. *Leukemia* **27,** 1080–9 (2013).

101. Reckel, S. *et al.* Structural and functional dissection of the DH and PH domains of oncogenic Bcr-Abl tyrosine kinase. *Nat. Commun.* **8,** (2017).

102. Reckel, S. *et al.* Differential signaling networks of Bcr-Abl p210 and p190 kinases in leukemia cells defined by functional proteomics. *Leukemia* 1–11 (2017). doi:10.1038/leu.2017.36

103. Cutler, J. A. *et al.* Differential signaling through p190 and p210 BCR-ABL fusion proteins revealed by interactome and phosphoproteome analysis. *Leukemia* **31,** 1513–1524 (2017).

104. Zhang, H. *et al.* The Blk pathway functions as a tumor suppressor in chronic myeloid leukemia stem cells. *Nat. Genet.* **44,** 861–871 (2012).

105. Chen, Y., Hu, Y., Zhang, H., Peng, C. & Li, S. Loss of the Alox5 gene impairs leukemia stem cells and prevents chronic myeloid leukemia. *Nat. Genet.* **41,** 783–792 (2009).

106. Byrne, D. P., Foulkes, D. M. & Eyers, P. A. Pseudokinases: update on their functions and evaluation as new drug targets. *Future Med. Chem.* **2,** fmc-2016-0207 (2017).

107. Afzal, A. R. *et al.* Recessive Robinow syndrome, allelic to dominant brachydactyly type B, is caused by mutation of ROR2. *Nat. Genet.* **25,** 419 (2000).

108. Afzal, A. R. & Jeffery, S. One gene, two phenotypes: ROR2 mutations in autosomal recessive Robinow syndrome and autosomal dominant brachydactyly type B. *Hum. Mutat.* **22,** 1–11 (2003).

109. Oldridge, M. *et al.* Dominant mutations in ROR2, encoding an orphan receptor tyrosine kinase, cause brachydactyly type B. *Nat. Genet.* **24,** 275 (2000).

110. Al-Shawi, R., Ashton, S. V., Underwood, C. & Simons, J. P. Expression of the Ror1 and Ror2 receptor tyrosine kinase genes during mouse development. *Dev. Genes Evol.* **211,** 161–171 (2001).

111. Debebe, Z. & Rathmell, W. K. Ror2 as a therapeutic target in cancer. *Pharmacol. Ther.* **150,** 143–8 (2015).

112. O'Connell, M. P. *et al.* The orphan tyrosine kinase receptor, ROR2, mediates Wnt5A signaling in metastatic melanoma. *Oncogene* **29,** 34–44 (2010).

113. Morioka, K. *et al.* Orphan receptor tyrosine kinase ROR2 as a potential therapeutic target for osteosarcoma. *Cancer Sci.* **100,** 1227–1233 (2009).

114. Li, C. *et al.* Ror2 modulates the canonical Wnt signaling in lung epithelial cells through cooperation with Fzd2. *BMC Mol. Biol.* **9,** 1–11 (2008).

115. Daneshmanesh, A. H. *et al.* Orphan receptor tyrosine kinases ROR1 and ROR2 in hematological malignancies. *Leuk. Lymphoma* **54,** 843–850 (2013).

116. Zhang, S. *et al.* The onco-embryonic antigen ROR1 is expressed by a variety of human cancers. *Am. J. Pathol.* **181,** 1903–1910 (2012).

117. Oishi, I. *et al.* The receptor tyrosine kinase Ror2 is involved in non-canonical Wnt5a/JNK signalling pathway. *Genes to Cells* **8,** 645–654 (2003).

118. Kani, S. *et al.* The receptor tyrosine kinase Ror2 associates with and is activated by casein kinase I??? *J. Biol. Chem.* **279,** 50102–50109 (2004).

119. Yamamoto, H., Yoo, S. K., Nishita, M., Kikuchi, A. & Minami, Y. Wnt5a modulates glycogen synthase kinase 3 to induce phosphorylation of receptor tyrosine kinase Ror2. *Genes to Cells* **12,** 1215–1223 (2007).

120. Ho, H.-Y. H. *et al.* Wnt5a-Ror-Dishevelled signaling constitutes a core developmental pathway that controls tissue morphogenesis. *Proc. Natl. Acad. Sci.* **109,** 4044–4051 (2012).

121. Rasmussen, N. R. *et al.* Receptor tyrosine kinase-like orphan receptor 2 (Ror2) expression creates a poised state of wnt signaling in renal cancer. *J. Biol. Chem.* **288,** 26301–26310 (2013).

122. O'Connell, M. P. & Weeraratna, A. T. Hear the wnt ror: How melanoma cells adjust to changes in Wnt. *Pigment Cell Melanoma Res.* **22,** 724–739 (2009).

123. Mikels, A., Minami, Y. & Nusse, R. Ror2 receptor requires tyrosine kinase activity to mediate Wnt5A signaling. *J. Biol. Chem.* **284,** 30167–30176 (2009).

124. Artim, S. C., Mendrola, J. M. & Lemmon, M. A. Assessing the range of kinase autoinhibition mechanisms in the insulin receptor family. *Biochem. J.* **448,** 213–20 (2012).

125. Mendrola, J. M., Shi, F., Park, J. H. & Lemmon, M. A. Receptor tyrosine kinases with intracellular pseudokinase domains. *Biochem. Soc. Trans.* **41,** 1029–1036 (2013).

126. Therrien, M. *et al.* KSR, a novel protein kinase required for RAS signal transduction. *Cell* **83,** 879–888 (1995).

127. Sundaram, M. & Han, M. The C. elegans ksr-1 gene encodes a novel Raf-related kinase involved in Ras-mediated signal transduction. *Cell* **83,** 889–901 (1995).

128. Brennan, D. F. *et al.* A Raf-induced allosteric transition of KSR stimulates phosphorylation of MEK. *Nature* **472,** 366–9 (2011).

129. Hannigan, G. E., McDonald, P. C., Walsh, M. P. & Dedhar, S. Integrin-linked kinase: Not so pseudo after all. *Oncogene* **30,** 4375–4385 (2011).

130. Dhawan, N. S., Scopton, A. P. & Dar, A. C. Small molecule stabilization of the

KSR inactive state antagonizes oncogenic Ras signalling. *Nature* **537,** 112–116 (2016).

131. Dang, C. V., Reddy, E. P., Shokat, K. M. & Soucek, L. Drugging the 'undruggable' cancer targets. *Nat. Rev. Cancer* **17,** (2017).

132. Fire, A. *et al.* Potent and specific genetic interference by double-stranded RNA in caenorhabditis elegans. *Nature* **391,** 806–811 (1998).

133. Hutvágner, G. & Zamore, P. D. A microRNA in a multiple-turnover RNAi enzyme complex. *Science* **297,** 2056–60 (2002).

134. Bumcrot, D., Manoharan, M., Koteliansky, V. & Sah, D. W. Y. RNAi therapeutics: a potential new class of pharmaceutical drugs. *Nat. Chem. Biol.* **2,** 711–719 (2006).

135. Hutvagner, G. & Simard, M. J. Argonaute proteins: Key players in RNA silencing. *Nat. Rev. Mol. Cell Biol.* **9,** 22–32 (2008).

136. Reynolds, A. *et al.* Rational siRNA design for RNA interference. *Nat. Biotechnol.* **22,** 326–330 (2004).

137. Paddison, P. J., Caudy, A. A., Bernstein, E., Hannon, G. J. & Conklin, D. S. Short hairpin RNAs (shRNAs) induce sequence-specific silencing in mammalian cells. *Genes Dev.* **16,** 948–958 (2002).

138. Heikkila, R. *et al.* A c-myc antisense oligodeoxynucleotide inhibits entry into S phase but not progress from G0 to G1. *Nature* **328,** 445–449 (1987).

139. Zamecnik, P. C., Goodchild, J., Taguchi, Y. & Sarin, P. S. Inhibition of replication and expression of human T-cell lymphotropic virus type III in cultured cells by exogenous synthetic oligonucleotides complementary to viral RNA. *Proc Natl Acad Sci U S A* **83,** 4143–4146 (1986).

140. Mendell, J. R. *et al.* Eteplirsen for the treatment of Duchenne muscular dystrophy. *Ann. Neurol.* **74,** 637–647 (2013).

141. Gaj, T., Gersbach, C. a & Barbas, C. F. ZFN, TALEN, and CRISPR/Cas-based methods for genome engineering. *Trends Biotechnol.* **31,** 397–405 (2013).

142. Jinek, M. *et al.* A Programmable Dual-RNA – Guided DNA Endonuclease in Adaptice Bacterial Immunity. *Science* **337,** 816–822 (2012).

143. Ran, F. A. *et al.* Genome engineering using the CRISPR-Cas9 system. *Nat. Protoc.* **8,** 2281–308 (2013).

144. Wang, H. *et al.* One-step generation of mice carrying mutations in multiple genes by CRISPR/Cas-mediated genome engineering. *Cell* **153,** 910–8 (2013).

145. Cong, L. *et al.* Multiplex genome engineering using CRISPR/Cas systems. *Science* **339,** 819–23 (2013).

146. Schmid-Burgk, J. L., Höning, K., Ebert, T. S. & Hornung, V. CRISPaint allows modular base-specific gene tagging using a ligase-4-dependent mechanism. *Nat. Commun.* **7,** 12338 (2016).

147. Silva, J. M. *et al.* Second-generation shRNA libraries covering the mouse and

human genomes. *Nat. Genet.* **37,** 1281–1288 (2005).

148. Hart, T. *et al.* High-Resolution CRISPR Screens Reveal Fitness Genes and Genotype-Specific Cancer Liabilities Screens Reveal Fitness Genes. *Cell* **163,** 1–12 (2015).

149. Shalem, O. *et al.* Genome-scale CRISPR-Cas9 knockout screening in human cells. *Science (80-.).* **343,** 84–87 (2014).

150. Chen, S. *et al.* Genome-wide CRISPR screen in a mouse model of tumor growth and metastasis. *Cell* **160,** 1246–1260 (2015).

151. Flowers, G. P., Sanor, L. D. & Crews, C. M. Lineage tracing of genome-edited alleles reveals high fidelity axolotl limb regeneration. *Elife* **6,** 1–15 (2017).

152. Coelho, T. *et al.* Safety and Efficacy of RNAi Therapy for Transthyretin Amyloidosis. *N. Engl. J. Med.* **369,** 819–829 (2013).

153. Juliano, R. L. The delivery of therapeutic oligonucleotides. *Nucleic Acids Res.* **44,** 6518–6548 (2016).

154. Tabernero, J. *et al.* First-in-humans trial of an RNA interference therapeutic targeting VEGF and KSP in cancer patients with liver involvement. *Cancer Discov.* **3,** 406–417 (2013).

155. Conde, J., Oliva, N., Atilano, M., Song, H. S. & Artzi, N. Self-assembled RNA-triple-helix hydrogel scaffold for microRNA modulation in the tumour microenvironment. *Nat. Mater.* **15,** 353–363 (2016).

156. Conde, J. & Artzi, N. Are RNAi and miRNA therapeutics truly dead? *Trends Biotechnol.* **33,** 141–144 (2015).

157. Lee, S. H., Kang, Y. Y., Jang, H. E. & Mok, H. Current preclinical small interfering RNA (siRNA)-based conjugate systems for RNA therapeutics. *Adv. Drug Deliv. Rev.* **104,** 78–92 (2016).

158. Wu, S. Y., Lopez-Berestein, G., Calin, G. A. & Sood, A. K. RNAi therapies: Drugging the undruggable. *Sci. Transl. Med.* **6,** 1–8 (2014).

159. Burslem, G. M. & Crews, C. M. Small-Molecule Modulation of Protein Homeostasis. *Chem. Rev.* **117,** 11269–11301 (2017).

160. Lin, Y. H. & Pratt, M. R. A Dual Small-Molecule Rheostat for Precise Control of Protein Concentration in Mammalian Cells. *ChemBioChem* **15,** 805–809 (2014).

161. Navarro, R., Chen, L. C., Rakhit, R. & Wandless, T. J. A Novel Destabilizing Domain Based on a Small-Molecule Dependent Fluorophore. *ACS Chem. Biol.* **11,** 2101–2104 (2016).

162. Nora, E. P. *et al.* Targeted Degradation of CTCF Decouples Local Insulation of Chromosome Domains from Genomic Compartmentalization. *Cell* **169,** 930–944.e22 (2017).

163. Zhang, L., Ward, J. D., Cheng, Z. & Dernburg, A. F. The auxin-inducible degradation (AID) system enables versatile conditional protein depletion in C. elegans. *Development* 4374–4384 (2015). doi:10.1242/dev.129635

164. Wilmington, S. R. & Matouschek, A. An inducible system for rapid degradation of specific cellular proteins using proteasome adaptors. *PLoS One* **11,** (2016).

165. Weintraub, A. S. *et al.* YY1 Is a Structural Regulator of Enhancer-Promoter Loops. *Cell* **171,** 1573–1588.e28 (2017).

166. Buckley, D. L. *et al.* HaloPROTACS: Use of Small Molecule PROTACs to Induce Degradation of HaloTag Fusion Proteins. *ACS Chem. Biol.* **10,** 1831–1837 (2015).

167. Liang, J. & Shang, Y. Estrogen and Cancer. *Annu. Rev. Physiol.* **75,** 225–240 (2013).

168. Dauvois, S., Danielian, P. S., White, R. & Parker, M. G. Antiestrogen ICI 164,384 reduces cellular estrogen receptor content by increasing its turnover. *Proc. Natl. Acad. Sci. U. S. A.* **89,** 4037–4041 (1992).

169. Wakeling, A. E., Dukes, M. & Bowler, J. A Potent Specific Pure Antiestrogen with Clinical Potential. *Am. Assoc. Cancer Res.* 3867–3873 (1991).

170. Lai, A. *et al.* Identification of GDC-0810 (ARN-810), an Orally Bioavailable Selective Estrogen Receptor Degrader (SERD) that Demonstrates Robust Activity in Tamoxifen-Resistant Breast Cancer Xenografts. *J. Med. Chem.* **58,** 4888–4904 (2015).

171. McDonnell, D. P., Wardell, S. E. & Norris, J. D. Oral Selective Estrogen Receptor Downregulators (SERDs), a Breakthrough Endocrine Therapy for Breast Cancer. *J. Med. Chem.* **58,** 4883–4887 (2015).

172. Wu, Y.-L. *et al.* Structural basis for an unexpected mode of SERM-mediated ER antagonism. *Mol. Cell* **18,** 413–24 (2005).

173. Wittmann, B. M., Sherk, A. & McDonnell, D. P. Definition of functionally important mechanistic differences among selective estrogen receptor down-regulators. *Cancer Res.* **67,** 9549–60 (2007).

174. Krönke, J. *et al.* Lenalidomide causes selective degradation of IKZF1 and IKZF3 in multiple myeloma cells. *Science* **343,** 301–5 (2014).

175. Lu, G. *et al.* The myeloma drug lenalidomide promotes the cereblon-dependent destruction of Ikaros proteins. *Science* **343,** 305–9 (2014).

176. Gandhi, A. K. *et al.* Immunomodulatory agents lenalidomide and pomalidomide co-stimulate T cells by inducing degradation of T cell repressors Ikaros and Aiolos via modulation of the E3 ubiquitin ligase complex CRL4CRBN. *Br. J. Haematol.* **164,** 811–821 (2014).

177. Krönke, J. *et al.* Lenalidomide induces ubiquitination and degradation of CK1α in del(5q) MDS. *Nature* **523,** 183–8 (2015).

178. Chamberlain, P. P. *et al.* Structure of the human Cereblon–DDB1–lenalidomide complex reveals basis for responsiveness to thalidomide analogs. *Nat. Struct. Mol. Biol.* **21,** 803–809 (2014).

179. Fischer, E. S. *et al.* Structure of the DDB1-CRBN E3 ubiquitin ligase in complex with thalidomide. *Nature* **512,** 49–53 (2014).

180. Petzold, G., Fischer, E. S. & Thomä, N. H. Structural basis of lenalidomide-

induced CK1α degradation by the CRL4CRBN ubiquitin ligase. *Nature* (2016). doi:10.1038/nature16979

181. Matyskiela, M. E. *et al.* A novel cereblon modulator recruits GSPT1 to the CRL4CRBN ubiquitin ligase. *Nature* **535,** 252–257 (2016).

182. Han, T. *et al.* Anticancer sulfonamides target splicing by inducing RBM39 degradation via recruitment to DCAF15. *Science (80-.).* **356,** (2017).

183. Uehara, T. *et al.* Selective degradation of splicing factor CAPERα By anticancer sulfonamides. *Nat. Chem. Biol.* **13,** 675–680 (2017).

184. Neklesa, T. K. *et al.* Small-molecule hydrophobic tagging-induced degradation of HaloTag fusion proteins. *Nat. Chem. Biol.* **7,** 538–43 (2011).

185. Tae, H. S. *et al.* Identification of Hydrophobic Tags for the Degradation of Stabilized Proteins. *ChemBioChem* **13,** 538–541 (2012).

186. Long, M. J. C., Gollapalli, D. R. & Hedstrom, L. Inhibitor Mediated Protein Degradation. *Chem. Biol.* **19,** 629–637 (2012).

187. Xie, T. *et al.* Pharmacological targeting of the pseudokinase Her3. *Nat. Chem. Biol.* **10,** 1006–1012 (2014).

188. Gustafson, J. L. *et al.* Small-Molecule-Mediated Degradation of the Androgen Receptor through Hydrophobic Tagging. *Angew. Chemie Int. Ed.* **54,** 9659–9662 (2015).

189. Karin, M. & Ben-Neriah, Y. Phosphorylation Meets Ubiquitination: The Control of NF-κB Activity. *Annu. Rev. Immunol.* **18,** 621–663 (2000).

190. Glickman, M. H. & Ciechanover, A. The Ubiquitin-Proteasome Proteolytic Pathway: Destruction for the Sake of Construction. *Physiol. Rev.* **82,** 373–428 (2002).

191. Goldstein, G. *et al.* Isolation of a polypeptide that has lymphocyte-differentiating properties and is probably represented universally in living cells. *Proc. Natl. Acad. Sci.* **72,** 11–15 (1975).

192. Goldknopf, I. L. & Busch, H. Isopeptide linkage between nonhistone and histone 2A polypeptides of chromosomal conjugate-protein A24. *Proc. Natl. Acad. Sci.* **74,** 864–868 (1977).

193. Hershko, A. & Tomkins, G. M. Studies on the Degradation of Tyrosine Aminotransferase in Hepatoma Cells in Culture: INFLUENCE OF THE COMPOSITION OF THE MEDIUM AND ADENOSINE TRIPHOSPHATE DEPENDENCE. *J. Biol. Chem.* **246,** 710–714 (1971).

194. Yau, R. & Rape, M. The increasing complexity of the ubiquitin code. *Nat. Cell Biol.* **18,** 579–586 (2016).

195. Swatek, K. N. & Komander, D. Ubiquitin modifications. *Cell Res.* **26,** 399–422 (2016).

196. Sakamoto, K. M. *et al.* Protacs: chimeric molecules that target proteins to the Skp1-Cullin-F box complex for ubiquitination and degradation. *Proc. Natl. Acad. Sci. U. S. A.* **98,** 8554–8559 (2001).

197. Schneekloth, J. S. *et al.* Chemical Genetic Control of Protein Levels: Selective in Vivo Targeted Degradation. *J. Am. Chem. Soc.* **126,** 3748–3754 (2004).

198. Schneekloth, A. R., Pucheault, M., Tae, H. S. & Crews, C. M. Targeted intracellular protein degradation induced by a small molecule: En route to chemical proteomics. *Bioorg. Med. Chem. Lett.* **18,** 5904–8 (2008).

199. Itoh, Y., Kitaguchi, R., Ishikawa, M., Naito, M. & Hashimoto, Y. Design, synthesis and biological evaluation of nuclear receptor-degradation inducers. *Bioorganic Med. Chem.* **19,** 6768–6778 (2011).

200. Hines, J., Gough, J. D., Corson, T. W. & Crews, C. M. Posttranslational protein knockdown coupled to receptor tyrosine kinase activation with phosphoPROTACs. *Proc. Natl. Acad. Sci. U. S. A.* **110,** 8942–7 (2013).

201. Okuhira, K. *et al.* in **1366,** 549–560 (2016).

202. Okuhira, K. *et al.* Specific degradation of CRABP-II via cIAP1-mediated ubiquitylation induced by hybrid molecules that crosslink cIAP1 and the target protein. *FEBS Lett.* **585,** 1147–1152 (2011).

203. Sekine, K. *et al.* Small molecules destabilize cIAP1 by activating auto-ubiquitylation. *J. Biol. Chem.* **283,** 8961–8968 (2008).

204. Zhang, D., Baek, S. H., Ho, A. & Kim, K. Degradation of target protein in living cells by small-molecule proteolysis inducer. *Bioorganic Med. Chem. Lett.* **14,** 645–648 (2004).

205. Fan, X., Jin, W. Y., Lu, J., Wang, J. & Wang, Y. T. Rapid and reversible knockdown of endogenous proteins by peptide-directed lysosomal degradation. *Nat. Neurosci.* **17,** 471–480 (2014).

206. Kibel, A., Iliopoulos, O., DeCaprio, J. a & Kaelin, W. G. Binding of the von Hippel-Lindau tumor suppressor protein to Elongin B and C. *Science* **269,** 1444–1446 (1995).

207. Iwai, K. *et al.* Identification of the von Hippel-lindau tumor-suppressor protein as part of an active E3 ubiquitin ligase complex. *Proc. Natl. Acad. Sci. U. S. A.* **96,** 12436–12441 (1999).

208. Kamura, T. *et al.* Activation of HIF1alpha ubiquitination by a reconstituted von Hippel-Lindau (VHL) tumor suppressor complex. *Proc. Natl. Acad. Sci. U. S. A.* **97,** (2000).

209. Maxwell, P. H. *et al.* The tumour suppressor protein VHL targets hypoxia-inducible factors for oxygen-dependent proteolysis. *Nature* **399,** 271–275 (1999).

210. Jaakkola, P. *et al.* Targeting of HIF-alpha to the von Hippel-Lindau ubiquitylation complex by O2-regulated prolyl hydroxylation. *Science* **292,** 468–472 (2001).

211. Ivan, M. *et al.* HIFalpha targeted for VHL-mediated destruction by proline hydroxylation: implications for O2 sensing. *Science* **292,** 464–8 (2001).

212. Hon, W.-C. *et al.* Structural basis for the recognition of hydroxyproline in HIF-1 alpha by pVHL. *Nature* **417,** 975–978 (2002).

213. Buckley, D. L. *et al.* Small-molecule inhibitors of the interaction between the E3

ligase VHL and HIF1α. *Angew. Chem. Int. Ed. Engl.* **51,** 11463–7 (2012).

214. Buckley, D. L. *et al.* Targeting the von Hippel–Lindau E3 Ubiquitin Ligase Using Small Molecules To Disrupt the VHL/HIF-1α Interaction. *J. Am. Chem. Soc.* **134,** 4465–4468 (2012).

215. Galdeano, C. *et al.* Structure-Guided Design and Optimization of Small Molecules Targeting the Protein-Protein Interaction between the von Hippel-Lindau (VHL) E3 Ubiquitin Ligase and the Hypoxia Inducible Factor (HIF) Alpha Subunit with in Vitro Nanomolar Affinities. *J. Med. Chem.* **57,** 8657–63 (2014).

216. Negoro, N. *et al.* Discovery of TAK-875: A Potent, Selective, and Orally Bioavailable GPR40 Agonist. *ACS Med. Chem. Lett.* **1,** 290–294 (2010).

217. Frost, J. *et al.* Potent and selective chemical probe of hypoxic signalling downstream of HIF-α hydroxylation via VHL inhibition. *Nat. Commun.* **7,** 1–12 (2016).

218. Kobayashi, K. *et al.* RICK/Rip2/CARDIAK mediates signalling for receptors of the innate and adaptive immune systems. *Nature* **416,** 194–9 (2002).

219. Kulak, N. a, Pichler, G., Paron, I., Nagaraj, N. & Mann, M. Minimal, encapsulated proteomic-sample processing applied to copy-number estimation in eukaryotic cells. *Nat. Methods* **11,** 319–24 (2014).

220. Wiśniewski, J. R. *et al.* Extensive quantitative remodeling of the proteome between normal colon tissue and adenocarcinoma. *Mol. Syst. Biol.* **8,** (2012).

221. Zhao, L. *et al.* Intracellular water-specific MR of microbead-adherent cells: the HeLa cell intracellular water exchange lifetime. *NMR Biomed.* **21,** 159–164 (2008).

222. Laurence, H. ATP-competitive inhibitors block protein kinase recruitment to the Hsp90-Cdc37 system. *Nat. Chem. Biol.* 1–8 (2013). doi:10.1038/nchembio.1212

223. Jewell, U. R. *et al.* Induction of HIF-1alpha in response to hypoxia is instantaneous. *FASEB J.* **15,** 1312–1314 (2001).

224. Mattiroli, F. & Sixma, T. K. Lysine-targeting specificity in ubiquitin and ubiquitin-like modification pathways. *Nat. Struct. Mol. Biol.* **21,** 308–16 (2014).

225. Hagai, T., Tóth-Petróczy, Á., Azia, A. & Levy, Y. The origins and evolution of ubiquitination sites. *Mol. Biosyst.* **8,** 1865 (2012).

226. Guharoy, M., Bhowmick, P. & Tompa, P. Design principles involving protein disorder facilitate specific substrate selection and degradation by the ubiquitin-proteasome system. *J. Biol. Chem.* **291,** 6723–31 (2016).

227. Jordan, V. C. Tamoxifen: A most unlikely pioneering medicine. *Nat. Rev. Drug Discov.* **2,** 205–213 (2003).

228. Harper, M. J. & Walpole, a L. A new derivative of triphenylethylene: effect on implantation and mode of action in rats. *J. Reprod. Fertil.* **13,** 101–119 (1967).

229. Furr, B. J. *et al.* ICI 176,334: a novel non-steroidal, peripherally selective antiandrogen. *J. Endocrinol.* **113,** R7-9 (1987).

230. Cyrus, K. *et al.* Impact of linker length on the activity of PROTACs. *Mol. BioSyst.* **7,** 359–364 (2011).

231. Puppala, D., Lee, H., Kim, K. B. & Swanson, H. I. Development of an aryl hydrocarbon receptor antagonist using the proteolysis-targeting chimeric molecules approach: a potential tool for chemoprevention. *Mol. Pharmacol.* **73,** 1064–1071 (2008).

232. Sakamoto, K. M. *et al.* Development of Protacs to target cancer-promoting proteins for ubiquitination and degradation. *Mol. Cell. Proteomics* **2,** 1350–1358 (2003).

233. Degorce, S. L. *et al.* Investigation of (E)-3-[4-(2-oxo-3-aryl-chromen-4-yl)oxyphenyl]acrylic acids as oral selective estrogen receptor down-regulators. *J. Med. Chem.* **58,** 3522–3533 (2015).

234. Eichner, L. J. & Giguère, V. Estrogen related receptors (ERRs): A new dawn in transcriptional control of mitochondrial gene networks. *Mitochondrion* **11,** 544–552 (2011).

235. Giguère, V. Transcriptional control of energy homeostasis by the estrogen-related receptors. *Endocr. Rev.* **29,** 677–696 (2008).

236. Luo, C. *et al.* ERRα Maintains Mitochondrial Oxidative Metabolism and Constitutes an Actionable Target in PGC1α-Elevated Melanomas. *Mol. Cancer Res.* **15,** 1366–1375 (2017).

237. Du, Y. *et al.* The discovery of novel, potent ERR-alpha inverse agonists for the treatment of triple negative breast cancer. *Eur. J. Med. Chem.* **136,** 457–467 (2017).

238. Fiori, J. L. *et al.* The cannabinoid receptor inverse agonist AM251 regulates the expression of the EGF receptor and its ligands via destabilization of oestrogen-related receptor alpha protein. *Br J Pharmacol* **164,** 1026–1040 (2011).

239. Patch, R. J. *et al.* Identification of diaryl ether-based ligands for estrogen-related receptor α as potential antidiabetic agents. *J. Med. Chem.* **54,** 788–808 (2011).

240. Omlin, A. *et al.* AZD3514, an oral selective androgen receptor down-regulator in patients with castration-resistant prostate cancer - Results of two parallel first-in-human phase I studies. *Invest. New Drugs* **33,** 679–690 (2015).

241. Safran, M. *et al.* Mouse model for noninvasive imaging of HIF prolyl hydroxylase activity: Assessment of an oral agent that stimulates erythropoietin production. *Proc. Natl. Acad. Sci.* **103,** 105–110 (2006).

242. Ju, D., He, J., Zhao, L., Zheng, X. & Yang, G. Estrogen related receptor α-induced adipogenesis is PGC-1β-dependent. *Mol. Biol. Rep.* **39,** 3343–54 (2012).

243. Nie, Y. & Wong, C. Suppressing the activity of ERRa in 3T3-L1 adipocytes reduces mitochondrial biogenesis but enhances glycolysis and basal glucose uptake. *J. Cell. Mol. Med.* **13,** 3051–3060 (2009).

244. Schneekloth, J. S. *et al.* Chemical Genetic Control of Protein Levels: Selective in Vivo Targeted Degradation. *J. Am. Chem. Soc.* **126,** 3748–3754 (2004).

245. Ito, T. *et al.* Identification of a primary target of thalidomide teratogenicity. *Science* **327,** 1345–1350 (2010).

246. Winter, G. E. *et al.* Phthalimide conjugation as a strategy for in vivo target protein degradation. *Science* **348,** 1376–81 (2015).

247. Lu, J. *et al.* Hijacking the E3 Ubiquitin Ligase Cereblon to Efficiently Target BRD4. *Chem. Biol.* **22,** 755–763 (2015).

248. Remillard, D. *et al.* Degradation of the BAF Complex Factor BRD9 by Heterobifunctional Ligands. *Angew. Chemie Int. Ed.* **56,** 5738–5743 (2017).

249. Toure, M. & Crews, C. M. Small-molecule PROTACS: New approaches to protein degradation. *Angew. Chemie - Int. Ed.* **55,** 1966–1973 (2016).

250. Lai, A. C. *et al.* Modular PROTAC Design for the Degradation of Oncogenic BCR-ABL. *Angew. Chemie Int. Ed.* **55,** 807–810 (2016).

251. Ottis, P. *et al.* Assessing Different E3 Ligases for Small Molecule-induced Protein Ubiquitination and Degradation. *ACS Chem. Biol.* acschembio.7b00485 (2017). doi:10.1021/acschembio.7b00485

252. Ohoka, N. *et al.* In Vivo Knockdown of Pathogenic Proteins via Specific and Nongenetic IAP-dependent Protein Erasers (SNIPERs). *J. Biol. Chem.* jbc.M116.768853 (2017). doi:10.1074/jbc.M116.768853

253. Okuhira, K. *et al.* Development of hybrid small molecules that induce degradation of estrogen receptor-alpha and necrotic cell death in breast cancer cells. *Cancer Sci.* **104,** 1492–1498 (2013).

254. Jin, X. *et al.* MAGE-TRIM28 complex promotes the Warburg effect and hepatocellular carcinoma progression by targeting FBP1 for degradation. *Oncogenesis* **6,** e312 (2017).

255. Lee, J., Udugamasooriya, D. G., Lim, H.-S. & Kodadek, T. Potent and selective photo-inactivation of proteins with peptoid-ruthenium conjugates. *Nat. Chem. Biol.* **6,** 258–260 (2010).

256. Cox, A. D., Fesik, S. W., Kimmelman, A. C., Luo, J. & Der, C. J. Drugging the undruggable RAS: Mission Possible? *Nat. Rev. Drug Discov.* **13,** 828–851 (2014).

257. Zhu, Z. & Cuozzo, J. Review Article: High-Throughput Affinity-Based Technologies for Small-Molecule Drug Discovery. *J. Biomol. Screen.* **14,** 1157–1164 (2009).

258. Lipinski, C. A., Lombardo, F., Dominy, B. W. & Feeney, P. J. Experimental and Computational Approaches to Estimate Solubility and Permeability in Drug Discovery and Develop ment Settings. *Adv. Drug Deliv. Rev.* **23,** 3–25 (1997).

259. Raina, K. *et al.* PROTAC-induced BET protein degradation as a therapy for castration-resistant prostate cancer. *Proc Natl Acad Sci U S A* **113,** 7124–7129 (2016).

260. Neklesa, T. K., Winkler, J. D. & Crews, C. M. Targeted protein degradation by PROTACs ☆. *Pharmacol. Ther.* (2017). doi:10.1016/j.pharmthera.2017.02.027

261. Douglass, E. F., Miller, C. J., Sparer, G., Shapiro, H. & Spiegel, D. A. A comprehensive mathematical model for three-body binding equilibria. *J. Am. Chem. Soc.* **135,** 6092–6099 (2013).

262. Fischer, E. S., Park, E., Eck, M. J. & Thomä, N. H. SPLINTS: Small-molecule protein ligand interface stabilizers. *Curr. Opin. Struct. Biol.* **37,** 115–122 (2016).

263. Paltoglou, S. & Roberts, B. J. HIF-1α and EPAS ubiquitination mediated by the VHL tumour suppressor involves flexibility in the ubiquitination mechanism, similar to other RING E3 ligases. *Oncogene* **26,** 604–609 (2007).

264. Zhang, Z. R., Bonifacino, J. S. & Hegde, R. S. Deubiquitinases sharpen substrate discrimination during membrane protein degradation from the ER. *Cell* **154,** 609–622 (2013).

265. Noblin, D. J. *et al.* A HaloTag-based small molecule microarray screening methodology with increased sensitivity and multiplex capabilities. *ACS Chem. Biol.* **7,** 2055–63 (2012).

266. Los, G. V *et al.* HaloTag: A novel protein labeling technology for cell imaging and protein analysis. *ACS Chem. Biol.* **3,** 373–382 (2008).

267. Wagner, S. a. *et al.* A Proteome-wide, Quantitative Survey of In Vivo Ubiquitylation Sites Reveals Widespread Regulatory Roles. *Mol. Cell. Proteomics* **10,** M111.013284-M111.013284 (2011).

268. Ye, Y. & Rape, M. Building ubiquitin chains: E2 enzymes at work. *Nat. Rev. Mol. Cell Biol.* **10,** 755–64 (2009).

269. Tebar, F., Bohlander, S. K. & Sorkin, A. Clathrin Assembly Lymphoid Myeloid Leukemia (CALM) Protein: Localization in Endocytic-coated Pits, Interactions with Clathrin, and the Impact of Overexpression on Clathrin-mediated Traffic. *Mol. Biol. Cell* **10,** 2687–2702 (1999).

270. Bielefeld-Sevigny, M. AlphaLISA immunoassay platform- the 'no-wash' high-throughput alternative to ELISA. *Assay Drug Dev. Technol.* **7,** 90–2 (2009).

271. Krissinel, E. & Henrick, K. Inference of Macromolecular Assemblies from Crystalline State. *J. Mol. Biol.* **372,** 774–797 (2007).

272. Deshaies, R. J. & Joazeiro, C. a P. RING domain E3 ubiquitin ligases. *Annu. Rev. Biochem.* **78,** 399–434 (2009).

273. Min, J.-H. *et al.* Structure of an HIF-1alpha -pVHL complex: hydroxyproline recognition in signaling. *Science* **296,** 1886–1889 (2002).

274. Nguyen, T. Van *et al.* Glutamine Triggers Acetylation-Dependent Degradation of Glutamine Synthetase via the Thalidomide Receptor Cereblon. *Mol. Cell* **61,** 809–820 (2016).

275. Robb, C. M. *et al.* Chemically induced degradation of CDK9 by a proteolysis targeting chimera (PROTAC). *Chem. Commun.* (2017). doi:10.1039/C7CC03879H

276. Olson, C. M. *et al.* Pharmacological perturbation of CDK9 using selective CDK9 inhibition or degradation. *Nat. Chem. Biol.* (2017). doi:10.1038/nchembio.2538

277. Burslem, G. M. *et al.* The Advantages of Targeted Protein Degradation Over Inhibition: An RTK Case Study. *Cell Chem. Biol.* 1–14 (2017). doi:10.1016/j.chembiol.2017.09.009

278. Bondeson, D. P. *et al.* Catalytic in vivo protein knockdown by small-molecule PROTACs. *Nat. Chem. Biol.* **11,** 611–617 (2015).

279. Zengerle, M., Chan, K.-H. & Ciulli, A. Selective Small Molecule Induced Degradation of the BET Bromodomain Protein BRD4. *ACS Chem. Biol.* **10,** 1770–7 (2015).

280. Gadd, M. S. *et al.* Structural basis of PROTAC cooperative recognition for selective protein degradation. *Nat. Chem. Biol.* **13,** 514–521 (2017).

281. Chessum, N. E. A. *et al.* Demonstrating In-Cell Target Engagement using a Pirin Protein Degradation Probe (CCT367766). *J. Med. Chem.* acs.jmedchem.7b01406 (2017). doi:10.1021/acs.jmedchem.7b01406

282. Duda, D. M. *et al.* Structural insights into NEDD8 activation of cullin-RING ligases: conformational control of conjugation. *Cell* **134,** 995–1006 (2008).

283. Liu, J. & Nussinov, R. The mechanism of ubiquitination in the cullin-RING E3 ligase machinery: Conformational control of substrate orientation. *PLoS Comput. Biol.* **5,** (2009).

284. Liu, J. & Nussinov, R. Flexible cullins in cullin-RING E3 ligases allosterically regulate ubiquitination. *J. Biol. Chem.* **286,** 40934–40942 (2011).

285. Liu, J. & Nussinov, R. Molecular Dynamics Reveal the Essential Role of Linker Motions in the Function of Cullin–RING E3 Ligases. *J. Mol. Biol.* **396,** 1508–1523 (2010).

286. Vijayan, R. S. K. *et al.* Conformational analysis of the DFG-out kinase motif and biochemical profiling of structurally validated type II inhibitors. *J. Med. Chem.* **58,** 466–479 (2015).

287. Qian, F. *et al.* Inhibition of Tumor Cell Growth, Invasion, and Metastasis by EXEL-2880 (XL880, GSK1363089), a Novel Inhibitor of HGF and VEGF Receptor Tyrosine Kinases. *Cancer Res.* **69,** 8009–8016 (2009).

288. Duncan, J. S. *et al.* Dynamic reprogramming of the kinome in response to targeted MEK inhibition in triple-negative breast cancer. *Cell* **149,** 307–321 (2012).

289. Karaman, M. W. *et al.* A quantitative analysis of kinase inhibitor selectivity. *Nat. Biotechnol.* **26,** 127–132 (2008).

290. Fabian, M. A. *et al.* A small molecule-kinase interaction map for clinical kinase inhibitors. *Nat. Biotechnol.* **23,** 329–36 (2005).

291. Field, S. D., Arkin, J., Li, J. & Jones, L. H. Selective Downregulation of JAK2 and JAK3 by an ATP-Competitive pan-JAK Inhibitor. *ACS Chem. Biol.* acschembio.7b00116 (2017). doi:10.1021/acschembio.7b00116

292. Mcalister, G. C. *et al.* MultiNotch MS3 Enables Accurate, Sensitive, and Multiplexed Detection of Differential Expression across Cancer Cell Line

Proteomes Graeme C. McAlister, 1 David P. Nusinow, 1. *Anal. Chem.* **86,** 7150–7158 (2014).

293. McAlister, G. C. *et al.* Increasing the multiplexing capacity of TMTs using reporter ion isotopologues with isobaric masses. *Anal. Chem.* **84,** 7469–7478 (2012).

294. Bier, D., Thiel, P., Briels, J. & Ottmann, C. Stabilization of Protein–Protein Interactions in chemical biology and drug discovery. *Prog. Biophys. Mol. Biol.* **119,** 10–19 (2015).

295. Briesewitz, R., Ray, G. T., Wandless, T. J. & Crabtree, G. R. Affinity modulation of small-molecule ligands by borrowing endogenous protein surfaces. *Proc. Natl. Acad. Sci. U. S. A.* **96,** 1953–8 (1999).

296. Petzold, G., Fischer, E. S. & Thomä, N. H. Structural basis of lenalidomide-induced CK1α degradation by the CRL4CRBN ubiquitin ligase. *Nature* **532,** 127–130 (2016).

297. Hughes, S. J. & Ciulli, A. Molecular recognition of ternary complexes: a new dimension in the structure-guided design of chemical degraders. *Essays Biochem.* **61,** 505–516 (2017).

298. Maniaci, C. *et al.* Homo-PROTACs: bivalent small-molecule dimerizers of the VHL E3 ubiquitin ligase to induce self-degradation. *Nat. Commun.* **8,** 830 (2017).

299. O'Hare, T., Zabriskie, M. S., Eiring, A. M. & Deininger, M. W. Pushing the limits of targeted therapy in chronic myeloid leukaemia. *Nat Rev Cancer* **12,** 513–526 (2012).

300. Lozzio, C. & Lozzio, B. Human Chronic Myelogenous Leukemia Cell-Line With Positive Philadelphia Chromosome. *Blood* **45,** 321–334 (1975).

301. Hantschel, O. *et al.* BCR-ABL uncouples canonical JAK2-STAT5 signaling in chronic myeloid leukemia. *Nat. Chem. Biol.* **8,** 285–293 (2012).

302. Hoelbl, A. *et al.* Stat5 is indispensable for the maintenance of Bcr/Abl-positive leukaemia. *EMBO Mol. Med.* **2,** 98–110 (2010).

303. Eskiocak, B., Ali, A. & White, M. a. The estrogen-related receptor α inverse agonist XCT 790 is a nanomolar mitochondrial uncoupler. *Biochemistry* **53,** 4839–4846 (2014).

304. Nagar, B., Hantschel, O., Young, M. a, Scheffzek, K. & Veach, D. Structural basis for the autoinhibition of c-Abl kinase. *Cell* **112,** 859–871 (2003).

305. Hantschel, O. *et al.* A myristoyl/phosphotyrosine switch regulates c-Abl. *Cell* **112,** 845–857 (2003).

306. Adrián, F. J. *et al.* Allosteric inhibitors of Bcr-abl–dependent cell proliferation. *Nat. Chem. Biol.* **2,** 95–102 (2006).

307. Zhang, J. *et al.* Targeting Bcr-Abl by combining allosteric with ATP-binding-site inhibitors. *Nature* **463,** 501–506 (2010).

308. Mao, J.-H. *et al.* As4S4 targets RING-type E3 ligase c-CBL to induce degradation of BCR-ABL in chronic myelogenous leukemia. *Proc. Natl. Acad. Sci.* **107,** 21683–21688 (2010).

309. Sun, H. *et al.* Bcr-Abl ubiquitination and Usp9x inhibition block kinase signaling and promote CML cell apoptosis. *Blood* **117,** 3151–3162 (2011).

310. Quintás-Cardama, A. *et al.* Reverse phase protein array profiling reveals distinct proteomic signatures associated with chronic myeloid leukemia progression and with chronic phase in the CD34-positive compartment. *Cancer* **118,** 5283–92 (2012).

311. Zhuang, C. *et al.* CDK1-mediated phosphorylation of Abi1 attenuates Bcr-Abl-induced F-actin assembly and tyrosine phosphorylation of WAVE complex during mitosis. *J. Biol. Chem.* **286,** 38614–38626 (2011).

312. Yoon, P. *et al.* Activation of mammalian target of rapamycin and the p70 S6 kinase by arsenic trioxide in BCR-ABL-expressing cells. *Mol. Cancer Ther.* **5,** 2815–2823 (2006).

313. Carayol, N. *et al.* Suppression of programmed cell death 4 (PDCD4) protein expression by BCR-ABL-regulated engagement of the mTOR/p70 S6 kinase pathway. *J. Biol. Chem.* **283,** 8601–8610 (2008).

314. Sheng, Z., Ma, L., Sun, J. E., Zhu, L. J. & Green, M. R. BCR-ABL suppresses autophagy through ATF5-mediated regulation of mTOR transcription. *Blood* **118,** 2840–2848 (2011).

315. Chen, J. *et al.* SHP-2 phosphatase is required for hematopoietic cell transformation by Bcr-Abl. *Blood* **109,** 778–785 (2007).

316. Harvey, A. J. & Crompton, M. R. Use of RNA interference to validate Brk as a novel therapeutic target in breast cancer: Brk promotes breast carcinoma cell proliferation. *Oncogene* **22,** 5006–5010 (2003).

317. Hantschel, O. Unexpected Off-Targets and Paradoxical Pathway Activation by Kinase Inhibitors. *ACS Chem. Biol.* **10,** 234–245 (2015).

318. Papa, F. R., Zhang, C., Shokat, K. & Walter, P. Bypassing a kinase activity with an ATP-competitive drug. *Science* **302,** 1533–7 (2003).

319. Muvaffak, A. *et al.* Evaluating TBK1 as a Therapeutic Target in Cancers with Activated IRF3. *Mol. Cancer Res.* **12,** 1055–66 (2014).

320. Barbie, D. A. *et al.* Systematic RNA interference reveals that oncogenic KRAS-driven cancers require TBK1. *Nature* **462,** 108–112 (2009).

321. Crew, A. P. *et al.* Identification and Characterization of Von Hippel-Lindau-Recruiting Proteolysis Targeting Chimeras (PROTACs) of TANK-Binding Kinase 1. *J. Med. Chem.* acs.jmedchem.7b00635 (2017). doi:10.1021/acs.jmedchem.7b00635

322. Inglese, J. *et al.* High-throughput screening assays for the identification of chemical probes. *Nat. Chem. Biol.* **3,** 466–479 (2007).

323. Comess, K. M. *et al.* An Ultraefficient Affinity-Based High-Throughout Screening Process: Application to Bacterial Cell Wall Biosynthesis Enzyme MurF. *J. Biomol. Screen.* **11,** 743–754 (2006).

324. Goodnow, R. A., Dumelin, C. E. & Keefe, A. D. DNA-encoded chemistry: Enabling

the deeper sampling of chemical space. *Nat. Rev. Drug Discov.* **16,** 131–147 (2017).

325. Brenner, S. & Lerner, R. A. Encoded combinatorial chemistry. *Proc. Natl. Acad. Sci.* **89,** 5381–5383 (1992).

326. Chan, A. I., McGregor, L. M. & Liu, D. R. Novel selection methods for DNA-encoded chemical libraries. *Curr. Opin. Chem. Biol.* **26,** 55–61 (2015).

327. Mcgregor, L. M., Jain, T. & Liu, D. R. Identification of Ligand − Target Pairs from Combined Libraries of Small Molecules and Unpuri fi ed Protein Targets in Cell Lysates. *J. Am. Chem. Soc.* **136,** 3264–3270 (2014).

328. Chan, A. I., McGregor, L. M., Jain, T. & Liu, D. R. Discovery of a Covalent Kinase Inhibitor from a DNA-Encoded Small-Molecule Library × Protein Library Selection. *J. Am. Chem. Soc.* **139,** 10192–10195 (2017).

329. Pellecchia, M. *et al.* Perspectives on NMR in drug discovery: A technique comes of age. *Nat. Rev. Drug Discov.* **7,** 738–745 (2008).

330. Dalvit, C., Fogliatto, G. P., Stewart, A., Veronesi, M. & Stockman, B. WaterLOGSY as a method for primary NMR screening: Practical aspects and range of applicability. *J. Biomol. NMR* **21,** 349–359 (2001).

331. Wagstaff, J. L., Taylor, S. L. & Howard, M. J. Recent developments and applications of saturation transfer difference nuclear magnetic resonance (STD NMR) spectroscopy. *Mol. BioSyst.* **9,** 571–577 (2013).

332. Lo, M.-C. *et al.* Evaluation of fluorescence-based thermal shift assays for hit identification in drug discovery. *Anal. Biochem.* **332,** 153–9 (2004).

333. Phillips, K. & de la Peña, A. H. The combined use of the thermofluor assay and thermoQ analytical software for the determination of protein stability and buffer optimization as an aid in protein crystallization. *Curr. Protoc. Mol. Biol.* 1–15 (2011). doi:10.1002/0471142727.mb1028s94

334. Niesen, F. H., Berglund, H. & Vedadi, M. The use of differential scanning fluorimetry to detect ligand interactions that promote protein stability. *Nat. Protoc.* **2,** 2212–21 (2007).

335. Murphy, J. M. *et al.* A robust methodology to subclassify pseudokinases based on their nucleotide-binding properties. *Biochem. J.* **457,** 323–34 (2014).

336. Hildebrand, J. M. *et al.* Activation of the pseudokinase MLKL unleashes the four-helix bundle domain to induce membrane localization and necroptotic cell death. *Proc. Natl. Acad. Sci. U. S. A.* **111,** 15072–7 (2014).

337. Fedorov, O., Niesen, F. H. & Knapp, S. Kinase Inhibitor Selectivity Profiling Using Differential Scanning Fluorimetry. *Kinase* **795,** 109–118 (2012).

338. Layton, C. J. & Hellinga, H. W. Thermodynamic analysis of ligand-induced changes in protein thermal unfolding applied to high-throughput determination of ligand affinities with extrinsic fluorescent dyes. *Biochemistry* **49,** 10831–41 (2010).

339. Askin, S. *et al.* Selective protein unfolding: a universal mechanism of action for the development of irreversible inhibitors. *Chem. Commun.* 2–5 (2018).

doi:10.1039/C8CC00090E

340. Zuercher, W. J. Seeding collaborations to advance kinase science with the GSK Published Kinase Inhibitor Set (PKIS). *Curr. Top. Med. Chem.* 1–3 (2013).

341. Elkins, J. M. *et al.* Comprehensive characterization of the Published Kinase Inhibitor Set. *Nat. Biotechnol.* (2015). doi:10.1038/nbt.3374

342. Davis, M. I. *et al.* Comprehensive analysis of kinase inhibitor selectivity. *Nat. Biotechnol.* **29,** 1046–1051 (2011).

343. Lebakken, C. S. *et al.* Development and Applications of a Broad-Coverage, TR-FRET-Based Kinase Binding Assay Platform. *J. Biomol. Screen.* **14,** 924–935 (2009).

344. Statsuk, A. V *et al.* Tuning a three-component reaction for trapping kinase substrate complexes. *J. Am. Chem. Soc.* **130,** 17568–74 (2008).

345. Daub, H. *et al.* Kinase-Selective Enrichment Enables Quantitative Phosphoproteomics of the Kinome across the Cell Cycle. *Mol. Cell* **31,** 438–448 (2008).

346. Bantscheff, M. *et al.* Quantitative chemical proteomics reveals mechanisms of action of clinical ABL kinase inhibitors. *Nat. Biotechnol.* **25,** 1035–1044 (2007).

347. Rinehart, J. *et al.* Sites of Regulated Phosphorylation that Control K-Cl Cotransporter Activity. *Cell* **138,** 525–536 (2009).

348. Weekes, M. P. *et al.* Quantitative temporal viromics: An approach to investigate host-pathogen interaction. *Cell* **157,** 1460–1472 (2014).

349. Ting, L., Rad, R., Gygi, S. P. & Haas, W. MS3 eliminates ratio distortion in isobaric multiplexed quantitative proteomics. *Nat. Methods* **8,** 937–940 (2011).

350. Médard, G. *et al.* Optimized chemical proteomics assay for kinase inhibitor profiling. *J. Proteome Res.* **14,** 1574–1586 (2015).